AD-A131 330 EVALUATION OF LOW MELTING HALIDE SYSTEMS FOR BATTERY APPLICATIONS(U) TENNESSEE UNIV KNOXVILLE DEPT OF CHEMISTRY G MAMANTOV ET AL. APR 83 AFWAL-TR-83-2032 1/2

UNCLASSIFIED F33615-78-C-2075 F/G 10/3 NL

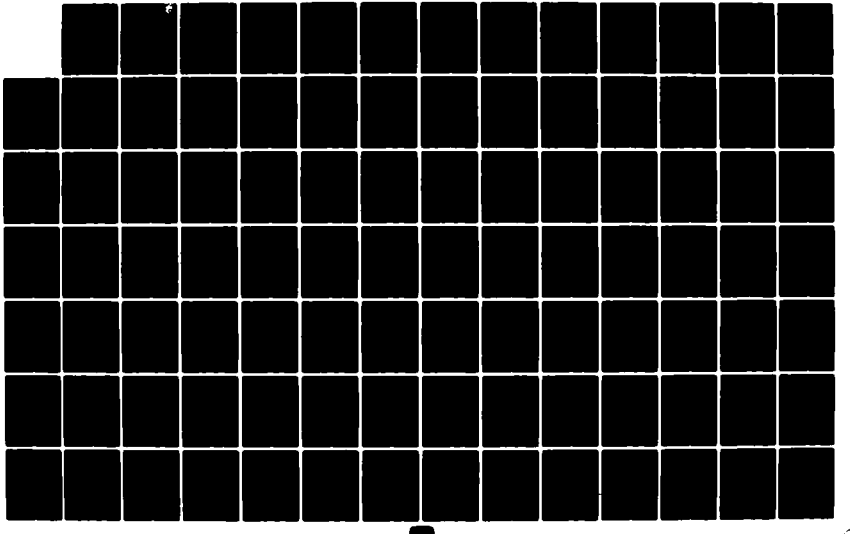

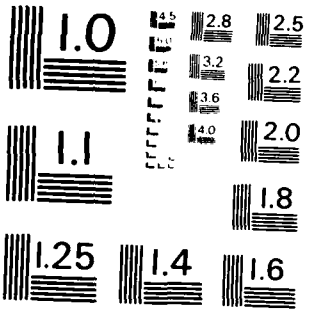

AFWAL-TR-83-2032

EVALUATION OF LOW MELTING HALIDE SYSTEMS FOR BATTERY APPLICATIONS

Dr G. Mamantov, Dr C. Petrovic

University of Tennessee
Department of Chemistry
Knowville Tennessee 37996-1600

APRIL 1983

FINAL REPORT FOR PERIOD SEPTEMBER 1978 - FEBRUARY 1983

AERO PROPULSION LABORATORY
AIR FORCE WRIGHT AERONAUTICAL LABORATORIES
AIR FORCE SYSTEMS COMMAND
WRIGHT-PATTERSON AIR FORCE BASE, OHIO 45433

NOTICE

When Government drawings, specifications, or other data are used for any purpose other than in connection with a definitely related Government procurement operation, the United States Government thereby incurs no responsibility nor any obligation whatsoever; and the fact that the government may have formulated, furnished, or in any way supplied the said drawings, specifications, or other data, is not to be regarded by implication or otherwise as in any manner licensing the holder or any other person or corporation, or conveying any rights or permission to manufacture use, or sell any patented invention that may in any way be related thereto.

This report has been reviewed by the Office of Public Affairs (ASD/PA) and is releasable to the National Technical Information Service (NTIS). At NTIS, it will be available to the general public, including foreign nations.

This technical report has been reviewed and is approved for publication.

James S. Cloyd

JAMES S. CLOYD
PROJECT ENGINEER

Donald P. Mortel

DONALD P. MORTEL
TECHNICAL AREA MANAGER
BATTERIES/FUEL CELLS GROUP

FOR THE COMMANDER

James D. Reams

JAMES D. REAMS
CHIEF, AEROSPACE POWER DIVISION
AERO PROPULSION LABORATORY

"If your address has changed, if you wish to be removed from our mailing list, or if the addressee is no longer employed by your organization please notify AFWAL/POOC *, W-PAFB, OH 45433 to help us maintain a current mailing list".*

Copies of this report should not be returned unless return is required by security considerations, contractual obligations, or notice on a specific document.

Unclassified

SECURITY CLASSIFICATION OF PAGE (When Data Entered)

REPORT DOCUMENTATION PAGE		READ INSTRUCTIONS BEFORE COMPLETING FORM
1. REPORT NUMBER AFWAL-TR-83-2032	2. GOVT ACCESSION NO. AD-A131330	3. RECIPIENT'S CATALOG NUMBER
4. TITLE (and Subtitle) EVALUATION OF LOW MELTING HALIDE SYSTEMS FOR BATTERY APPLICATIONS		5. TYPE OF REPORT & PERIOD COVERED Final Report for Period Sep 78 - Feb 83 6. PERFORMING ORG. REPORT NUMBER
7. AUTHOR(s) Dr. Gleb Mamantov Dr. Cedomir Petrovic		8. CONTRACT OR GRANT NUMBER(s) F33615-78-C-2075
9. PERFORMING ORGANIZATION NAME AND ADDRESS University of Tennessee Department of Chemistry Knoxville TN 37919		10. PROGRAM ELEMENT, PROJECT, TASK AREA & WORK UNIT NUMBERS 31452289
11. CONTROLLING OFFICE NAME AND ADDRESS Aero Propulsion Laboratory (AFWAL/POOC) Air Force Wright Aeronautical Laboratories (AFSC) Wright-Patterson Air Force Base Ohio 45433		12. REPORT DATE April 1983 13. NUMBER OF PAGES 159
14. MONITORING AGENCY NAME & ADDRESS(if different from Controlling Office)		15. SECURITY CLASS. (of this report) UNCLASSIFIED 15a. DECLASSIFICATION/DOWNGRADING SCHEDULE

16. DISTRIBUTION STATEMENT (of this Report)

Approved for public release; distribution unlimited.

17. DISTRIBUTION STATEMENT (of the abstract entered in Block 20, if different from Report)

18. SUPPLEMENTARY NOTES

19. KEY WORDS (Continue on reverse side if necessary and identify by block number)

electrolytes, molten salt, low melting point, conductivity, battery

20. ABSTRACT (Continue on reverse side if necessary and identify by block number)

This program involved evaluation of selected low temperature molten salt solvent systems containing inorganic and/or organic chlorides and bromides for battery applications. The research involved determination of the liquidus temperatures, the specific electrical conductivity, and the electrochemical span of selected halide systems. The studies of a few cathode and anode systems and of two prototype cells were also undertaken for a few promising solvent systems.

DD FORM 1 JAN 73 1473 EDITION OF 1 NOV 65 IS OBSOLETE

Unclassified

SECURITY CLASSIFICATION OF THIS PAGE (When Data Entered)

FOREWORD

This report describes experimental evaluation of some low melting halide systems for battery applications. This work was performed at the Department of Chemistry, The University of Tennessee, Knoxville, under Contract No. F33615-78-C-2075 with the Aero Propulsion Laboratory, Air Force Wright Aeronautical Laboratories, Wright-Patterson Air Force Base, Ohio. The Principal investigator was Professor Gleb Mamantov. The Air Force Project Officer was Mr. J. S. Cloyd, AFWAL/POOC, Wright-Patterson Air Force Base, Ohio.

The personnel working on the project consisted of Dr. Cedomir Petrovic, postdoctoral research associate, Jeff Cobb, Douglas Goff, Jeff Ledford, Walter Li, Jeff Nelson, and Robert Walton, undergraduate research assistants.

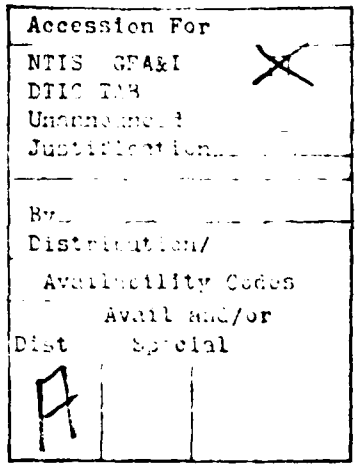

TABLE OF CONTENTS

LIST OF FIGURES

LIST OF FIGURES (Continued)

LIST OF TABLES

LIST OF TABLES (Continued)

LIST OF TABLES (Continued)

LIST OF TABLES (Continued)

1. INTRODUCTION

Molten alkali chloroaluminates are of considerable interest as solvents in several primary and secondary batteries presently under development (1-3). They have low liquidus temperatures, a relatively large electrochemical span and good specific electrical conductivity. For example, the liquidus temperature of the $AlCl_3$-NaCl binary molten salt system varies as a function of composition between 115 and 190°C; the potential span between the aluminum deposition and the chlorine evolution is 2.1 V, and the specific conductivity is in the 0.1-0.7 $ohm^{-1}cm^{-1}$ range (4). The acid-base properties of an aluminum chloride-alkali chloride system are a function of its composition (5). Thus, the chloride ion concentration in these melts and the Lewis acidity of the melts can be readily varied over several decades (5).

Even lower liquidus temperatures are possible in chloroaluminate melts in which an organic halide is substituted for an alkali halide. For example, some compositions of the $AlCl_3$-1-ethylpyridinium chloride and $AlCl_3$-ethylpyridinium bromide melts are liquid at room temperature (6-8). The former melt system has been studied at the F. J. Seiler Research Laboratory for possible battery applications (9).

Other low-temperature melt systems may also be useful for battery applications. Recent compilations list a number of binary and/or ternary systems in which $AlCl_3$, $AlBr_3$, $GaCl_3$, $SbCl_3$ and $FeCl_3$, among others, appear as one component (10,11). These compilations, however, do not attempt a critical evaluation of existing data and much of the information listed in them is conflicting. The more critical recent volume by Janz et al. (4) includes only a few chloroaluminate molten salt systems. Low melting salt systems which do not contain $AlCl_3$, such as $AlBr_3$-, $GaCl_3$- and $FeCl_3$- containing melts, have received little attention to date as possible solvents for battery uses.

The purpose of this three year project was to critically evaluate a wide range of binary and ternary low temperature molten salt systems for battery applications. These systems included chlorides and/or bromides of aluminum, antimony, iron and gallium as one component, and various alkali, alkaline earth, quaternary ammonium, n-butyl pyridinium and antimony chlorides and/or bromides as the other(s). During the first year of the project the liquidus range measurements were performed on the following molten salt systems: $AlCl_3$-LiCl-NaCl, $AlCl_3$-NaCl-KCl, $AlCl_3$-LiCl-KCl, $AlCl_3$-$BaCl_2$-NaCl,

$AlCl_3$-$CaCl_2$-NaCl, $AlCl_3$-NaBr, $AlBr_3$-Bu_4NBr and $AlBr_3$-Me_4NBr, as well as extensive electrical conductivity measurements on the $AlCl_3$-LiCl-NaCl molten salt system. In the second year, the liquidus range and/or electrical conductivity measurements were performed on the following molten salt systems: $AlCl_3$-LiCl-NaCl, $AlCl_3$-NaBr, $AlBr_3$-NaCl, $AlBr_3$-Bu_4NBr, $AlBr_3$-Me_4NBr, $AlCl_3$-$SbCl_3$, $AlCl_3$-$SbCl_3$-n-BuPyCl, $FeCl_3$-NaCl, $FeCl_3$-LiCl-NaCl, and $GaCl_3$-NaCl. At the end of the second year, four molten salt systems were selected for further work: $AlCl_3$-LiCl-NaCl, $AlCl_3$-$SbCl_3$-NaCl, $FeCl_3$-LiCl-NaCl, and $AlCl_3$-Me_4NCl-NaCl. The liquidus range and electrical conductivity studies were continued during the third year of this project, as well as some vapor pressure and Raman spectroscopic studies. The compatibility of Nafion, a possible battery separator, LiAl alloy anode, and TiS_2 cathode with chloroaluminate melts was investigated. The study of the low temperature molten salt cell Na/β"-alumina/SCl_3^+ in $AlCl_3$-LiCl-NaCl was also initiated during this period. Following the instructions of the sponsoring agency, the study of the $AlCl_3$-Me_4NCl-NaCl system was terminated at the end of the third year. During an extension of the project, additional studies of the $FeCl_3$-LiCl-NaCl system and the cyclic voltammetry of the $AlCl_3$-$SbCl_3$-NaCl system were performed, the study of the Na/SCl_3^+ cell was continued, and two other cells, the primary (thermal) cell Na/Nafion/SCl_3^+ in $AlCl_3$-LiCl-NaCl and the rechargeable cell Na/β"-alumina/$AlCl_3$-$SbCl_3$-NaCl were investigated.

2. EXPERIMENTAL

2.1 Preparative

Samples of the melts studied in the present work were prepared by the standard procedures employed in our Laboratory. Anhydrous aluminum chloride (Fluka, puris, distilled) was digested overnight at 210°C with high purity aluminum (Alfa-Ventron, m6N) in evacuated, sealed glass vessels and subsequently redistilled in the same vessels. Anhydrous aluminum bromide (Fluka, purum, distilled) was digested at 140°C and redistilled in the same manner. Alkali chlorides and bromides (Fisher and Baker), calcium chloride (Mallinckrodt, anhydrous), and barium chloride (Vaughn, anhydrous) were dried in vacuum at 400°C for five days. Tetrabutyl ammonium bromide (Eastman) was dried in vacuum at 90°C for seven days; tetramethyl ammonium bromide (Eastman) was dried at 160°C for the same length of time. Tetramethyl ammonium chloride (Eastman) was dried in vacuum at 105°C for two weeks. Various methods of preparation of tetrabutyl ammonium chloride are discussed in Section 3.7. Purified antimony chloride (Mallinckrodt, anhydrous, digested with antimony and distilled under vacuum) was obtained from the laboratory of Dr. G. P. Smith, Oak Ridge National Laboratory. Alternately, it was prepared from the commercial antimony chloride (Alfa-Ventron, anhydrous) by distilling twice under vacuum. Ferric chloride (Alfa-Ventron, anhydrous) was also distilled under vacuum. Its purification is discussed in more detail in Section 3.16. Gallium chloride (Alfa-Ventron, 99.999%) was used as received.

Samples of the melts, 6-10 g each, for the liquidus range and/or electrical conductivity measurements, were prepared using an analytical balance in a dry box (Vacuum Atmospheres), with the moisture and oxygen levels of <2 ppm. All the subsequent operations were performed either in evacuated and sealed Pyrex vessels or in the dry box.

2.2 Liquidus Range

Differential scanning calorimetry was used wherever possible for the liquidus range measurements. For the measurements on viscous samples, which supercool readily, and where crystallization, once induced, proceeds very slowly, the visual observation method was used as a superior alternative. For oxidizing samples, such as melts containing $FeCl_3$, the latter method was the only choice.

A commercial differential scanning calorimeter, Perkin Elmer DSC-1B, was used to determine the phase transition temperatures. The data were recorded

on a Moseley Autograph 2D-2A X-Y recorder with 5mV full scale sensitivity. A low pass RC filter was used to reduce the noise. In view of the very small size of samples used in the DSC experiments (1.5 to 2.0 mg), special care was taken to insure that the DSC samples were representative of the average composition of the melts. The samples were prepared in specially designed melt tubes with thin walled capillary sidearms. By quenching these sample tubes in an ice-water bath, the melt in the sidearms was rapidly frozen. Samples for the DSC measurements were taken from these sidearms and sealed in aluminum sample pans (Perkin Elmer Co.) in the dry box, and were kept under dry nitrogen atmosphere until and during the DSC experiments. The samples were scanned at 5°C/min. At this slow speed no appreciable instrumental distortion of the DSC curves was observed. The calorimeter was calibrated at the same scanning speed with sealed high purity indium and tin standards with the melting temperatures of 156.2 and 231.9°C, respectively. Only the melting curves were used for collecting the data. Due to severe supercooling, of the order of 20-50°C, the cooling curves were of little value for our work.

The solidus temperature in the present report is defined as the "extrapolated onset" temperature, i.e. the intersection of the extrapolated linear section of the ascending melting peak with the extrapolated baseline. The liquidus temperature is defined as the maximum of the last melting peak on the DSC curve. Since there is no agreement in the literature regarding the correct method of extracting the melting temperatures from the DSC data (12-14), the first deviation of the melting peak from the baseline, the "extrapolated onset", and the peak maximum temperatures having all been used, a short discussion of the method is needed here.

A comparison of our values for the solidus temperature for the $AlCl_3$-NaCl salt system with the literature data did not help resolve the issue due to the scatter of the literature data. Our "extrapolated onset" value for the solidus temperature of the $AlCl_3$-NaCl samples, 114°C, was in good agreement with the literature value of 115°C (15), obtained by the visual observation technique. Our "first deviation from the baseline" value of 104°C for the same system, however, was in fair agreement with the more recent literature value of 107.2°C (16), also determined by the visual method. An independent experimental method, the measurement of the electrical conductivity of the solid chloroaluminate melts as a function of temperature through the melting process did not yield a clear cut solidus

temperature either. Even though the conductivity change during the melting process was nearly four orders of magnitude, the change itself was gradual and difficult to interpret. These measurements are discussed in more detail in Section 3.1. The measurements on $AlCl_3$-NaCl samples at Oak Ridge National Laboratory using a Perkin-Elmer DSC-2 instrument, which has a superior sensitivity and signal-to-noise ratio as well as a flat baseline, settled the issue by demonstrating that the "first deviation" temperature was a function of the sensitivity limit of the instrument (Figure 1). In our measurements with the DSC-1B instrument the "first deviation" temperature was determined by a combination of the maximum amplifier gain, the instrumental noise level, and the baseline curvature, and, therefore, does not have much physical meaning.

The above result also settled the method of extracting the liquidus temperature from a DSC curve. If the "extrapolated onset" temperature is the true melting point of a pure compound, and if the slope of the leading edge of its melting peak is determined by the thermal resistance of the sample pan - sample interface and of the sample itself (12), then the sample of a pure compound is completely molten by the time the maximum of the melting peak is reached (14). In that case the liquidus temperature of a multicomponent sample is neither the temperature of the return to the baseline, nor the "extrapolated return" temperature in the DSC recordings, because the multicomponent system is presumably also completely molten by the time the last maximum of the melting curve is reached. Therefore, the maximum of the last peak should be read as the liquidus temperature. The thermal resistance probably plays a role here as well, but it is not clear how to perform the thermal lag correction in this case. The liquidus temperature data in this Report were read as the extrapolated maxima of the last melting peak in the DSC recordings, and are not corrected for the thermal lag.

Samples for the visual determination of the liquidus range were sealed in evacuated Pyrex tubes and suspended in a silicone oil thermostat. The temperature was scanned using a proportional temperature controller, built in our electronics shop, and modified by an addition of a clock motor. The scanning rate was ca. 5°C/hr. The high temperature limit of the bath, deteremined by the silicone oil, was ca. 180°C. The temperature of the bath was read with a copper-constantan thermocouple and a Fluke Model 895 DC differential voltmeter.

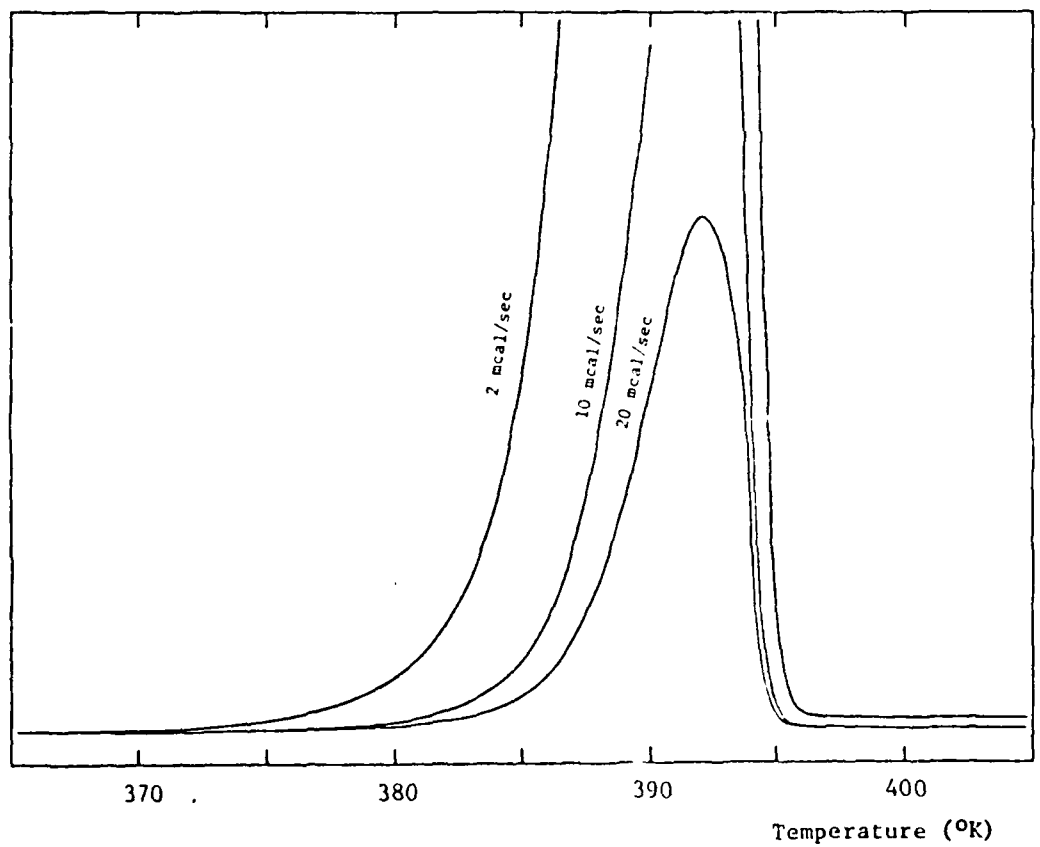

Figure 1. DSC Recordings of 61.0-39.0 Mole % $AlCl_3$-NaCl at Sensitivity of 2, 10, and 20 mcal/sec Full Scale.

The solidus temperature in the visual measurements was determined as the temperature of the last change in the appearance of the solid samples, followed by the first sign of the liquid phase. The liquidus temperature was taken as the temperature at which the last residue of the solid phase disappeared. With the exception of the ferric chloride containing samples, both transition temperatures were quite distinct.

2.3 Electrical Conductivity

The specific electrical conductivity measurements were performed by the conventional AC method. The equipment consisted of a Hewlett-Packard wide band oscillator Model 200 CD, an RC bridge built in our electronics shop, General Radio precision decade resistors and capacitors and a Tektronix Model 549 oscilloscope. The furnace with an aluminum block body and non-inductive cartridge heaters was controlled by a proportional controller also built in our electronics shops, or by a Bayley Model 124 proportional temperature controller. The temperature of the cell was read with a chromel-alumel and a copper-constantan thermocouple and a Fluke Model 895 DC differential voltmeter.

Small volume capillary conductivity cells with platinum foil electrodes were built of Pyrex (Figure 2). They were calibrated at 25°C with the 1.0 demal KCl solution according to the standard procedure of Jones and Bradshaw (17). The values of the cell constants were in the 215 to 265 cm^{-1} range. The calculated temperature dependence of the cell constants was of the order of 0.00015 $cm^{-1}deg^{-1}$. Since the calculated change of the cell constants over the 300°C temperature range was only 0.05 cm^{-1}, it was ignored in further work.

The measurements were performed at the frequency of 1.0 kHz. The frequency dispersion of the melts was not studied, since the temperature of the furnace was not sufficiently stable to permit the retuning of the RC bridge for different frequencies.

The measurements of the AC conductivity in the solid phase were performed with the same equipment used for the molten salt conductivity studies, except for the conductivity cell, which was of the conventional low resistance liquid type. The molten samples were frozen in the cell by quenching in the ice-water bath, and then annealed prior to the experiment at 10-20°C below the solidus temperature of the sample. Since the high resistance limit of our RC bridge was ca. 10 megohms, the measurements on the solid samples

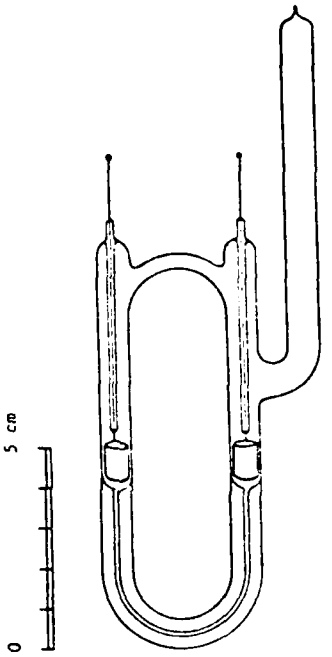

Figure 2. Electrical Conductivity Cell.

were limited to the temperatures above 75°C for the $AlCl_3$-NaCl samples and above 55°C for the $AlCl_3$-LiCl-NaCl samples. The heating rate in our experiments was ca. 2.5°C/hr. Both the resistance and the capacitance of solid samples were measured. However, the capacitance was too small to be measured with our RC bridge until a sample was well within its liquidus range.

The temperatures listed in the specific conductivity tables in this report were measured with the chromel-alumel thermocouple, calibrated at the Metrology Laboratory of ORNL against a standard platinum resistance thermometer. The corrected temperature T_c is given as:

$$T_c = T - \Delta T$$

where T is the measured temperature and

$$\begin{aligned}\Delta T = & -5.29222\times10^{-1} + 1.50805\times10^{-2}T \\ & +6.04628\times10^{-4}T^2 - 1.59570\times10^{-5}T^3 \\ & +2.03140\times10^{-7}T^4 - 1.27380\times10^{-2}T^5 \\ & +3.81065\times10^{-12}T^6 - 4.37159\times10^{-15}T^7 \end{aligned} \quad (1)$$

The large number of terms in this expression was necessitated by a change in the shape of the calibration curve between 150 and 175°C. The correction expression is exact only to 260°C and should be used with caution above this temperature. Since the specific conductivity data in this report extend for many melt compositions to 300°C, and for some melts to as high as 350°C, it was not practical to correct some data and not correct the others. Therefore the temperatures in all the specific conductivity tables in this report are listed as measured, i.e. uncorrected.

2.4 Vapor Pressure

Two experimental methods were used for the vapor pressure measurements. The first employed a differential transducer with vacuum as a reference. Thus it yielded the absolute pressure above a studied melt sample under the chosen experimental conditions. The second method utilized a mercury manometer with a melt sample of known vapor pressure as a reference. Since it measured the pressure difference above the two melt samples under the identical conditions, it was a true differential technique.

The transducer vapor pressure apparatus (Figure 3) consisted of a MKS Baratron type 221A differential pressure transducer (0-1000 torr pressure range and 0.1 torr resolution) attached to an evacuated and sealed Pyrex bulb containing the sample melt via a Kovar seal and a Cajon VCR high vacuum

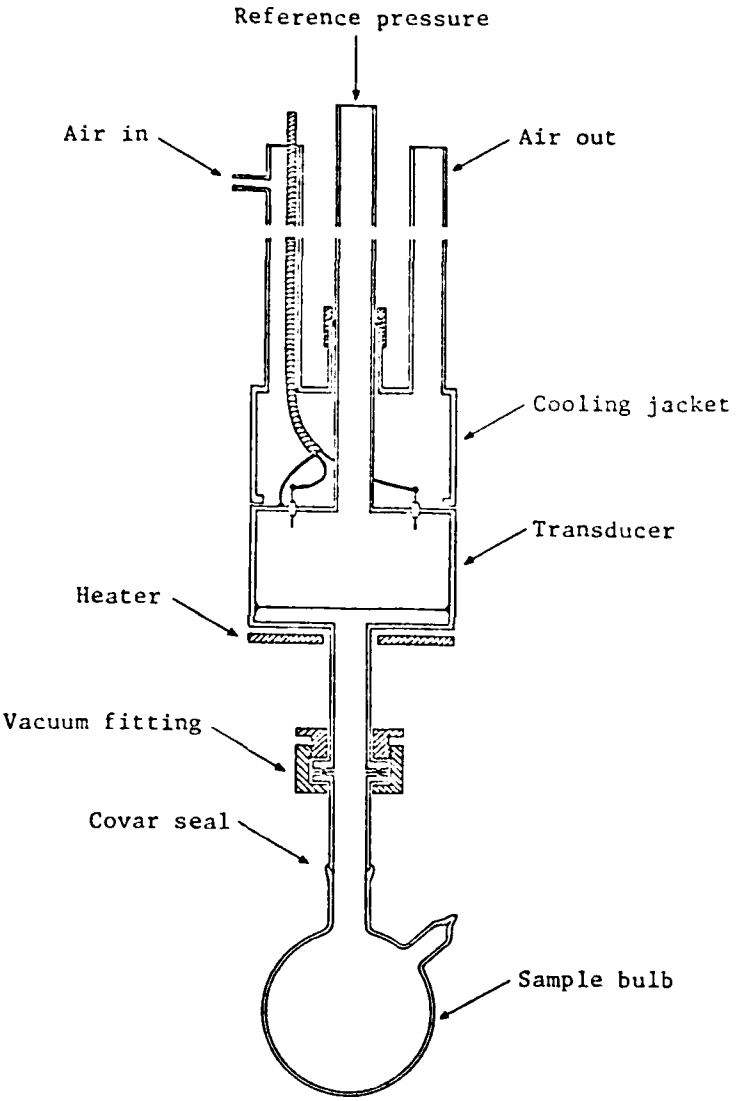

Figure 3. Vapor Pressure Apparatus.

fitting with a nickel gasket. The reference pressure in the transducer was maintained at zero by continuous evacuation. The high temperature operating limit of the transducer was extended to ca. 230°C by protecting the electrical feed-throughs on its reference side and the teflon insulated leads with an air cooled stainless steel jacket. The temperature of the vapor pressure apparatus was maintained constant using an aluminum block furnace controlled by a proportional temperature controller. The temperature of the sample side of the transducer was maintained a few degrees above the temperature of the melt to safeguard against the condensation of the volatile melt components inside the transducer cavity. The output of the transducer was amplified using the MKS type 221A electronics and displayed on a Keithley Model 177 digital voltmeter.

The vapor pressure apparatus was baked out for 48 hours at 120°C under vacuum prior to an experiment. A sample of the melt was transferred into the sample bulb in the dry box, and the bulb was sealed under vacuum. After the sample was molten and brought back to the room temperature, a residual pressure was observed in the cell. This pressure may have been due to the HCl formed in the reaction of $AlCl_3$ from the melt sample with the residual moisture adsorbed on the glass and stainless steel surfaces of the pressure apparatus. The residual pressure problem was dealt with by adding a Pyrex sidearm with a breakable seal to allow one more evacuation of the cell prior to the beginning of measurements. In the end, the transducer method was abandoned as too time consuming and unreliable.

The differential vapor pressure cell (Figure 4) consisted of two melt compartments connected by a capillary mercury manometer. After the cell was baked out in vacuum, as described in the previous paragraph, the mercury was introduced into the capillary followed by the sample and reference melts. The two filling arms were sealed in vacuum and, as the last step, the pressure equalizing tube was sealed between the two melt compartments. The difference between the vapor pressure of the sample melt and the reference melt was read to 0.1 torr with the aid of a cathetometer. Since the sample and the reference compartments are identical, and since the composition of the sample is similar to the composition of the reference melt, any residual moisture effects in the differential pressure cell are expected to cancel out.

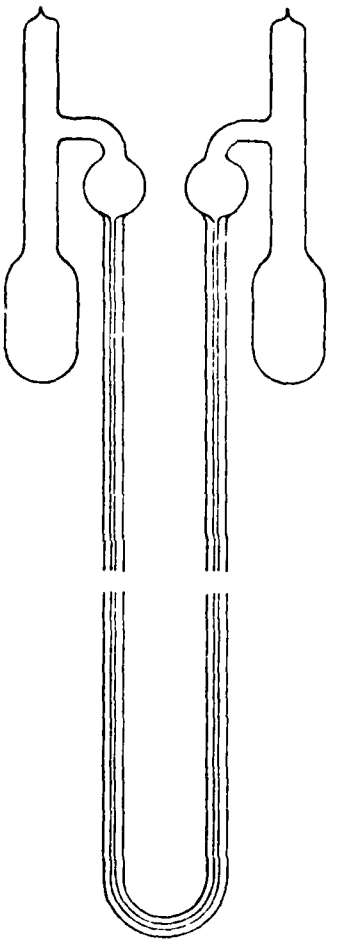

Figure 4. Differential Vapor Pressure Cell.

2.5 Raman Spectroscopy

Samples for the Raman spectroscopy were sealed in evacuated 6mm square Pyrex cells. The temperature of the nichrome resistor wire wound furnace was regulated with a variable transformer.

The spectrometer consisted of a Spectra Physics Model 171 argon ion laser and a Jobin Yvon Ramanor 2000M double pass monochromator controlled by a ISA Model 980015 stepping motor controller. The RCA Model 31034 photomultiplier tube was operated at room temperature. The photon counting electronics consisted of a Pacific Model AD 126 amplifier discriminator and a Model 126 photometer. A Houston Omnigraphic strip chart recorder was used to record the spectra.

2.6 Cyclic Voltammetry

The cyclic voltammetry measurements were performed in evacuated and sealed Pyrex cells. Since the design of the cells and the choice of electrodes varied with the melts being studied, the details of the cells are discussed together with the results of voltammetric measurements.

A Princeton Applied Research Model 174A Polarographic Analyzer and a Model 175 Universal Programmer were used for the cyclic voltammetry scans. The current-voltage curves were recorded on a Houston Omnigraphic Model 2000 X-Y Recorder. The electrode potentials were measured using a Keithley Model 616 Digital Electrometer.

3. RESULTS

3.1 $AlCl_3$-LiCl-NaCl System

The $AlCl_3$-LiCl-NaCl molten salt system appears attractive as a solvent for battery use. The addition of LiCl to the $AlCl_3$-NaCl system, the most widely used of the chloroaluminate systems, lowers the liquidus range of the latter without altering drastically most of its other physical and chemical properties. The ionic mobility of the Li^+ cation is lower than the mobility of the Na^+ cation, due to the smaller ionic radius of the former and its stronger interaction with the anionic species in these melts. Therefore, the specific electrical conductivity of the $AlCl_3$-LiCl melts is lower by approximately 20% at the corresponding compositions. However, there is no appreciable difference in the electrochemical span of the two binary melt systems, since their limiting cathodic potentials are determined by the aluminum deposition process, and not by the alkali metal deposition.

Our data for three sections of the $AlCl_3$-LiCl-NaCl phase diagram are listed in Table 1 and shown in Figure 5. The LiCl to NaCl mole ratio in these pseudobinary sections was maintained constant, 3:1, 1:1 and 1:3, respectively. The phase diagram of the $AlCl_3$-LiCl-NaCl system is not available in the literature, although several compositions of this system have been studied at the F. J. Seiler Research Laboratory (18). The phase diagrams of the two binary aluminum chloride-alkali chloride subsystems, $AlCl_3$-LiCl and $AlCl_3$-NaCl, however, have been extensively studied (4,15,16).

The liquidus curves of the three sections of the $AlCl_3$-LiCl-NaCl ternary system resemble the liquidus curve of the $AlCl_3$-NaCl system. Their minima are displaced towards the alkali chloride rich compositions with respect to the eutectic composition of the $AlCl_3$-NaCl system. This displacement is more than 2 mole % for the 3:1 section, ca. 3 mole % for the 1:3 section, and as much as 4 mole % $AlCl_3$ for the 1:1 LiCl to NaCl section. The last section also exhibits the lowest liquidus temperatures. In view of the similarity of the two alkali cations, as well as the similarity of the phase diagrams of the $AlCl_3$-LiCl and $AlCl_3$-NaCl binary systems, the similarity of the liquidus curves of the three studied sections seems reasonable. The solidus temperature of all three sections, 86°C, is the same. Thus it is lower by ca. 30°C than the solidus temperature of the $AlCl_3$-NaCl binary system. A new feature of the data for the 1:3 section, which does not appear in the 1:1 section, is an intermediate phase transition at 97°C in the melts with less than 58 mole

TABLE 1

PHASE DIAGRAM DATA FOR $AlCl_3$-LiCl-NaCl SYSTEM

Composition (Mole %)			Solidus Temperature (°C)	Intermediate Transition (°C)	Liquidus Temperature (°C)
$AlCl_3$	LiCl	NaCl			
52.0	24.0	24.0	86		105
54.0	23.0	23.0	86		101
56.0	22.0	22.0	86		96
58.0	21.0	21.0	86		100.5
60.0	20.0	20.0	86		124
62.0	19.0	19.0	86		136.5
64.0	18.0	18.0	86		151
68.0	16.0	16.0	86		168
53.4	35.0	11.6	86		119
56.0	33.0	11.0	86		112
58.0	31.5	10.5	86		105
60.0	30.0	10.0	86		107
62.0	28.5	9.5	86		132
64.0	27.0	9.0	86		150
68.0	24.0	8.0	86		172
52.0	12.0	36.0	86	98	128
54.0	11.5	34.5	86	?	120
56.0	11.0	33.0	86	96	110
59.0	10.2	30.8	86	?	103
60.0	10.2	30.0	86	103	113
62.0	9.5	28.5	86	103	130
64.0	9.0	27.0	86	102	139
68.0	8.0	24.0	86	103	162
55.0	27.5	17.5	86		103

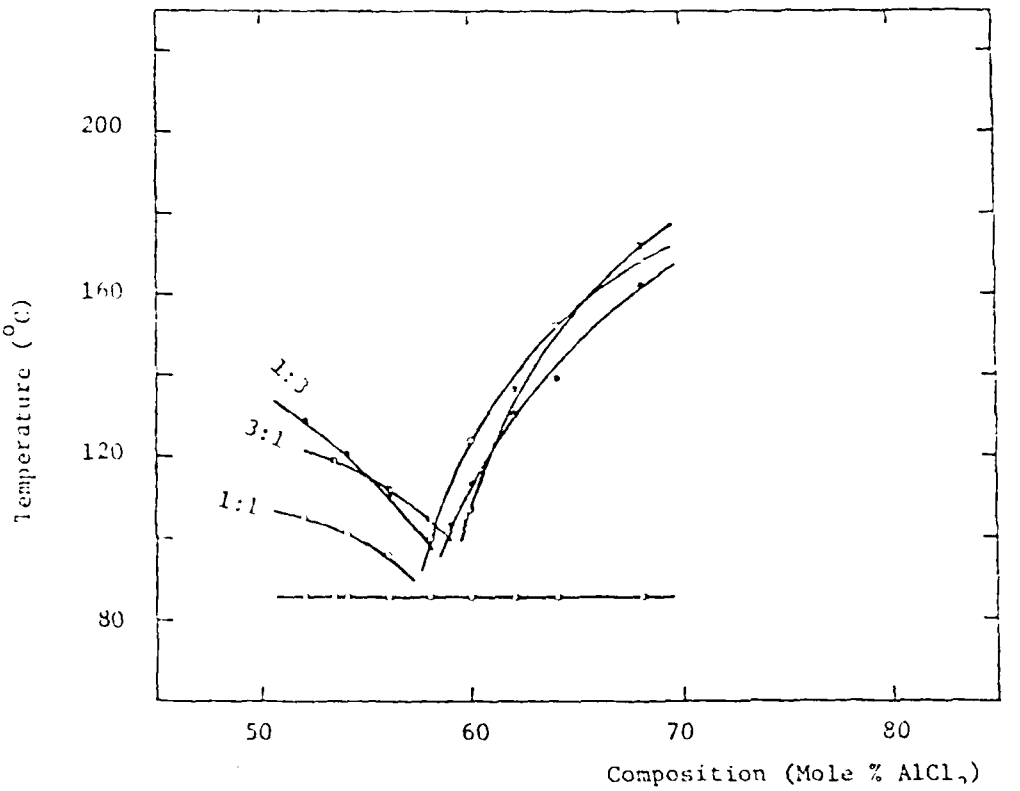

Figure 5. Phase Diagram Data for the $AlCl_3$-LiCl-NaCl System.
LiCl to NaCl mole ratios are indicated on the liquidus curves.

% $AlCl_3$, and at 103°C in the melts in which $AlCl_3$ is over 58 mole %. The nature of this transition is not clear.

Our specific electrical conductivity data for the $AlCl_3$-LiCl-NaCl molten salt system are listed in Tables 2 to 14, and the conductivity vs. temperature plots are shown in Figures 6 and 7. The conductivity measurements were performed in the temperature range from the melting point of the samples to 300°C. In the very acidic melts, which have considerable vapor pressure, the upper temperature limit was lowered accordingly. The reproducibility of the data was checked by performing measurements on two different samples of the 54.0-23.0-23.0 mole % melt. The agreement of the measured conductivities was within 0.25% and was probably limited by the reproducibility of the sample compositions. During the course of this work conductivity data for 7 compositions of $AlCl_3$-LiCl-NaCl melts have been published (19). Our results are in agreement to 1.5% with the literature values for the two melts for which the compositions coincide. The data were fitted by the least squares method to a polynomial equation of the second order in temperature:

$$\kappa = A_o + A_1 T + A_2 T^2 \qquad (2)$$

where κ is the specific conductivity in $ohm^{-1}cm^{-1}$, and T is the absolute temperature. The coefficients, A_o, A_1 and A_2 are listed in Table 15. The temperature correction given in Equation 1 should be applied to all the specific conductivity values calculated from the Equation 2.

A comparison of the conductivity of the melts with the same $AlCl_3$ mole fraction, but different LiCl to NaCl mole ratio is not very revealing. The specific conductivity of the melts with 3:1 LiCl to NaCl mole ratio is consistently lower than the conductivity of the corresponding 1:1 melts. In the most acidic melts this difference is about 10%. This is in agreement with the lower ionic mobility of the Li^+ ion compared to the mobility of the Na^+ ion, both in aqueous solutions (20) and in the binary chloroaluminate melts, and is probably due to the more covalent character of the interaction of the Li^+ cation with the other species in these melts.

The electrical conductivity of the 54.0-23.0-23.0 mole % $AlCl_3$-LiCl-NaCl and the 66.0-34.0 mole % $AlCl_3$-NaCl samples was studied as a function of temperature through the solid-liquid phase transition. These data are shown in Figure 8. The conductivity of these samples changes by four orders of magnitude during the phase transition, and its temperature dependence drops from 25 deg^{-1} at 60°C in the solid to 0.19 deg^{-1} at 120°C in the melt for the

TABLE 2

SPECIFIC CONDUCTIVITY DATA FOR $AlCl_3$-LiCl-NaCl SYSTEM AT 1.0 KHz

COMPOSITION: 52.0-24.0-24.0 (Mole %)

Temperature (°C)	Specific Conductivity ($ohm^{-1}cm^{-1}$)
120.0	0.2377*
130.0	0.2637*
140.0	0.2894*
150.0	0.3155
160.0	0.3400
170.0	0.3645
180.0	0.3889
190.0	0.4129
200.0	0.4370
210.0	0.4608
220.0	0.4844
230.0	0.5075
240.0	0.5298
250.0	0.5522
260.0	0.5743
270.0	0.5956
279.3	0.6162
290.0	0.6377
298.3	0.6549

*Calculated from Eqn. 2.

TABLE 3

SPECIFIC CONDUCTIVITY DATA FOR $AlCl_3$-LiCl-NaCl SYSTEM AT 1.0 KHz

COMPOSITION: 54.0-23.0-23.0 (Mole %)

Temperature (°C)	Specific Conductivity ($ohm^{-1}cm^{-1}$)
110.0	0.1895
119.2	0.2122
130.0	0.2344
140.0	0.2568
150.0	0.2794
159.3	0.3002
170.0	0.3240
182.5	0.3519
190.0	0.3690
200.0	0.3909
210.0	0.4120
220.0	0.4333
230.0	0.4545
240.0	0.4754
250.0	0.4959
261.0	0.5183
270.0	0.5362
280.0	0.5558
290.0	0.5752
300.0	0.5944

TABLE 4

SPECIFIC CONDUCTIVITY DATA FOR $AlCl_3$-LiCl-NaCl SYSTEM AT 1.0 KHz

COMPOSITION: 56.0-22.0-22.0 (Mole %)

Temperature (°C)	Specific Conductivity ($ohm^{-1}cm^{-1}$)
100.0	0.1404*
110.0	0.1620*
120.0	0.1835*
130.0	0.2043*
140.0	0.2265
150.7	0.2483
160.0	0.2674
170.0	0.2881*
180.0	0.3081
190.0	0.3285
200.0	0.3486
210.0	0.3684
220.0	0.3882
231.0	0.4097
240.0	0.4271
250.0	0.4464
260.6	0.4667
269.8	0.4840
280.0	0.5027
290.0	0.5200
300.0	0.5387

* Calculated from Eqn. 2.

TABLE 5

SPECIFIC CONDUCTIVITY DATA FOR $AlCl_3$-LiCl-NaCl SYSTEM AT 1.0 KHz

COMPOSITION: 58.0-21.0-21.0 (Mole %)

Temperature (°C)	Specific Conductivity ($ohm^{-1}cm^{-1}$)
120.0	0.1629*
130.0	0.1821*
140.0	0.2023
150.0	0.2196
160.0	0.2378
170.0	0.2568
180.0	0.2755
190.0	0.2939
200.0	0.3121
210.0	0.3301
220.0	0.3480
230.0	0.3657
240.0	0.3832
250.0	0.4005
260.0	0.4178
270.0	0.4346
280.0	0.4517
290.0	0.4683
300.0	0.4847

*Calculated from Eqn. 2.

TABLE 6

SPECIFIC CONDUCTIVITY DATA FOR $AlCl_3$-LiCl-NaCl SYSTEM AT 1.0 KHz

COMPOSITION: 60.0-20.0-20.0 (Mole %)

Temperature (°C)	Specific Conductivity ($ohm^{-1}cm^{-1}$)
130.0	0.1667*
140.0	0.1837*
150.0	0.2009
160.0	0.2175
170.0	0.2351
180.0	0.2523
190.0	0.2683
200.0	0.2862*
210.0	0.3036
220.0	0.3202
230.0	0.3373
239.9	0.3553
250.0	0.3728*
259.4	0.3905
270.0	0.4085
280.0	0.4256
290.0	0.4424
300.0	0.4601

* Calculated from Eqn. 2.

TABLE 7

SPECIFIC CONDUCTIVITY DATA FOR $AlCl_3$-LiCl-NaCl SYSTEM AT 1.0 KHz

COMPOSITION: 62.0-19.0-19.0 (Mole %)

Temperature (°C)	Specific Conductivity ($ohm^{-1} cm^{-1}$)
150.0	0.1783
160.0	0.1940
170.0	0.2101
180.0	0.2259
190.0	0.2417
200.0	0.2581
210.0	0.2747
220.0	0.2915
230.0	0.3090
240.0	0.3256
250.0	0.3432
260.0	0.3587
270.0	0.3755
280.0	0.3925
290.0	0.4095
300.0	0.4254

TABLE 8

SPECIFIC CONDUCTIVITY DATA FOR $AlCl_3$-LiCl-NaCl SYSTEM AT 1.0 KHz

COMPOSITION: 64.0-18.0-18.0 (Mole %)

Temperature (°C)	Specific Conductivity ($ohm^{-1} cm^{-1}$)
160.0	0.1801*
170.0	0.1941*
181.4	0.2098
190.8	0.2231
200.0	0.2360
210.0	0.2503
219.8	0.2641
230.6	0.2791
241.0	0.2934
250.0	0.3069
260.0	0.3208
269.8	0.3349

*Calculated from Eqn. 2.

TABLE 9

SPECIFIC CONDUCTIVITY DATA FOR $AlCl_3$-LiCl-NaCl SYSTEM AT 1.0 KHz

COMPOSITION: 68.0-16.0-16.0 (Mole %)

Temperature (°C)	Specific Conductivity ($ohm^{-1}cm^{-1}$)
180.0	0.1790
190.0	0.1907
200.0	0.2027
210.0	0.2134
220.0	0.2250
230.0	0.2368
240.0	0.2482
250.0	0.2603

TABLE 10

SPECIFIC CONDUCTIVITY DATA FOR $AlCl_3$-LiCl-NaCl SYSTEM AT 1.0 KHz

COMPOSITION: 53.4-35.0-11.6 (Mole %)

Temperature (°C)	Specific Conductivity ($ohm^{-1}cm^{-1}$)
130.0	0.2283
140.0	0.2506
150.0	0.2730
160.0	0.2949
170.0	0.3170
180.0	0.3385
190.0	0.3607
200.0	0.3825*
210.0	0.4038
220.0	0.4250
230.0	0.4462
240.0	0.4666
249.8	0.4868
260.0	0.5074
270.0	0.5270
280.0	0.5464
290.0	0.5654
300.0	0.5854*

* Calculated from Eqn. 2.

TABLE 11

SPECIFIC CONDUCTIVITY DATA FOR $AlCl_3$-LiCl-NaCl SYSTEM AT 1.0 KHz

COMPOSITION: 56.0-33.0-11.6 (Mole %)

Temperature (°C)	Specific Conductivity ($ohm^{-1}cm^{-1}$)
130.0	0.1912*
140.0	0.2116*
151.0	0.2338
160.8	0.2534
170.0	0.2717
180.0	0.2914
190.0	0.3111
200.0	0.3301
210.0	0.3497
220.0	0.3688
230.0	0.3869
240.0	0.4053
251.9	0.4273
261.0	0.4436
270.0	0.4599
280.0	0.4779
290.0	0.4955
300.0	0.5126

*Calculated from Eqn. 2.

TABLE 12

SPECIFIC CONDUCTIVITY DATA FOR $AlCl_3$-LiCl-NaCl SYSTEM AT 1.0 KHz

COMPOSITION: 58.0-31.5-10.5 (Mole %)

Temperature (°C)	Specific Conductivity ($ohm^{-1}cm^{-1}$)
120.0	0.1526*
130.0	0.1711*
140.0	0.1902
150.0	0.2076
160.0	0.2255
170.0	0.2435
180.0	0.2612
190.0	0.2792
200.0	0.2968
209.9	0.3139
220.2	0.3316
230.0	0.3497
240.0	0.3667
250.0	0.3832
260.0	0.4002
270.0	0.4172
281.0	0.4348
292.7	0.4543
301.6	0.4689

*Calculated from Eqn. 2.

TABLE 13

SPECIFIC CONDUCTIVITY DATA FOR $AlCl_3$-LiCl-NaCl SYSTEM AT 1.0 KHz

COMPOSITION: 60.0-30.0-10.0 (Mole %)

Temperature (°C)	Specific Conductivity ($ohm^{-1}cm^{-1}$)
120.0	0.1389*
131.0	0.1571
140.3	0.1719
150.0	0.1874
159.8	0.2035
171.0	0.2217
180.0	0.2362
190.0	0.2526
200.0	0.2687
210.0	0.2847
222.6	0.3048
230.0	0.3162
240.0	0.3321
250.0	0.3481
260.0	0.3639
271.0	0.3812
280.0	0.3957*
290.0	0.4120
300.0	0.4269

* Calculated from Eqn. 2

TABLE 14

SPECIFIC CONDUCTIVITY DATA FOR $AlCl_3$-LiCl-NaCl SYSTEM AT 1.0 KHz
COMPOSITION: 68.0-24.0-8.0 (Mole %)

Temperature (°C)	Specific Conductivity ($ohm^{-1} cm^{-1}$)
170.0	0.1571*
180.0	0.1681*
190.0	0.1791*
200.0	0.1898
210.0	0.2011
220.3	0.2121
230.0	0.2228
240.0	0.2336
250.0	0.2446

* Calculated from Eqn. 2.

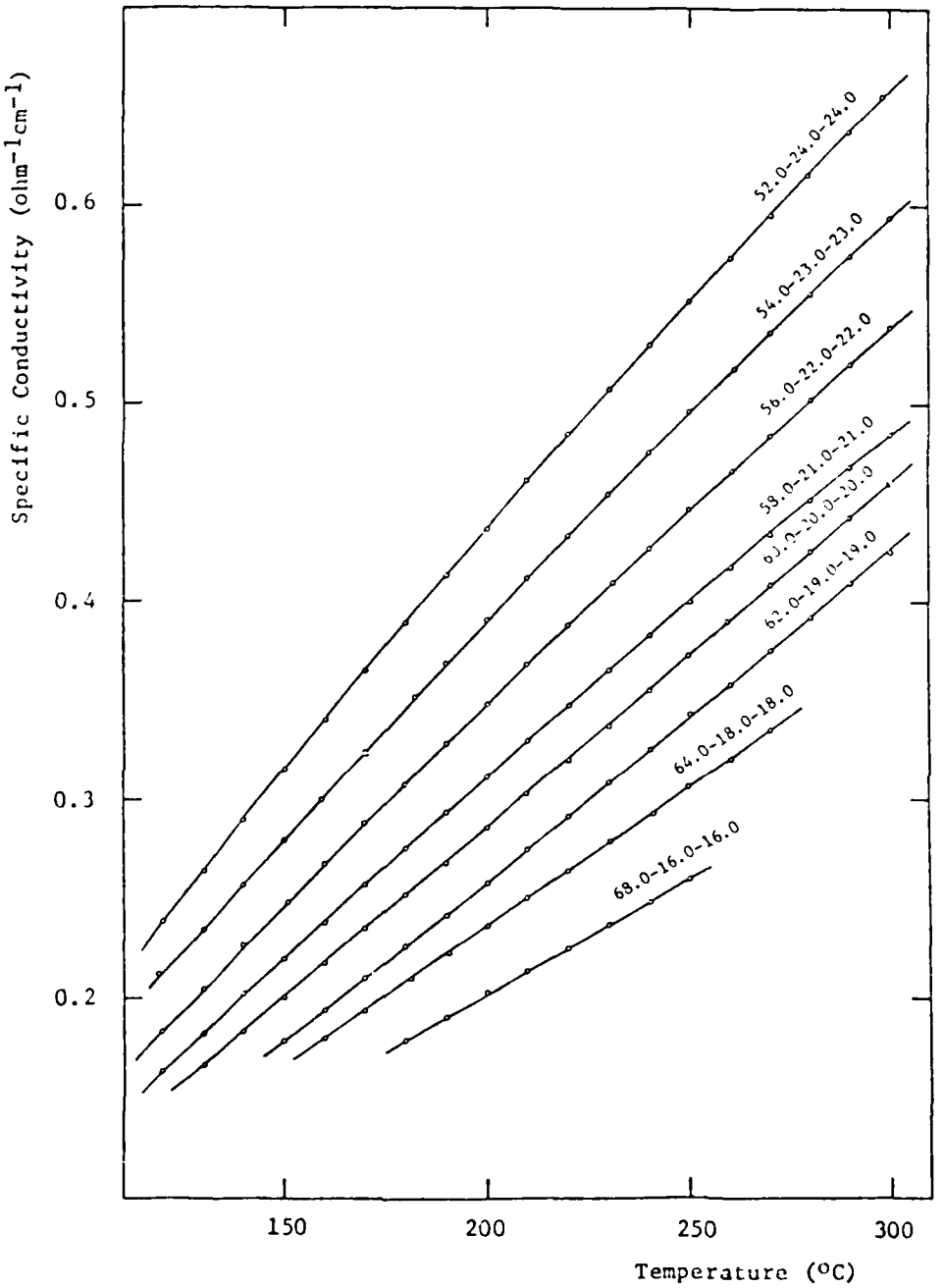

Figure 6. Specific Conductivity of $AlCl_3$-LiCl-NaCl System (LiCl-NaCl Mole Ratio 1:1).
Composition in mole % is indicated on the curves.

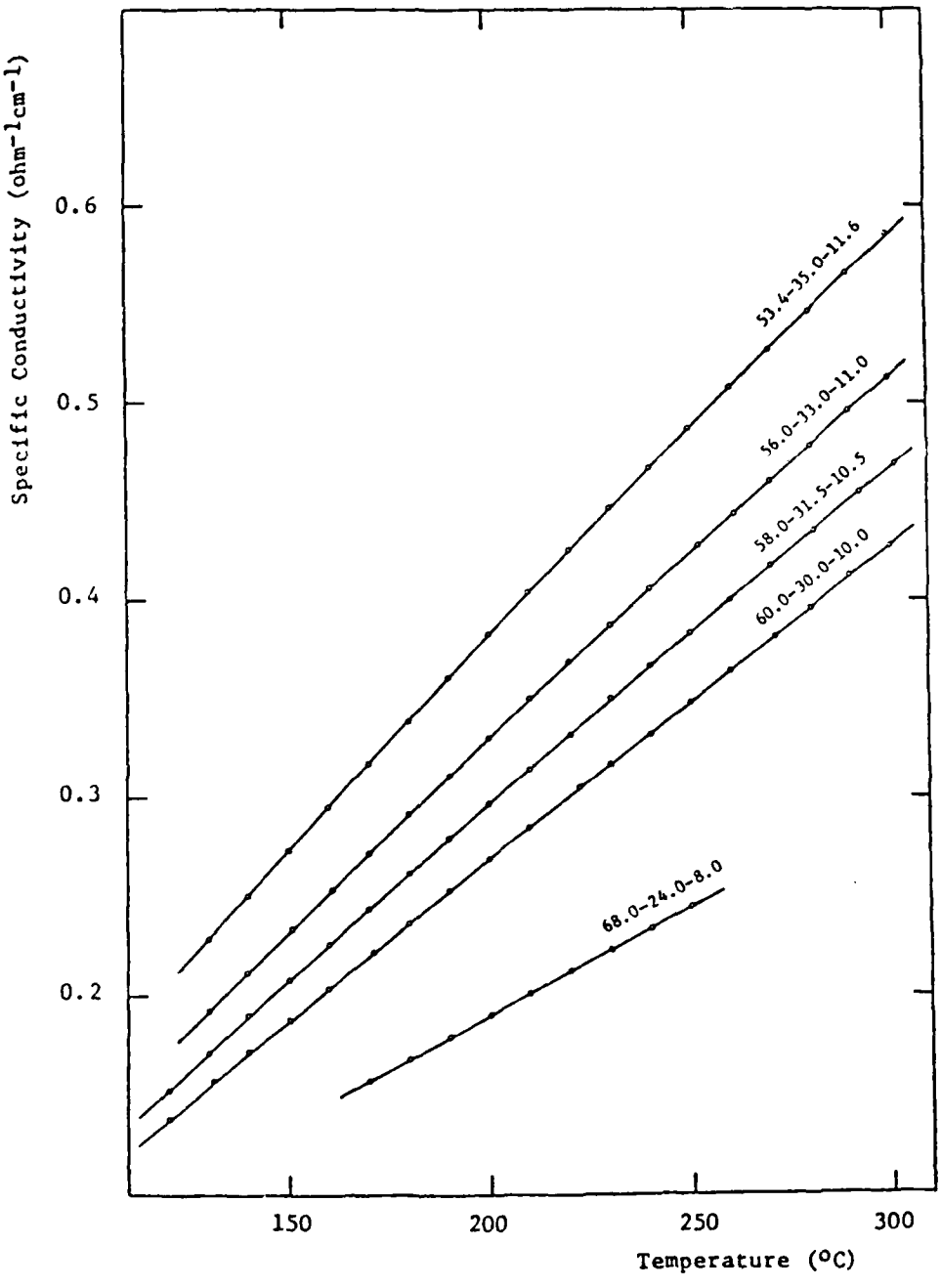

Figure 7. Specific Conductivity of $AlCl_3$-LiCl-NaCl System (LiCl-NaCl Mole Ratio 3:1).
Composition in mole % is indicated on the curves.

TABLE 15

TEMPERATURE DEPENDENCE OF THE SPECIFIC CONDUCTIVITY OF THE $AlCl_3$-LiCl-NaCl SYSTEM

Composision (Mole %)			Coefficients for Equation 2		
$AlCl_3$	LiCl	NaCl	A_o	$A_1 \times 10^3$	$A_2 \times 10^6$
		(LiCl-NaCl Mole Ratio 1:1)			
52.0	24.0	24.0	-1.02747	3.81867	-1.52860
54.0	23.0	23.0	-0.84931	3.09007	-0.99411
56.0	22.0	22.0	-0.79713	2.85035	-0.90625
58.0	21.0	21.0	-0.70954	2.51345	-0.74940
60.0	20.0	20.0	-0.48036	1.51815	0.21516
62.0	19.0	19.0	-0.44525	1.33423	0.32510
64.0	18.0	18.0	-0.39984	1.28372	0.12712
68.0	16.0	16.0	-0.30053	0.96894	0.19290
		(LiCl-NaCl Mole Ratio 3:1)			
53.4	35.0	11.6	-0.87078	3.15976	-1.08030
56.0	33.0	11.0	-0.79300	2.82780	-0.95952
58.0	31.5	10.5	-0.67084	2.33552	-0.61367
60.0	30.0	10.0	-0.53101	1.77409	-0.17893
68.0	24.0	8.0	-0.36936	1.27100	-0.18757

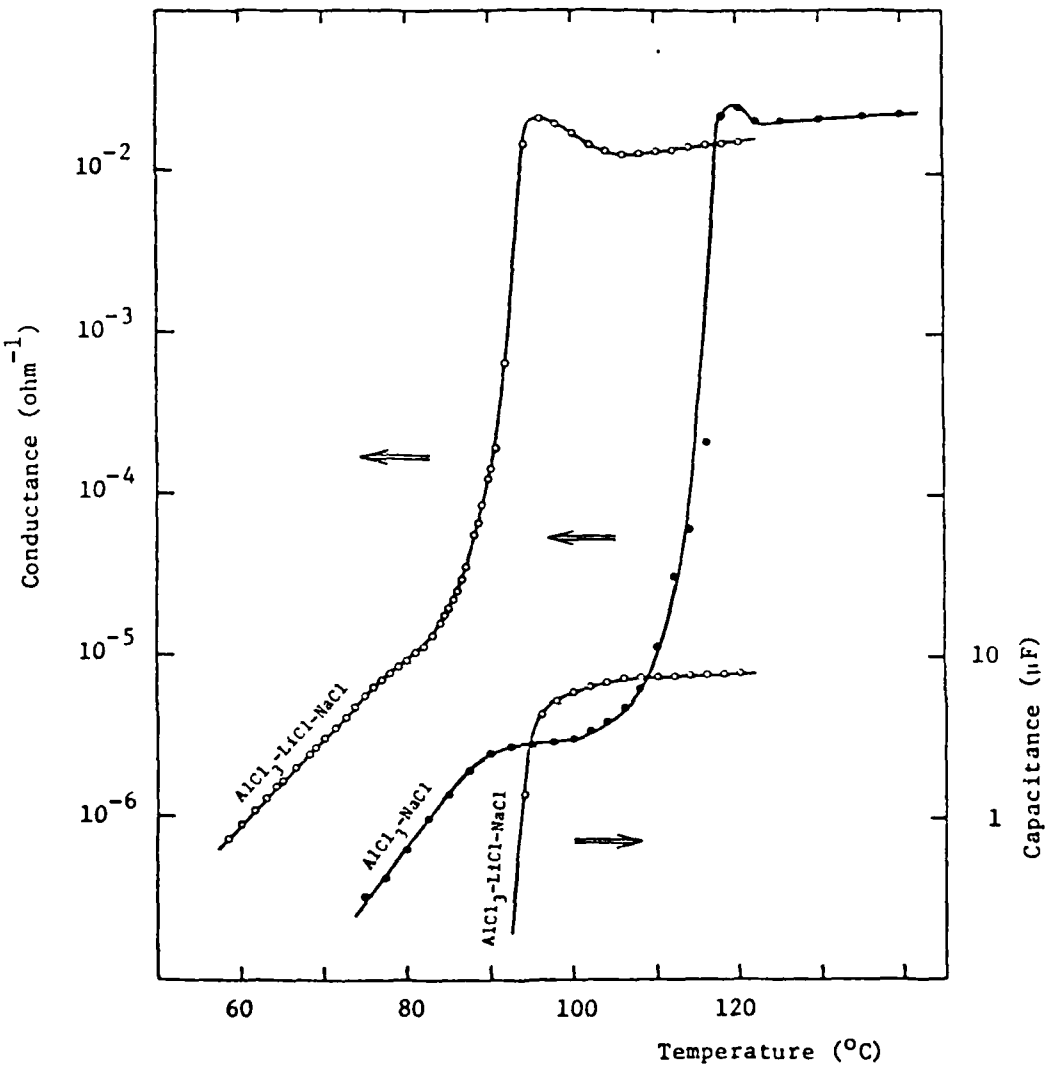

Figure 8. Conductance and Capacitance of 54.0-23.0-23.0 Mole % $AlCl_3$-LiCl-NaCl and 66.0-34.0 Mole % $AlCl_3$-NaCl Samples.

54.0-23.0-23.0 mole % $AlCl_3$-LiCl-NaCl sample. However, the change is quite gradual and without discontinuities. Both the conductivity and the capacitance assume their linear shape at ca. 106°C, in agreement with the DSC liquidus data (Table 1). The "extrapolated onset" of the steeply rising section of the conductivity curve at 85-86°C is also in agreement with the "extrapolated onset" on the DSC curve for the 54.0-23.0-23.0 mole % sample. Since our interest in these measurements was in the shape of the electrical conductivity vs. temperature curves, the cell used for these measurements was not calibrated, and only the reciprocal resistance is shown on the ordinate axis in this figure. The specific conductivity of the solid chloroaluminate, however, is a factor in the rate of self-discharge during storage of the low temperature secondary batteries which employ these melts as solvents. The specific conductivity of the solid 54.0-23.0-23.0 mole % $AlCl_3$-LiCl-NaCl is readily calculated from Figure 8, using the conductivity of the melt with the same composition, Table 3, to calibrate the conductivity cell. The linear, low temperature section of the 1/R curve for the 54.0-23.0-23.0 mole % $AlCl_3$-LiCl-NaCl sample extrapolates to 1.6×10^{-8} ohm^{-1} at 25°C. The corresponding value for the same, completely molten, sample at 120°C is 1.6×10^{-2} ohm^{-1}, and its specific conductivity is 0.2120 ohm^{-1} cm^{-1} (Table 3). Therefore, the extrapolated specific conductivity of the solid 54.0-23.0-23.0 mole % sample at 25°C is 2.1×10^{-7} $ohm^{-1}cm^{-1}$. Thus it is roughly an order of magnitude higher than the conductivity of the solid 66.0-34.0 mole % $AlCl_3$-NaCl at the same temperature and composition (Figure 8). This is expected in view of the lower solidus temperature of the $AlCl_3$-LiCl-NaCl. Since these values are extrapolated far beyond the experimentally measured range, however, they should be accepted with caution.

In summary, the specific conductivities of the $AlCl_3$-LiCl-NaCl molten salt system (0.1-0.7 $ohm^{-1}cm^{-1}$) are not substantially lower than the conductivities in the $AlCl_3$-NaCl system, and the electrochemical span in the two systems is the same (>2.0 V). The liquidus temperatures of the $AlCl_3$-LiCl-NaCl system ($\geq$86°C) are lower by ca. 30°C, and thus compare favorably with the liquidus temperatures of the $AlCl_3$-NaCl system. The $AlCl_3$-LiCl-NaCl system certainly merits further study as a very promising solvent for battery use.

3.2 Other Ternary $AlCl_3$-MCl Systems

We have performed preliminary measurements on two other ternary aluminum

chloride-alkali chloride systems: the $AlCl_3$-NaCl-KCl system and the $AlCl_3$-LiCl-KCl system. Our results (Table 16) indicate that the solidus temperatures of these two systems, ca. 100°C for the former, and ca. 98°C for the latter, are quite close to each other. The literature value of 93°C for the ternary eutectic temperature of the $AlCl_3$-NaCl-KCl system (21) is low in comparison to our value. Other reported values (cf. references in (21)) are even lower and are probably incorrect.

The phase diagram of the $AlCl_3$-LiCl-KCl system is available in the literature (22). The reported ternary eutectic temperature of 84-85°C seems also too low in comparison to our value of ca. 98°C. Our liquidus temperature data are also not in good agreement with the literature values. Considerably more work is required if the source of these disagreements is to be clarified.

3.3 $AlCl_3$-$BaCl_2$-NaCl System

The complete phase diagram of the $AlCl_3$-$BaCl_2$-NaCl ternary system has been studied recently (23). The melting point of 50°C has been reported for the ternary eutectic with the composition of 63.6-2.6-33.8 mole % (23). Since this is the lowest liquidus temperature reported to date for an inorganic chloroaluminate melt, it was of interest to verify the information.

The results of our DSC measurements are shown in Table 17. One of our samples was prepared to have exactly the same composition as quoted in the literature for the lowest melting ternary eutectic, and in the other two the mole fraction of $AlCl_3$ was varied. Thus the $BaCl_2$ to NaCl mole ratio was the same in all three samples.

Our results do not reproduce the above literature data. Our sample with the 63.6-2.6-33.8 mole % composition has the liquidus range of ca. 25°C, which indicates that the true eutectic composition is quite far from the cited composition. The 60.0-2.9-37.1 mole % sample, with the liquidus range of ca. 10°C, is much closer to the true eutectic point. We do not observe any phase transitions below 108°C. Since our results demonstrate that the addition of $BaCl_2$ lowers the solidus temperature of the $AlCl_3$-NaCl binary system by only 7°C, and does not change appreciably the liquidus temperatures at the studied compositions, the effect of $BaCl_2$ as an additive is marginal. In view of this result, a further study of this system is not justified.

TABLE 16

PHASE DIAGRAM DATA FOR OTHER TERNARY ALKALI CHLOROALUMINATE SYSTEMS

Composition (mole %)			Solidus Temperature (°C)	Liquidus Temperature (°C)
$AlCl_3$	NaCl	KCl		
55.0	31.6	13.4	100	118
61.2	24.8	14.0	100	108
63.4	22.4	14.2	101	147
$AlCl_3$	LiCl	KCl		
51.2	35.8	13.0	98	118
60.8	25.8	13.4	98	167

TABLE 17

PHASE DIAGRAM DATA FOR $AlCl_3$-$BaCl_2$-NaCl SYSTEM

Composition (mole %)			Solidus Temperature (°C)	Liquidus Temperature (°C)
$AlCl_3$	$BaCl_2$	NaCl		
56.0	3.2	40.8	108	136
60.0	2.9	37.1	108	118
63.6	2.6	33.8	108	134

3.4 $AlCl_3$-$CaCl_2$-NaCl System

No data are available in the literature for the $AlCl_3$-$CaCl_2$-NaCl system. Our DSC data for the samples with compositions similar to the $AlCl_3$-$BaCl_2$-NaCl compositions are shown in Table 18. These results indicate that the solidus temperature in the $AlCl_3$-$CaCl_2$-NaCl system is 108°C. The liquidus temperatures of the studied samples with the $CaCl_2$ are very close to the liquidus temperatures of the corresponding $AlCl_3$-$BaCl_2$-NaCl samples, and therefore to the liquidus temperatures of the binary $AlCl_3$-NaCl system at the same mole fraction of $AlCl_3$. Perhaps not unexpectedly, $CaCl_2$ and $BaCl_2$ have qualitatively the same effect on the $AlCl_3$-NaCl system. In short, the effect of $CaCl_2$ is not spectacular, and it does not seem very useful to pursue further measurements on this system.

3.5 $AlCl_3$-NaBr System

The addition of LiCl significantly lowers the liquidus temperatures of the binary $AlCl_3$-NaCl system. The $AlCl_3$-NaBr system was studied in order to determine the effect of the second halide ion, Br^-, on the $AlCl_3$-NaCl system. The $AlCl_3$-NaBr system is a subsystem of a more complex $AlCl_3$-$AlBr_3$-NaCl-NaBr system. The latter is still only a ternary system, since its four components are related by the equilibrium

$$AlCl_3 + 3NaBr = AlBr_3 + 3NaCl \qquad (3)$$

and its nominal composition can be expressed in terms of only three of its components. Therefore, the mole percentages of only one cation and one anion are sufficient to define the total nominal composition of the system. The literature data for the mixed chloride-bromide systems are not available.

Our phase diagram data for the $AlCl_3$-NaBr system are listed in Table 19 and the phase diagram based on these data is shown in Figure 9. The literature phase diagrams for the $AlCl_3$-NaCl system (15) and the $AlBr_3$-NaBr system (15) are also shown in this figure. The solidus temperature of the $AlCl_3$-NaBr system is a function of the composition. It gradually decreases from 86°C at 28 mole % NaBr to 72°C at 48 mole % NaBr. This effect is possibly due to the exchange of the Cl^- and Br^- ions in the haloaluminate species:

$$AlCl_4^- + Br^- = AlCl_3Br^- + Cl^- \qquad (4)$$

The liquidus curve of the $AlCl_3$-$NaBr_3$ system strongly resembles the $AlCl_3$-NaCl liquidus curve. Both have only one eutectic point in the low melting composition region, the $AlCl_3$-NaBr system at ca. 62 mole % $AlCl_3$, which is very close to the composition of the $AlCl_3$-NaCl eutectic of 61.4 mole %

TABLE 18

PHASE DIAGRAM DATA FOR $AlCl_3$-$CaCl_2$-NaCl SYSTEM

Composition (Mole %)			Solidus Temperature (°C)	Liquidus Temperature (°C)
$AlCl_3$	$CaCl_2$	NaCl		
56.0	3.7	40.3	108	136
60.0	3.3	36.7	108	121
64.0	3.0	33.0	107	137.5

TABLE 19

PHASE DIAGRAM DATA FOR $AlCl_3$-NaBr SYSTEMS

Composition (Mole %)		Solidus Temperature (°C)	Liquidus Temperature (°C)
AlCl3	NaBr		
52.0	48.0	72	127
56.0	44.0	80	117.5
60.0	40.0	80	100
64.0	36.0	83	112
68.0	32.0	85	146
72.0	28.0	86	165

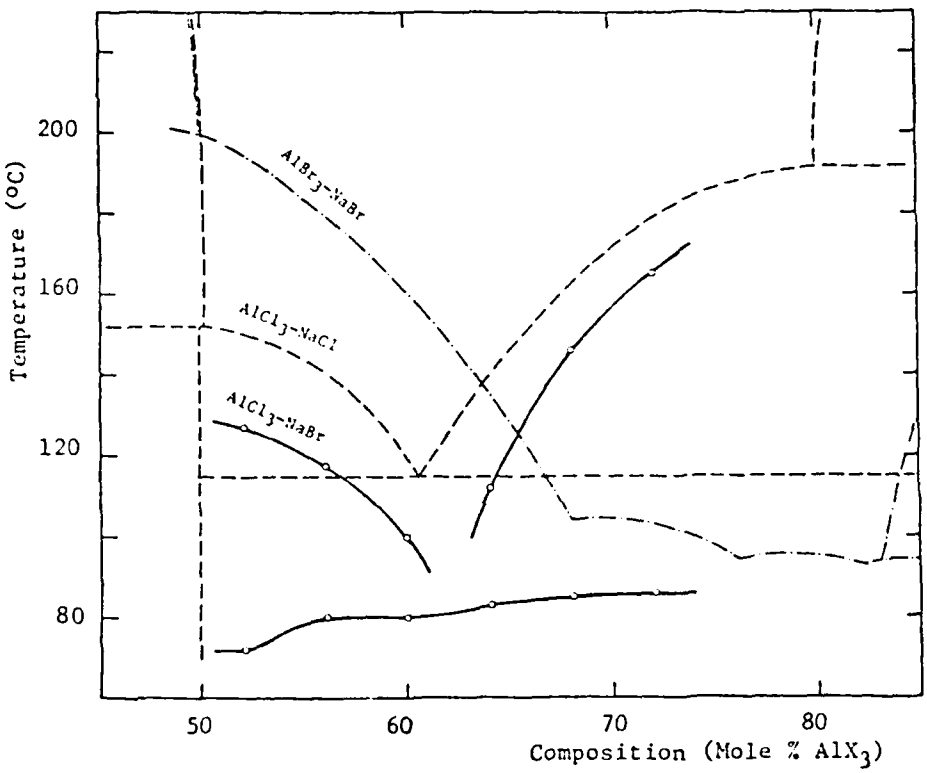

Figure 9. Phase Diagrams of $AlCl_3$-NaBr, $AlCl_3$-NaCl and $AlBr_3$-NaBr Systems.

$AlCl_3$. On the other hand, the $AlBr_3$-NaBr system has three minima at ca. 68, 78 and 81 mole % $AlBr_3$ due to the existence of several compounds stable in the solid phase. Phase diagrams of the other alkali bromide-aluminum bromide systems also exhibit at least two minima (24,25). The liquidus temperatures in the $AlCl_3$-NaBr system are lower than in the $AlCl_3$-NaCl system by as much as 32°C. Thus the effect of the Br^- ion is significant.

Our specific conductivity data for this system are listed in Tables 20 to 23, and shown in Figure 10. These conductivity vs. temperature plots are quite similar to the conductivity plots for the $AlCl_3$-LiCl-NaCl system which are also shown in the same figure. The difference in the specific conductivities of the two systems is within 7% for the 52.0 mole % $AlCl_3$ melts, and within 3% for the others. The specific conductivity of the pure bromide system, $AlBr_3$-NaBr, however, is lower than the conductivity of the $AlCl_3$-NaCl system by nearly an order of magnitude (26).

Data on the electrochemical span in the mixed chloride-bromide melts are available in literature. The bromine evolution potential has been reported as +1.61 V relative to the Al(III)/Al(0) reference potential (27), which should be compared to +2.09 V for the chlorine evolution potential in the $AlCl_3$-NaCl system. The data for the $AlCl_3$-NaBr-KBr melts show a potential of 1.71 V (27), which has been attributed to the mixed chlorine-bromine evolution. Thus the reduction of the electrochemical span in the mixed chloride-bromide systems amounts to 0.4 to 0.5 V.

Based on the liquidus temperature and specific conductivity data, the system $AlCl_3$-NaBr is quite comparable to the $AlCl_3$-LiCl-NaCl system. However, the electrochemical span in the $AlCl_3$-NaBr system is 0.4 to 0.5 V smaller than in the $AlCl_3$-NaCl system. From the battery use standpoint, this loss in the electrochemical span is not justified. About the same lowering of the liquidus temperatures of the $AlCl_3$-NaCl system can be accomplished by introducing LiCl as a third component, without paying any penalty in the electrochemical span.

3.6 $AlBr_3$-NaCl System

Our phase diagram data for the $AlBr_3$-NaCl system, the second subsystem of the $AlCl_3$-$AlBr_3$-NaCl-NaBr system, are listed in Table 24 and shown in Figure 11. The similarity of our phase diagram data with the phase diagram of the corresponding pure bromide system $AlBr_3$-NaBr, which is also shown in Figure 11, is obvious. The lowering of the liquidus temperature of the pure

TABLE 20

SPECIFIC CONDUCTIVITY DATA FOR $AlCl_3$-NaBr SYSTEM AT 1.0 KHz

COMPOSITION: 52.0-48.0 (Mole %)

Temperature (°C)	Specific Conductivity ($ohm^{-1} cm^{-1}$)
130.0	0.2386*
140.0	0.2654*
150.0	0.2919*
158.4	0.3147
169.3	0.3423
180.4	0.3703
190.8	0.3963
200.6	0.4207
210.1	0.4442
220.4	0.4698
229.4	0.4919
240.8	0.5186
250.9	0.5425
260.6	0.5660
269.4	0.5861
279.9	0.6095
290.2	0.6318
300.2	0.6530

* Calculated from Eqn. 2.

TABLE 21

SPECIFIC CONDUCTIVITY DATA FOR $AlCl_3$-NaBr SYSTEM AT 1.0 KHz

COMPOSITION: 60.0-40.0 (Mole %)

Temperature (°C)	Specific Conductivity ($ohm^{-1} cm^{-1}$)
110.3	0.1275
120.2	0.1440
131.5	0.1634
141.0	0.1797
150.0	0.1955*
160.4	0.2134
171.4	0.2325
181.2	0.2499
190.0	0.2652
200.3	0.2834
210.2	0.3009
220.1	0.3183
230.4	0.3363
240.7	0.3544
250.3	0.3712

* Calculated from Eqn. 2.

TABLE 22

SPECIFIC CONDUCTIVITY DATA FOR $AlCl_3$-NaBr SYSTEM AT 1.0 KHz

COMPOSITION: 64.0-36.0 (Mole %)

Temperature (°C)	Specific Conductivity ($ohm^{-1} cm^{-1}$)
120.0	0.1206*
130.4	0.1364
139.6	0.1498
150.9	0.1665
160.3	0.1808
170.0	0.1954
179.9	0.2104
189.9	0.2254
200.0	0.2410
209.6	0.2560
220.2	0.2722
230.0	0.2868
240.0	0.3024
249.8	0.3172

* Calculated from Eqn. 2.

TABLE 23

SPECIFIC CONDUCTIVITY DATA FOR $AlCl_3$-NaBr SYSTEM AT 1.0 KHz

COMPOSITION: 68.0-32.0 (Mole %)

Temperature (°C)	Specific Conductivity ($ohm^{-1}cm^{-1}$)
169.7	0.1624
177.8	0.1727
188.8	0.1868
198.1	0.1988
208.5	0.2124
217.7	0.2250
229.4	0.2400
239.1	0.2532
250.6	0.2686

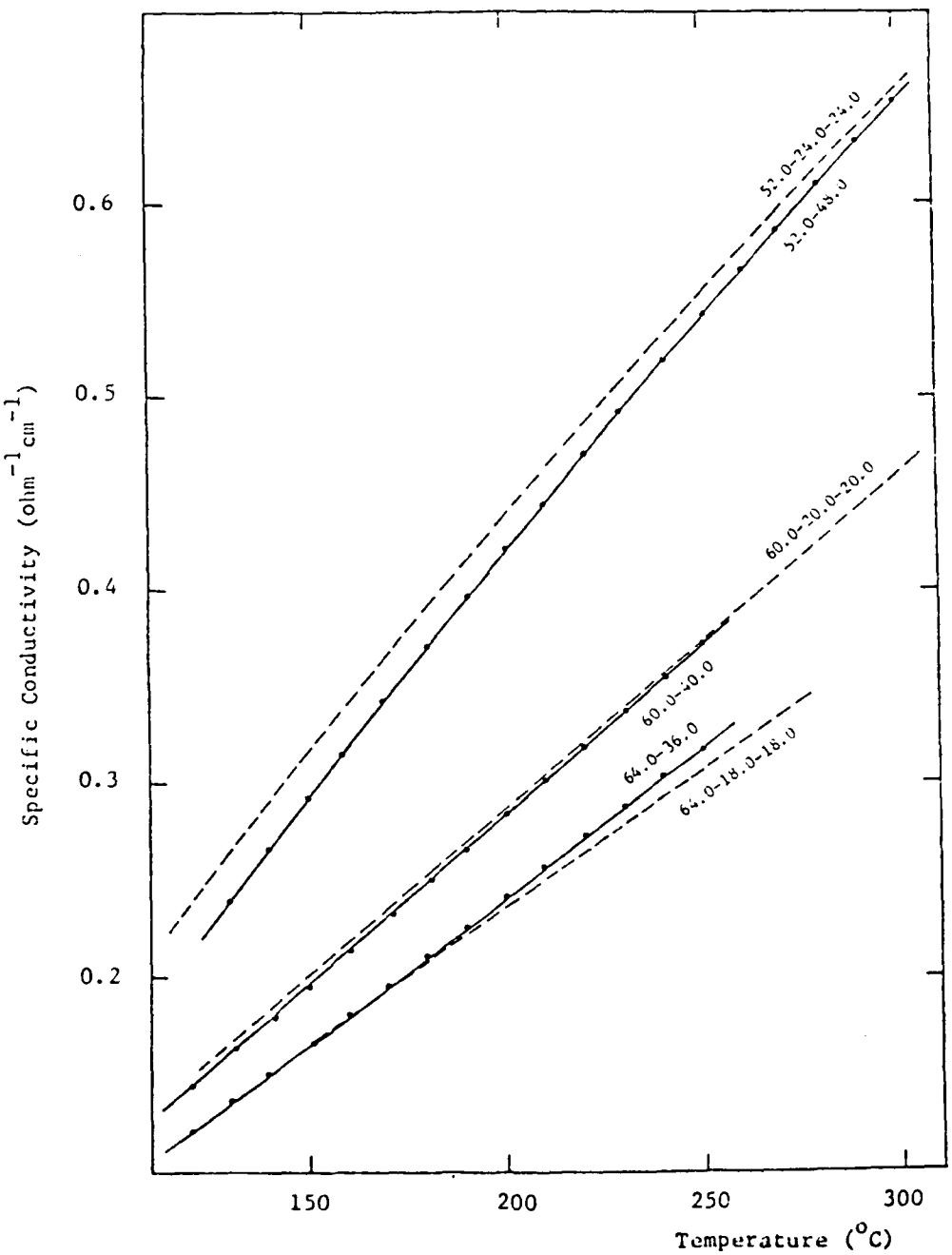

Figure 10. Specific Conductivity of $AlCl_3$-NaBr System (Full Line) and $AlCl_3$-LiCl-NaCl System (Dashed Line). Composition in mole % is indicated on the curves.

TABLE 24

PHASE DIAGRAM DATA FOR $AlBr_3$-NaCl SYSTEM

Composition (Mole %)		Solidus Temperature (°C)	Liquidus Temperature (°C)
$AlBr_3$	NaCl		
52.0	48.0	83	168
56.0	44.0	89	155
60.0	40.0	95	138
64.0	36.0	?	114
68.0	32.0	81	97
72.0	28.0	82	94

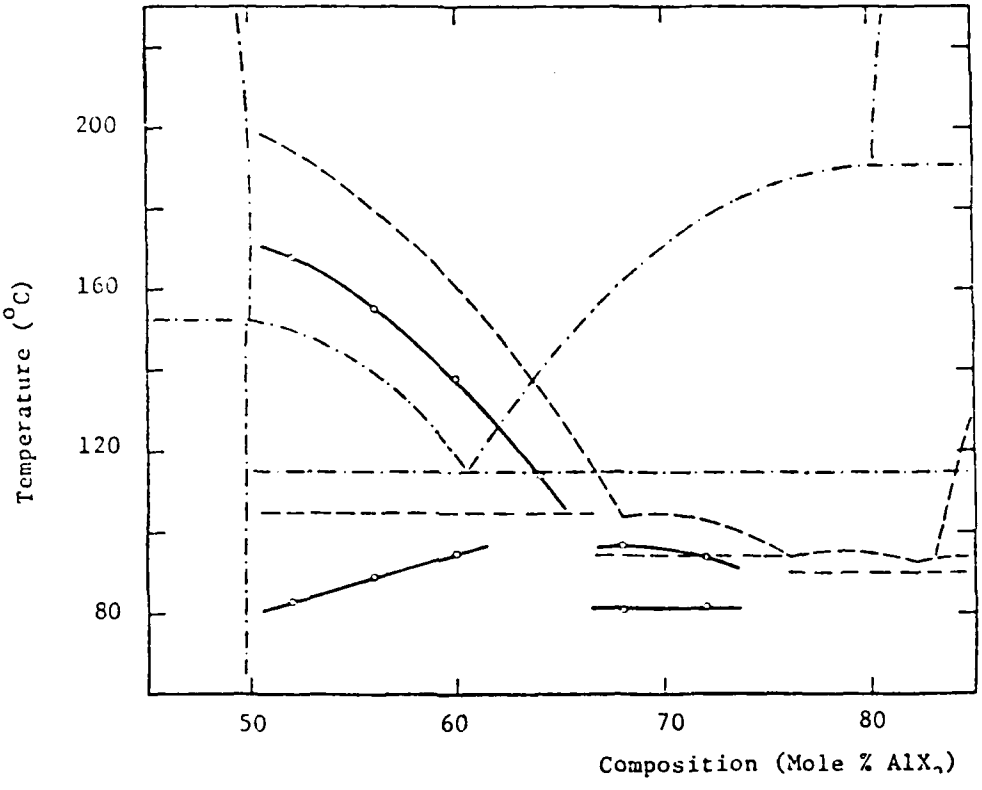

Figure 11. Phase Diagram Data for the $AlBr_3$-NaCl System. The phase diagrams of $AlBr_3$-NaBr system (dashed line) and $AlCl_3$-NaCl system (dot-dash line) are shown for reference.

bromide system by the addition of NaCl is only 7 to 10°C in the $AlBr_3$-rich composition region, and as much as 25°C in the region with less than 60 mole % $AlBr_3$. In that region, however, the liquidus temperatures of the $AlBr_3$-NaCl system are still above the liquidus temperatures of the $AlCl_3$-NaBr system. The bromide species, being in large excess, determine the shape of the phase diagram of the $AlBr_3$-NaCl system. The measured liquidus temperatures in this system are as low as 94°C, but the eutectic temperature is outside the studied composition region ($\geq$ 72 mole % $AlBr_3$).

Our specific conductivity data for the $AlBr_3$-NaCl system are listed in Tables 25 to 28 and shown in Figure 12. The conductivity *vs.* temperature plots are nearly linear and similar to the conductivity plots for the $AlCl_3$-LiCl-NaCl system, which are also shown in Figure 12. The values of the specific conductivity of the $AlBr_3$-NaCl melts, however, are considerably lower (*ca.* 20% for the 52.0-48.0 mole % melt, and up to 30% at 68.0 mole % $AlBr_3$).

In summary, the low melting region of the $AlBr_3$-NaCl system is shifted towards highly acidic compositions, so that the liquidus temperatures below 62 mole % $AlBr_3$ are actually higher than in the $AlCl_3$-NaCl system. The specific conductivity of the $AlBr_3$-NaCl system is 20 to 30% lower than in the $AlCl_3$-LiCl-NaCl system. Based on these data, the $AlBr_3$-NaCl system does not seem to offer much promise for the battery use.

3.7 $AlBr_3$-Bu_4NBr System

The low melting points of quaternary ammonium halides compared to alkali halides (74-420°C range, except for the tetramethyl and tetraethyl bromides which decompose before melting) as well as the chemical stability of their cations, give rise to expectations that the aluminum halide-quaternary ammonium halide molten salt systems may be low melting solvents of considerable promise for the battery applications. The quaternary ammonium cations, being basic, as well as chemically very stable due to the saturated character of their bonding, have similarities with the alkali cations. However, the large ionic radii of the quaternary ammonium cations introduce a new factor in the structure of their haloaluminates, and thus influence the physical and chemical properties, such as the viscosity, diffusion and electrical conductivity, of the quaternary ammonium haloaluminate melts. Also, the expected structural differences in the solid phase, due to the size of their cations, make it difficult to predict the shape of their phase diagrams. The aluminum

TABLE 25

SPECIFIC CONDUCTIVITY DATA FOR $AlBr_3$-NaCl SYSTEM AT 1.0 KHz

COMPOSITION: 52.0-48.0 (Mole %)

Temperature (°C)	Specific Conductivity ($ohm^{-1} cm^{-1}$)
188.6	0.3189
198.4	0.3408
290.4	0.3637
218.9	0.3848
228.9	0.4065
238.9	0.4281
249.5	0.4507
259.6	0.4718
270.7	0.4947
280.2	0.5141
290.6	0.5346
299.5	0.5521

TABLE 26

SPECIFIC CONDUCTIVITY DATA FOR $AlBr_3$-NaCl SYSTEM AT 1.0 KHz

COMPOSITION: 56.0-44.0 (Mole %)

Temperature (°C)	Specific Conductivity ($ohm^{-1}cm^{-1}$)
177.6	0.2318
189.2	0.2532
199.8	0.2729
208.5	0.2887
219.0	0.3079
229.8	0.3277
239.6	0.3456
249.6	0.3634

TABLE 27

SPECIFIC CONDUCTIVITY DATA FOR $AlBr_3$-NaCl SYSTEM AT 1.0 KHz

COMPOSITION: 64.0-36.0 (Mole %)

Temperature (°C)	Specific Conductivity ($ohm^{-1}cm^{-1}$)
137.7	0.09986
147.4	0.1115
158.8	0.1256
169.5	0.1389
178.9	0.1508
188.2	0.1626
198.7	0.1760
208.2	0.1882
219.7	0.2029
229.3	0.2157
238.7	0.2278
249.7	0.2421

TABLE 28

SPECIFIC CONDUCTIVITY DATA FOR $AlBr_3$-NaCl SYSTEM AT 1.0 KHz

COMPOSITION: 68.0-32.0 (Mole %)

Temperature (°C)	Specific Conductivity ($ohm^{-1} cm^{-1}$)
119.1	0.06191
130.9	0.07299
138.8	0.08052
149.5	0.09121
159.6	0.1014
171.0	0.1132
180.9	0.1234
189.7	0.1325
199.6	0.1428
209.9	0.1535
220.8	0.1653
229.8	0.1748
240.4	0.1862
250.3	0.1971

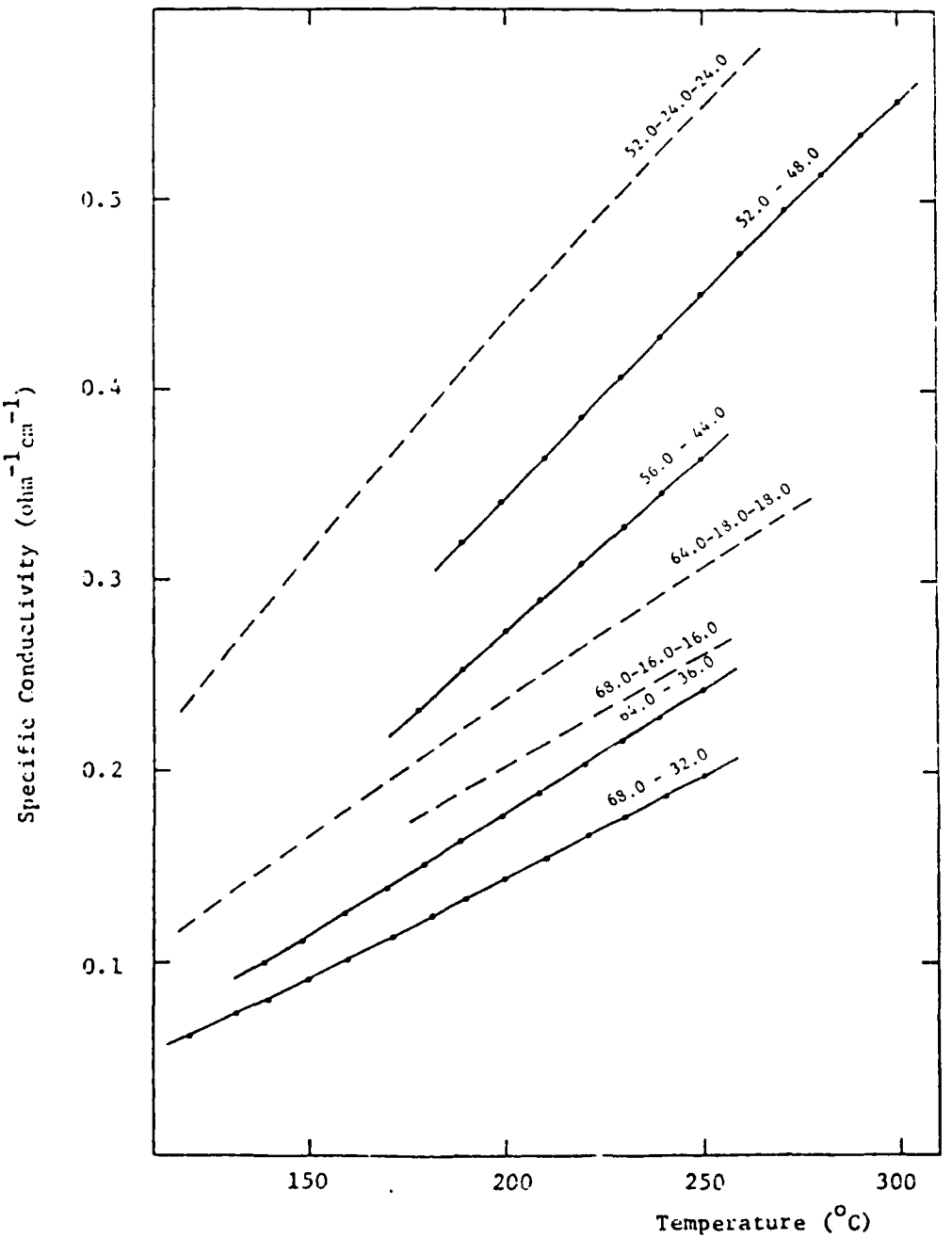

Figure 12. Specific Conductivity of $AlBr_3$-NaCl System (Full Line) and $AlCl_3$-LiCl-NaCl System (Dashed Line). Composition in mole % is indicated on the curves.

halide-quaternary ammonium halide molten salt systems have not been studied to date. Our studies were started with the aluminum bromide-quaternary ammonium bromide systems, since the quaternary ammonium chlorides are more difficult to prepare in the anhydrous form.

Based on the low melting point of the pure Bu_4NBr ($\geq$ 101°C) (28), the $AlBr_3$-Bu_4NBr system was expected to be a very low melting system. Our preliminary experiments indicated that the liquidus temperatures of the melts with more than 50 mole % Bu_4NBr were indeed below room temperature. Subsequent experiments have shown, however, that these melts were merely supercooled for unusually long periods of time (ca. 9 months for the 40.0-60.0 mole % melt, and ca. 1 year for the 30.0-70.0 mole % melt). The true liquidus temperature of these two melts is 111°C for the 40.0-60.0 mole % melt, and 89°C for the 30.0-60.0 mole % melt. The solidus temperature in the Bu_4NBr-rich composition region is 62°C. All the melts appear to be thermally stable below ca. 140°C, since no sign of decomposition was observed for at least 20 days at this temperature.

Our specific conductivity data for the $AlBr_3$-Bu_4NBr system are listed in Tables 29 to 34 and shown in Figure 13. The conductivity of these melts, less than 0.03 $ohm^{-1}cm^{-1}$ at 220°C, is quite low. In view of the high viscosity of these melts, however, and of the large size of the Bu_4N^+ cation, which is presumably the conducting species in these melts, such low specific conductivity seems to be reasonable. The conductivity vs. temperature plots exhibit a very pronounced curvature. With the exception of the 30.0-70.0 mole % melt, the conductivity at a given temperature has little dependence on the composition of the melt.

In summary, even though the liquidus temperatures in the $AlBr_3$-Bu_4NBr melts are quite low ($\geq$ 62°C), their very low specific conductivity, as well as their electrochemical span, smaller by 0.4 to 0.5 V than in the chloride melts, severely limit the potential usefulness of these melts for battery applications.

3.8 $AlBr_3$-Me_4NBr System

In view of the smaller size of the Me_4N^+ ion compared to the Bu_4N^+ ion, the $AlBr_3$-Me_4NBr system is probably the more interesting of the two bromide systems. The solidus temperature in the $AlBr_3$ rich composition region of the $AlBr_3$-Me_4NBr system is in the 70-80°C range. Due to the severe supercooling of these melts, similar to the supercooling of the $AlBr_3$-Bu_4NBr system, we do

TABLE 29

SPECIFIC CONDUCTIVITY DATA FOR $AlBr_3$-Bu_4NBr SYSTEM AT 1.0 KHz

COMPOSITION: 30.0-70.0 (Mole %)

Temperature (°C)	Specific Conductivity ($ohm^{-1}cm^{-1}$)
95.4	0.001238
105.1	0.001736
114.3	0.002328
125.2	0.003190
135.5	0.004159
144.8	0.005252
154.2	0.006587
164.8	0.008356
172.8	0.010221
182.9	0.012342
195.0	0.015118
205.3	0.017712
214.9	0.020414

TABLE 30

SPECIFIC CONDUCTIVITY DATA FOR $AlBr_3$-Bu_4NBr SYSTEM AT 1.0 KHz

COMPOSITION: 40.0-60.0 (Mole %)

Temperature (°C)	Specific Conductivity ($ohm^{-1} cm^{-1}$)
127.1	0.006026
137.9	0.007592
147.2	0.009165
157.6	0.011114
167.6	0.013130
176.5	0.015143
186.8	0.017667
196.0	0.020560

TABLE 31

SPECIFIC CONDUCTIVITY DATA FOR $AlBr_3$-Bu_4NBr SYSTEM AT 1.0 KHz

COMPOSITION: 50.0-50.0 (Mole %)

Temperature (°C)	Specific Conductivity ($ohm^{-1} cm^{-1}$)
152.1	0.01049
161.2	0.01235
171.2	0.01448
180.4	0.01669
189.2	0.01883
198.6	0.02136
209.1	0.02427
218.6	0.02696

TABLE 32

SPECIFIC CONDUCTIVITY DATA FOR $AlBr_3$-Bu_4NBr SYSTEM AT 1.0 KHz

COMPOSITION: 60.0-40.0 (Mole %)

Temperature (°C)	Specific Conductivity ($ohm^{-1} cm^{-1}$)
113.9	0.004614
118.6	0.005142
122.7	0.005609
128.4	0.006297
135.2	0.007195
145.2	0.008585
154.2	0.009871
163.3	0.01152
172.4	0.01312

TABLE 33

SPECIFIC CONDUCTIVITY DATA FOR $AlBr_3$-Bu_4NBr SYSTEM AT 1.0 KHz

COMPOSITION: 64.0-36.0 (Mole %)

Temperature (°C)	Specific Conductivity ($ohm^{-1}cm^{-1}$)
99.2	0.003440
110.5	0.004499
118.6	0.005361
129.3	0.006654
139.4	0.007970
150.0	0.009484
160.4	0.01112
171.1	0.01291
181.6	0.01478
193.5	0.01704
200.6	0.01843
209.4	0.02022
219.0	0.02223

TABLE 34

SPECIFIC CONDUCTIVITY DATA FOR $AlBr_3$-Bu_4NBr SYSTEM AT 1.0 KHz

COMPOSITION: 68.0-32.0 (Mole %)

Temperature (°C)	Specific Conductivity ($ohm^{-1} cm^{-1}$)
85.0	0.002423
92.5	0.002966
102.2	0.003758
112.3	0.004685
122.5	0.005743
133.8	0.007053
144.8	0.008438
157.7	0.01024
169.5	0.01206
178.5	0.01351
192.2	0.01585
203.9	0.01796
212.6	0.01958
219.6	0.02092

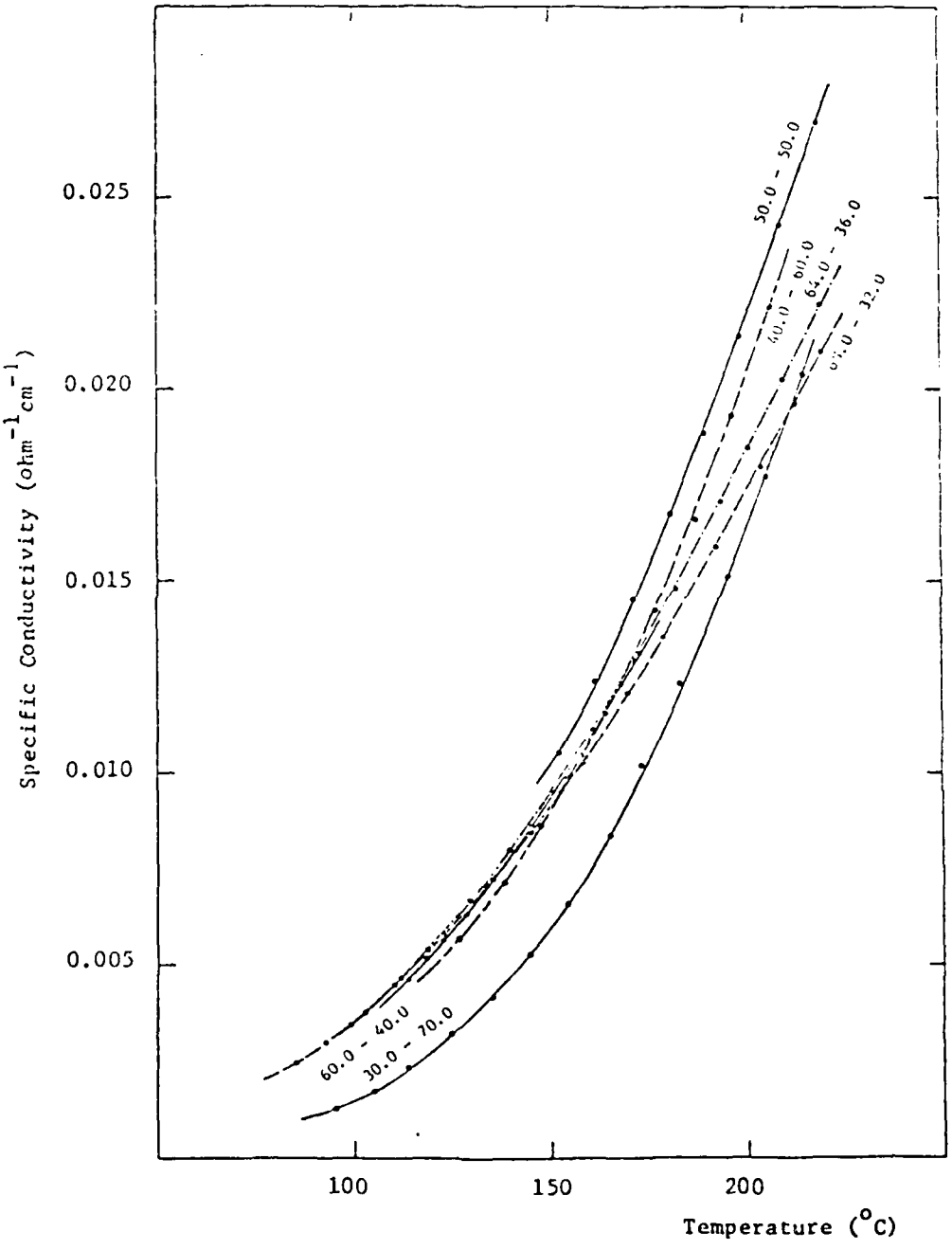

Figure 13. Specific Conductivity of $AlBr_3$-Bu_4NBr System. Composition in mole % is indicated on the curves.

not have liquidus temperature data for this composition region. The melts with less than 50 mole % $AlBr_3$, however, do not reach their liquidus temperature even at 230°C (the decomposition temperature of pure Me_4NBr (29)), at which temperature they also decompose. This is an important difference between the two quaternary ammonium bromide systems. The $AlBr_3$-Me_4NBr melts are, however, also thermally stable below ca. 130-140°C for extended periods of time.

Our specific conductivity data for the 70.0-30.0 mole % $AlBr_3$-Me_4NBr melt are listed in Table 35 and shown in Figure 14. These conductivity data are ca. 70% higher than the values for the 68.0-32.0 mole % $AlBr_3$-Bu_4NBr melt at the same temperature. This higher conductivity is presumably due to the smaller size and consequently higher mobility of the Me_4N^+ cation compared to the Bu_4N^+ cation. The conductivity of the $AlCl_3$-Me_4NBr melt, however, is still too low to justify a further study of this system.

3.9 $AlCl_3$-Bu_4NCl System

Our phase diagram data for the $AlCl_3$-Bu_4NCl system, the first of the quaternary ammonium chloride systems studied, are listed in Table 36 and the phase diagram based on these data is shown in Figure 15. This diagram exhibits a maximum at 50 mole % $AlCl_3$ due to the formation of the 1:1 compound Bu_4NAlCl_4. The melting point of this compound is 125-130°C. The existence of this compound is in agreement with the general pattern of the formation of 1:1 compounds in the inorganic aluminum chloride-alkali chloride systems. The maximum in the liquidus curve divides the phase diagram into two composition regions, each with one eutectic.

The solidus temperature in the low $AlCl_3$ composition region is in the 35-38°C range. These melts appear to be very viscous and readily supercool to low temperatures; it is difficult to establish with certainty their solidus temperatature. The 30.0-70.0 mole % melt appears to not solidify completely in our experiments. The eutectic composition in this region is probably located between 35 and 40 mole % $AlCl_3$.

The solidus temperature in the high $AlCl_3$ composition region also has a very low value of 40.5°C. These melts seem to be considerably less viscous and supercool less extensively than the melts with the low $AlCl_3$ content. Therefore the phase transitions in this composition region are identified with relative ease. The eutectic composition is between 64 and 68 mole % $AlCl_3$.

TABLE 35

SPECIFIC CONDUCTIVITY DATA FOR $AlBr_3$-Me_4NBr SYSTEM AT 1.0 KHz

COMPOSITION: 70.0-30.0 (Mole %)

Temperature (°C)	Specific Conductivity ($ohm^{-1}cm^{-1}$)
108.4	0.00728
118.3	0.00887
129.8	0.0110
144.8	0.0141
148.4	0.0150
167.3	0.0196
188.2	0.0254
208.0	0.0314
224.2	0.0367

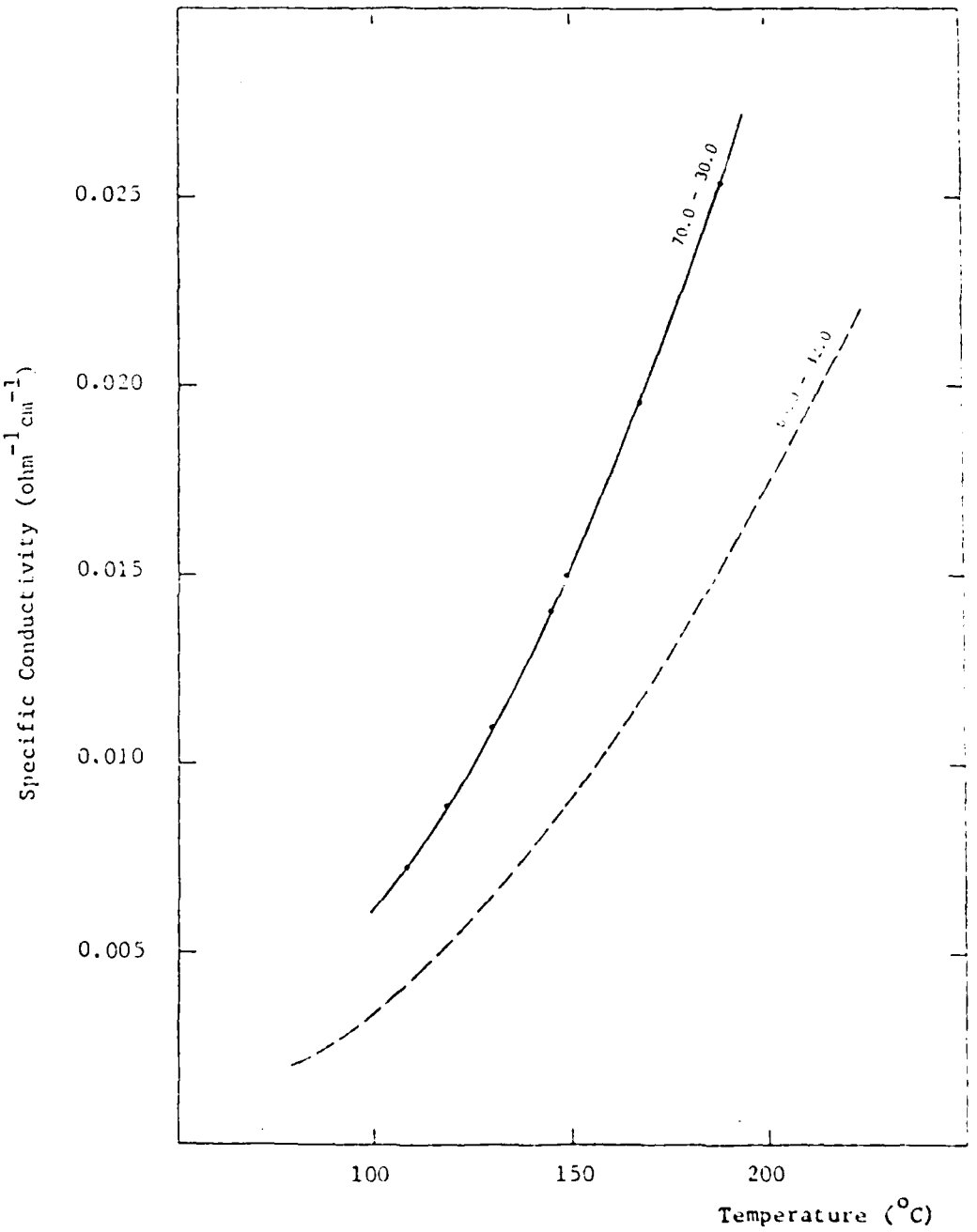

Figure 14. Specific Conductivity of $AlBr_3$–Me_4NBr 70.0–30.0 Mole % Melt (Full Line) and $AlBr_3$–Bu_4NBr 68.0–32.0 Mole % Melt (Dashed Line). Composition in mole % is indicated on the curves.

TABLE 36

PHASE DIAGRAM DATA FOR THE $AlCl_3$-Bu_4NCl SYSTEM

Composition (Mole %)		Solidus Temperature (°C)	Liquidus Temperature (°C)
$AlCl_3$	Bu_4NCl		
20.0	80.0	35	60
30.0	70.0	-	56
40.0	60.0	38	76.0
52.0	48.0	40.4	123.3
56.0	44.0	40.4	101.1
60.0	40.0	40.4	72.7
64.0	36.0	-	41.4
68.0	32.0	40.4	46.8

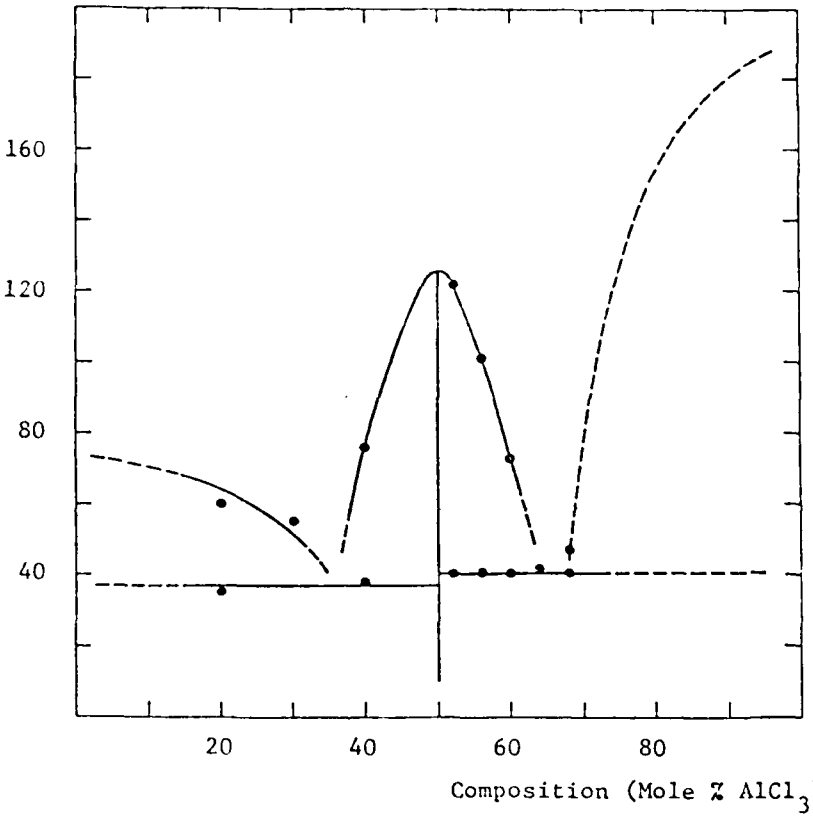

Figure 15. Phase Diagram of the $AlCl_3$-Bu_4NCl System.

The phase diagram shown in Figure 15 is tentative. More extensive data are required to pinpoint the details of the low melting regions and the region above 70 % $AlCl_3$, as well as to establish with more certainty the solidus temperature in the low $AlCl_3$ composition region.

The Bu_4NCl used to prepare the $AlCl_3$-Bu_4NCl melts for our phase diagram measurement (Eastman, dried under vacuum at ca. 70°C) was not of sufficient purity for the specific conductivity work. Recrystallization of commercial Bu_4NCl from various combinations of mixed solvents turned out to be difficult. We have prepared this salt by two different methods. In the first, the Bu_4NCl was prepared by titrating the aqueous solution of Bu_4NOH (Fluka, 40%), which is commercially available with better purity than Bu_4NCl, with HCl. This was followed by the vacuum evaporation of water. Since Bu_4NCl decomposes slowly at temperatures above ca. 80°C, the salt was maintained below this temperature during the vacuum drying, and the removal of the last residue of water was very slow. In the second method, the starting material, Bu_4NHSO_4 (Fluka, puriss 99%), was recrystallized from acetone, and the aqueous solution of the purified product was titrated with $BaCl_2$. The resulting Bu_4NCl solution was filtered, and water and HCl were removed by vacuum evaporation. The salt was finally dried under vacuum below 80°C, and the removal of the residual moisture was again very time consuming. The Bu_4NCl obtained by the second method appeared to be of higher purity than the salt prepared by the first method. Upon melting, it yielded a nearly colorless liquid. However, it was prepared too late to be used for the electrical conductivity measurements in view of the superior thermal stability of Me_4NCl compared to Bu_4NCl, as well as the very limited amount of time left until the end of this project, it was decided to initiate the study of the $AlCl_3$-Me_4NCl molten salt system instead of continuing the work on the $AlCl_3$-Bu_4NCl system.

3.10 $AlCl_3$-Me_4NCl System

In contrast to Bu_4NCl, Me_4NCl starts thermally decomposing only above 320°C (29). It is also commercially available with reasonably high purity, and is easy to prepare in a dry form. The Me_4NCl used for our study (Eastman) did not require further purification beyond drying under vacuum at 110°C for 14 days. The above advantages, however, were expected to be partially offset by the high melting point of Me_4NCl (420°C (29)), and, as a consequence, higher liquidus temperatures in the $AlCl_3$-Me_4NCl system than in the $AlCl_3$-Bu_4NCl system.

The results of our liquidus range measurements on the $AlCl_3$-Me_4NCl system are listed in Table 37. The liquidus temperatures in the composition region with up to 60 mole % $AlCl_3$ are unexpectedly high (>185°C). This temperature should be compared to the values below 130°C for the corresponding composition region of the $AlCl_3$-Bu_4NCl system. The eutectic composition in the $AlCl_3$ rich region of the $AlCl_3$-Me_4NCl system is probably close to 67 mole % $AlCl_3$. The solidus temperature, however, is difficult to establish. The presence of the liquid phase in equilibrium with the solid phase in the 64.0-36.0 mole % $AlCl_3$-Me_4NCl composition at the room temperature indicates that the solidus temperature in this composition region is below the room temperature. However, we do not have sufficient data to determine the solidus temperature with certainty.

Although our initial results for the $AlCl_3$-Me_4NCl system were very promising, no further measurements on this system were performed due to the lack of time.

3.11 $AlCl_3$-Me_4NCl-NaCl System

NaCl is a necessary constituent of an $AlCl_3$-Me_4NCl based melt if it is to be used as a solvent in a battery which employs β-alumina or any other Na^+ solid separator. Thus the study of the $AlCl_3$-Me_4NCl-NaCl system is a natural extension of our study of the $AlCl_3$-Me_4NCl system.

Our liquidus data for the $AlCl_3$-Me_4NCl-NaCl system are listed in Table 38 and shown in Figure 16. This figure also shows the liquidus data from Table 37 for the binary $AlCl_3$-Me_4NCl system, which is a subsystem of the ternary $AlCl_3$-Me_4NCl-NaCl system. The liquidus temperatures in these two systems are roughly comparable. The eutectic composition in the ternary system, however, appears to be shifted towards the lower mole fraction of $AlCl_3$. For example, the liquidus temperature of the 60.0-30.0-10.0 mole % $AlCl_3$-Me_4NCl-NaCl melt (116°C), is considerably lower than the liquidus temperature of the 60.0-40.0 mole % $AlCl_3$-Me_4NCl melt (>185°C). The solidus temperature of the $AlCl_3$-Me_4NCl-NaCl system could not be established in our measurements. It is expected, however, to be close to the solidus temperature of the $AlCl_3$-Me_4NCl melts. Our data are insufficient for determining the location of the ternary eutectic.

The $AlCl_3$-Me_4NCl-NaCl melts appear to be quite promising for use as battery solvents. The addition of NaCl to the $AlCl_3$-Me_4NCl melts is expected to have a favorable effect on their electrical conductivity. Such data,

TABLE 37
PHASE DIAGRAM DATA FOR THE $AlCl_3$-Me_4NCl SYSTEM

Composition (Mole %)		Liquidus Temperature (°C)
$AlCl_3$	Me_4NCl	
52.0	48.0	>185
56.0	44.0	>185
60.0	40.0	>185
64.0	36.0	141.5
68.0	32.0	96

TABLE 38

PHASE DIAGRAM DATA FOR THE $AlCl_3$-Me_4NCl-NaCl SYSTEM

Composition (Mole %)			Liquidus Temperature (°C)
$AlCl_3$	Me_4NCl	NaCl	
52.0	30.0	18.0	215
56.0	30.0	14.0	141
60.0	30.0	10.0	116

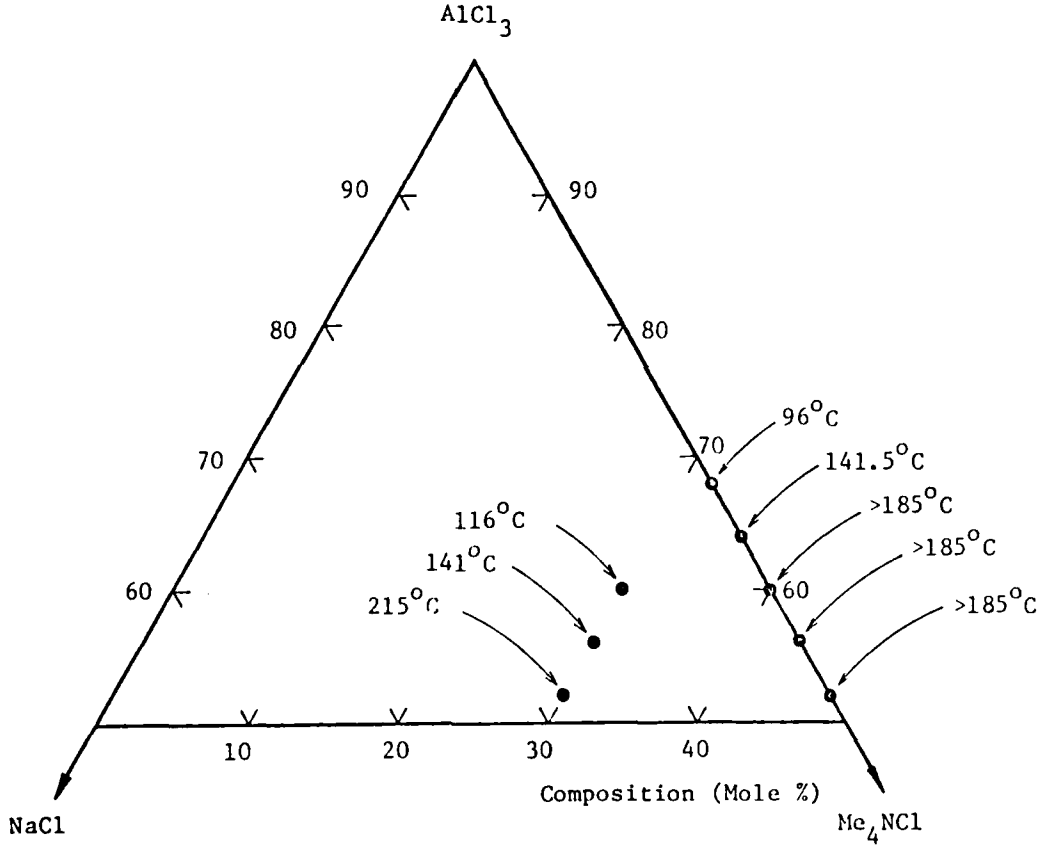

Figure 16. Liquidus Temperature Data for the $AlCl_3$-Me_4NCl-NaCl System.

however, are available for none of these systems. Due to the lack of time, our study of the $AlCl_3$-Me_4NCl-NaCl system, the last molten salt system to be studied in this project, had to be terminated.

3.12 $AlCl_3$-$SbCl_3$ System

The phase diagram of the $AlCl_3$-$SbCl_3$ system, based on the data of Kendall *et al.*, (15) and Niselsen *et al.*, (30) is shown in Figure 17. The eutectic temperature in this system is 70°C, and the eutectic composition is ~10 mole % $AlCl_3$. Since $SbCl_3$ is a weaker acid than $AlCl_3$, an acid-base equilibrium is expected to take place in their binary melts:

$$2SbCl_3 + Al_2Cl_6 \rightleftarrows 2SbCl_2^+ + 2AlCl_4^- \qquad (5)$$

The vapor pressure data for the $AlCl_3$-$SbCl_3$ melts indeed show a negative deviation from the additivity, and this deviation is most pronounced at the 1:1 $AlCl_3$-$SbCl_3$ mole ratio (30). However, the phase diagram of this system (Figure 17), gives no indication of the formation of a compound in the solid phase. Moreover, the Raman studies show no evidence for the presence of the $AlCl_4^-$ or $Al_2Cl_7^-$ ions in these melts (31). Since the molten pure $AlCl_3$ and $SbCl_3$ are both nonconducting molecular liquids, the electrical conductivity of the $AlCl_3$-$SbCl_3$ melts is expected to be very low.

The results of our specific conductivity measurements on the $AlCl_3$-$SbCl_3$ melts, performed in the composition region from 2.5 to 60.0 mole % $AlCl_3$, are listed in Tables 39 to 49 and shown in Figures 18 and 19. Due to the high volatility of the 60.0-40.0 mole % melt even at temperatures close to its liquidus point, our measurements on this melt were not very reproducible. Therefore, no measurements were performed on melts with more than 60 mole % $AlCl_3$.

The relatively high specific conductivity of the $AlCl_3$-$SbCl_3$ melts of up to 0.1 ohm^{-1} cm^{-1} (*ca.* 20% of the conductivity of the $AlCl_3$-LiCl-NaCl melts) is quite surprising. The conductivity *vs.* temperature curves of melts with a low mole fraction of $AlCl_3$ exibit pronounced deviations from linearity. The conductivity curves for the melts with 10 mole % $AlCl_3$ or less pass through a maximum. The highest conductivity at constant temperature is observed at a composition between 30 and 40 mole % $AlCl_3$.

It is possible to interpret the observed temperature dependence of the specific conductivity of the $AlCl_3$-$SbCl_3$ melts in terms of the change of the equilibrium constant for the ionization reaction (5) with temperature. Thus

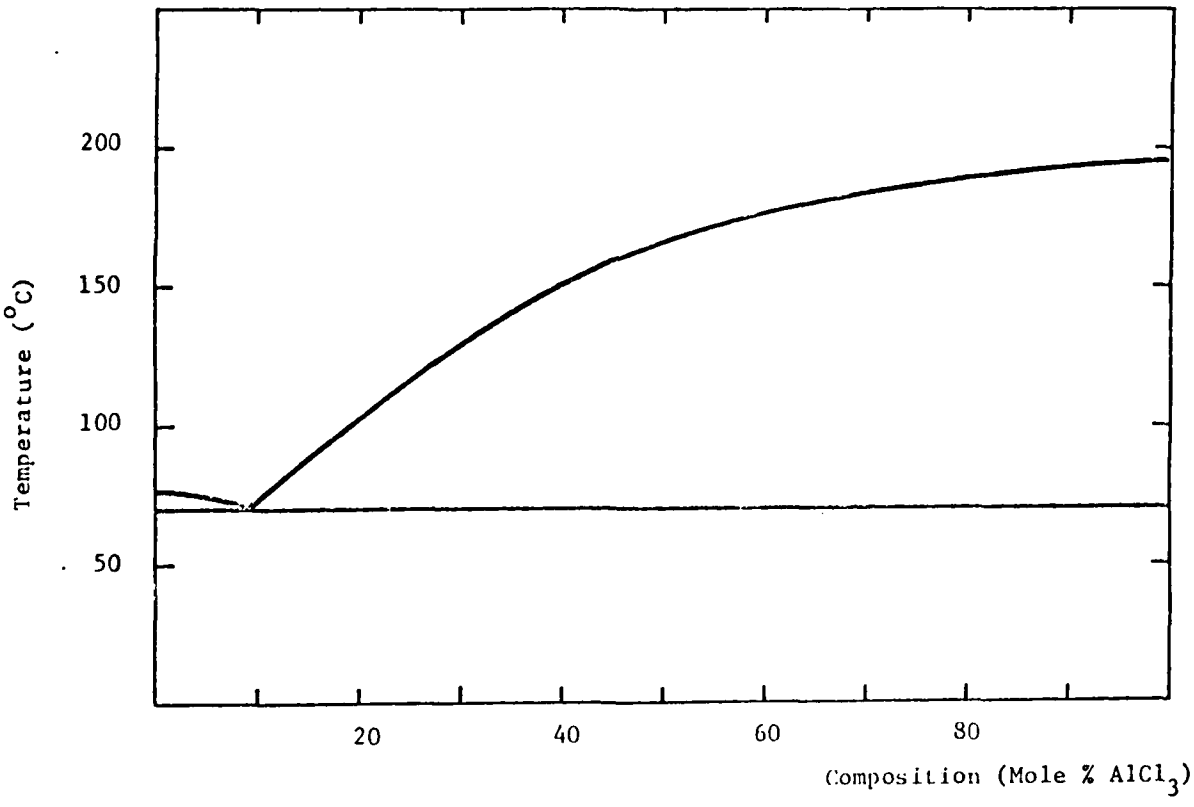

Figure 17. Phase Diagram of the $AlCl_3$-$SbCl_3$ System.

TABLE 39

SPECIFIC CONDUCTIVITY DATA FOR $AlCl_3$-$SbCl_3$ SYSTEM AT 1.0 KHz

COMPOSITION: 2.5-97.5 (Mole %)

Temperature (°C)	Specific Conductivity ($ohm^{-1} cm^{-1}$)
86.7	0.007845
95.6	0.008355
106.6	0.008919
116.6	0.009367
126.8	0.009750
134.9	0.010010
144.3	0.010255
154.6	0.010469
167.8	0.010638
178.0	0.010699
187.0	0.010708
200.2	0.010652
204.4	0.010601
212.9	0.010511
222.5	0.010364
231.3	0.010197

TABLE 40

SPECIFIC CONDUCTIVITY DATA FOR $AlCl_3$-$SbCl_3$ SYSTEM AT 1.0 KHz

COMPOSITION: 5.0-95.0 (Mole %)

Temperature (°C)	Specific Conductivity ($ohm^{-1}cm^{-1}$)
83.8	0.01399
93.1	0.01514
102.8	0.01623
113.2	0.01735
123.3	0.01825
134.0	0.01908
144.2	0.01974
154.1	0.02027
164.0	0.02071
173.8	0.02101
185.4	0.02122
193.3	0.02129
201.2	0.02133
206.5	0.02126
211.6	0.02120
217.6	0.02110
226.0	0.02089
232.0	0.02070

TABLE 41

SPECIFIC CONDUCTIVITY DATA FOR $AlCl_3$-$SbCl_3$ SYSTEM AT 1.0 KHz

COMPOSITION: 10.0-90.0 (Mole %)

Temperature (°C)	Specific Conductivity ($ohm^{-1}cm^{-1}$)
80.2	0.02326
90.0	0.02610
101.2	0.02864
109.9	0.03070
119.4	0.03276
129.2	0.03473
138.9	0.03646
148.7	0.03802
158.3	0.03938
167.6	0.04048
170.8	0.04090
180.1	0.04176
190.8	0.04252
199.8	0.04294
208.7	0.04320
218.9	0.04331
229.6	0.04320

TABLE 42

SPECIFIC CONDUCTIVITY DATA FOR $AlCl_3$-$SbCl_3$ SYSTEM AT 1.0 KHz

COMPOSITION: 15.0-85.0 (Mole %)

Temperature (°C)	Specific Conductivity ($ohm^{-1}cm^{-1}$)
108.8	0.03951
119.2	0.04306
128.8	0.04613
138.3	0.04891
147.8	0.05152
150.1	0.05214
157.0	0.05385
158.5	0.05415
170.2	0.05673
178.8	0.05837
190.0	0.06018
191.8	0.06051
200.0	0.06150
201.4	0.06171
210.8	0.06262
221.1	0.06329
230.2	0.06363
239.8	0.06370

TABLE 49

SPECIFIC CONDUCTIVITY DATA FOR $AlCl_3$-$SbCl_3$ SYSTEM AT 1.0 KHz

COMPOSITION: 60.0-40.0 (Mole %)

Temperature (°C)	Specific Conductivity ($ohm^{-1}cm^{-1}$)
193.3	0.06271
195.0	0.06344
202.0	0.06620
206.6	0.06747
211.6	0.06941
216.7	0.07125

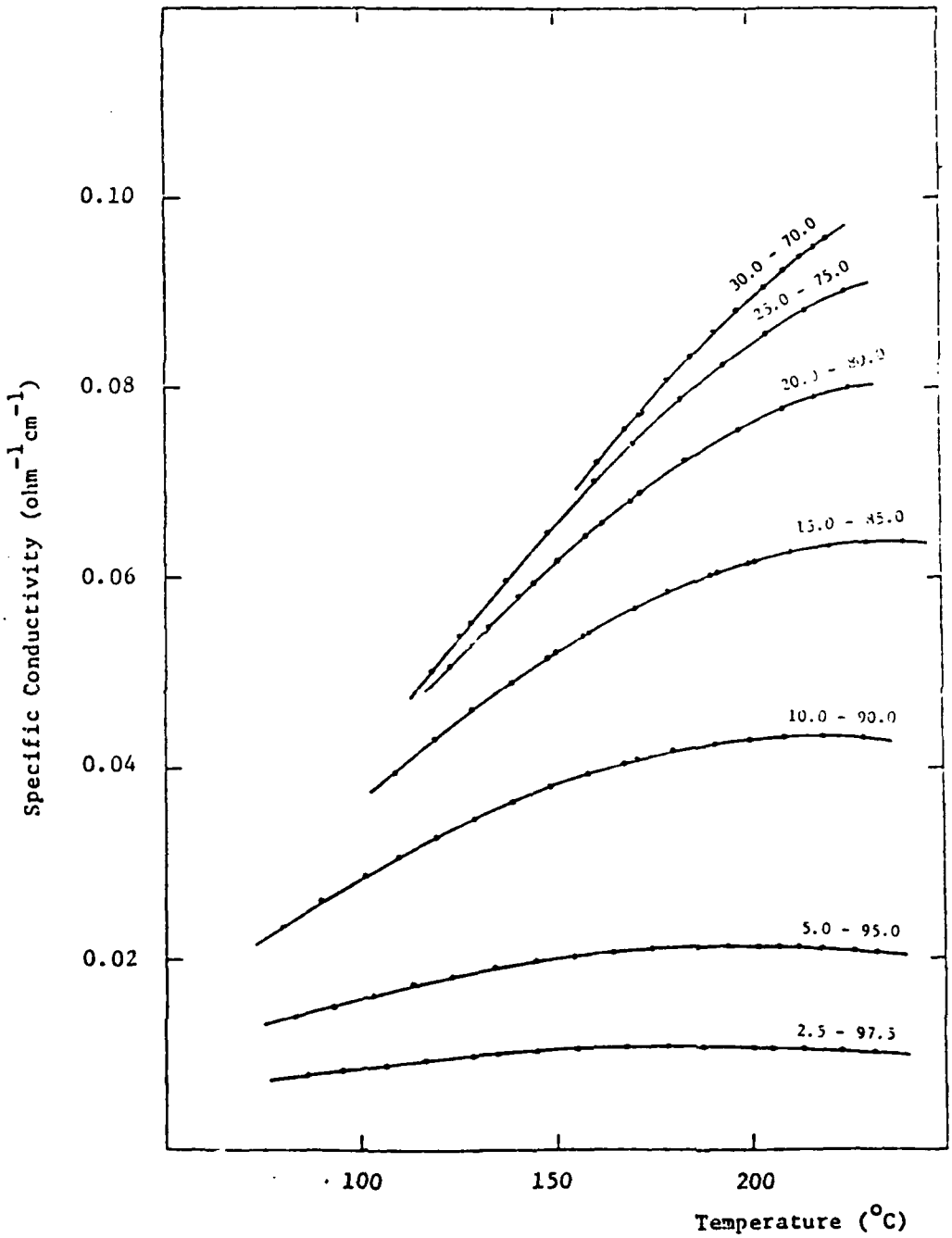

Figure 18. Specific Conductivity of $AlCl_3$-$SbCl_3$ System (Part 1). Composition in mole % is indicated on the curves.

TABLE 43

SPECIFIC CONDUCTIVITY DATA FOR $AlCl_3$-$SbCl_3$ SYSTEM AT 1.0 KHz

COMPOSITION: 20.0-80.0 (Mole %)

Temperature (°C)	Specific Conductivity ($ohm^{-1}cm^{-1}$)
123.0	0.05071
128.0	0.05285
132.2	0.05447
132.7	0.05480
140.5	0.05787
144.4	0.05942
150.8	0.06171
158.0	0.06430
162.0	0.06563
169.3	0.06801
172.1	0.06886
183.6	0.07223
197.4	0.07551
209.0	0.07771
217.3	0.07897
226.0	0.07998

TABLE 44

SPECIFIC CONDUCTIVITY DATA FOR $AlCl_3$-$SbCl_3$ SYSTEM AT 1.0 KHz

COMPOSITION: 25.0-75.0 (Mole %)

Temperature (°C)	Specific Conductivity ($ohm^{-1}cm^{-1}$)
125.5	0.05378
128.4	0.05527
137.5	0.05961
148.2	0.06461
160.4	0.07001
170.2	0.07407
182.4	0.07869
193.6	0.08242
204.6	0.08561
215.0	0.08815
225.1	0.09016

TABLE 45

SPECIFIC CONDUCTIVITY DATA FOR $AlCl_3$-$SbCl_3$ SYSTEM AT 1.0 KHz

COMPOSITION: 30.0-70.0 (Mole %)

Temperature (°C)	Specific Conductivity ($ohm^{-1}cm^{-1}$)
160.8	0.07205
168.2	0.07566
171.7	0.07728
172.4	0.07767
179.0	0.08067
184.8	0.08320
191.1	0.08579
197.1	0.08811
203.9	0.09058
209.2	0.09243
213.6	0.09382
217.0	0.09484
220.2	0.09575

AD-A131 330 EVALUATION OF LOW MELTING HALIDE SYSTEMS FOR BATTERY APPLICATIONS(U) TENNESSEE UNIV KNOXVILLE DEPT OF CHEMISTRY G MAMANTOV ET AL. APR 83 AFWAL-TR-83-2032 2/2

UNCLASSIFIED F33615-78-C-2075 F/G 10/3 NL

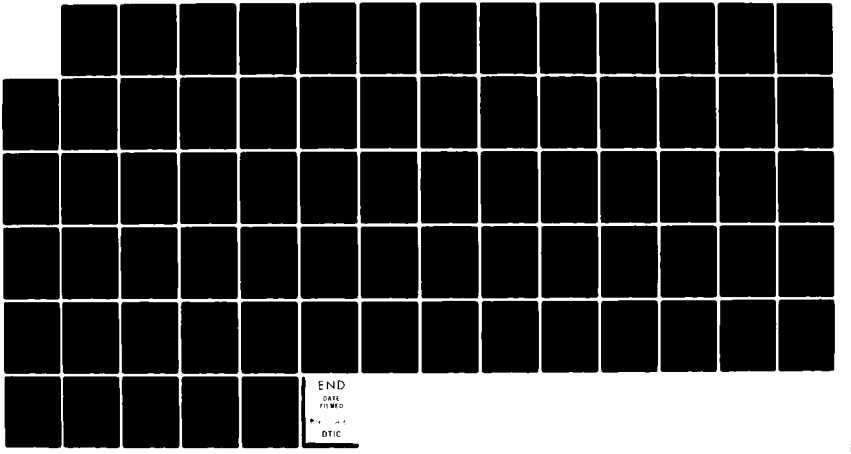

END

DATE FILMED

DTIC

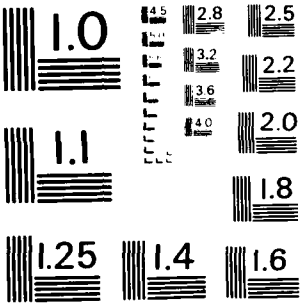

TABLE 46

SPECIFIC CONDUCTIVITY DATA FOR $AlCl_3$-$SbCl_3$ SYSTEM AT 1.0 KHz

COMPOSITION: 40.0-60.0 (Mole %)

Temperature (°C)	Specific Conductivity ($ohm^{-1}cm^{-1}$)
173.6	0.07461
177.3	0.07661
179.3	0.07835
185.5	0.08083
191.1	0.08400
197.4	0.08674
201.4	0.08891
204.9	0.09037
211.4	0.09311
214.0	0.09428
217.8	0.09575

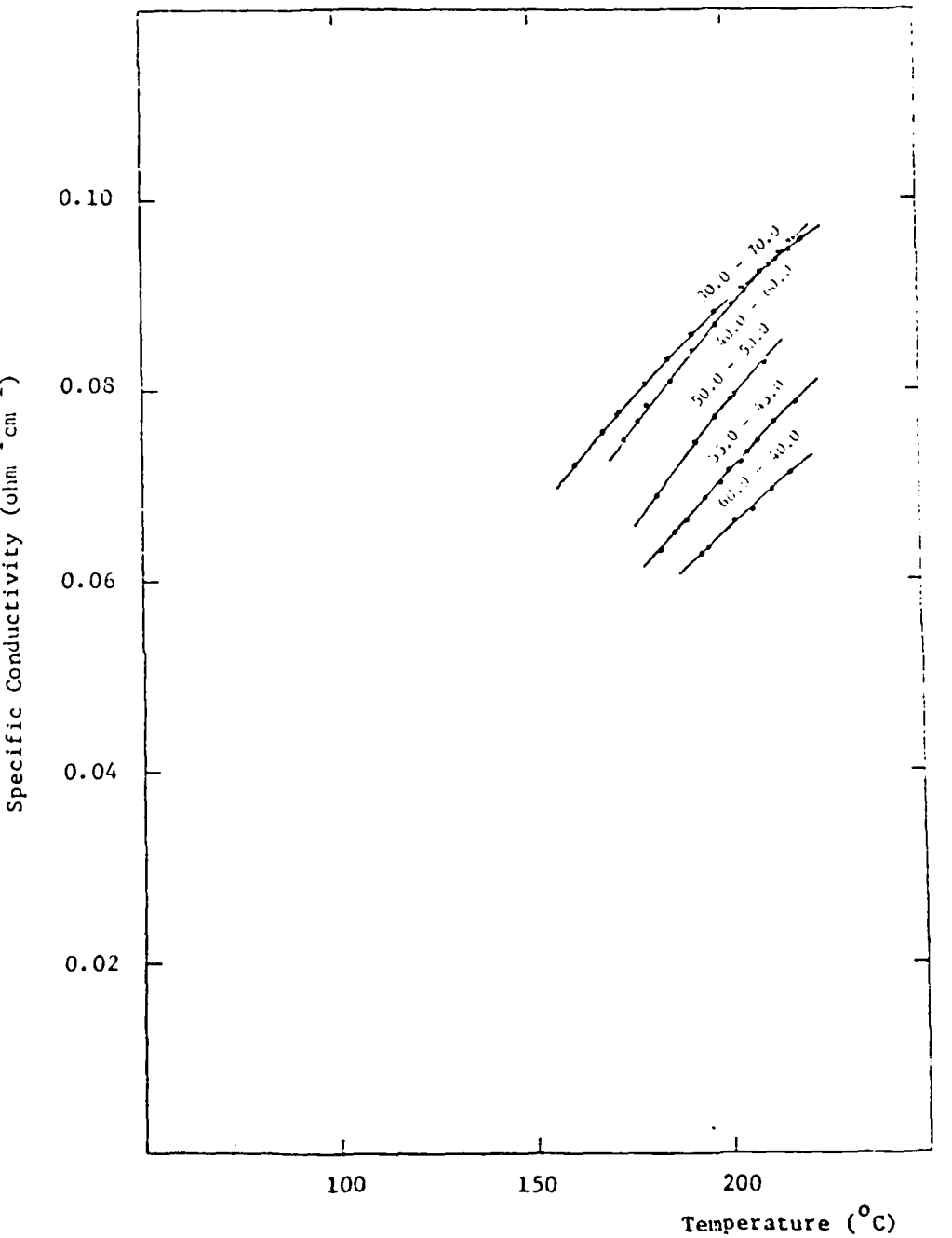

Figure 19. Specific Conductivity of $AlCl_3$-$SbCl_3$ System (Part 2). Composition in mole % is indicated on the curves.

the temperature of the melt increases, the total number of ions in the melt may decrease enough to compensate for the increasing ionic mobility in the melt. This interpretation, however, still requires an abnormally high ionic mobility for the $SbCl_2^+$ cation in these melts. An alternate, more realistic interpretation, which takes into account the polymeric structure of molten $SbCl_3$, proposes that a chloride chain conduction mechanism, similar to the proton jump conduction in aqueous solutions, acts in parallel to the classical diffusional conduction process. The observed temperature dependence of the specific conductivity than results from the breakdown of the $SbCl_3$ polymers as the melt temperature increases, and the consequent loss in the effectiveness of the chloride chain conduction. The two conduction mechanisms are discussed in greater detail in the Appendix.

In summary, the $AlCl_3$-$SbCl_3$ melts have very low liquidus temperatures, and unexpectedly high specific conductivity. The melts with less than 50 mole % $AlCl_3$ seem to be promising for use in batteries in which $SbCl_3$ is used as a cathode material.

3.13 $AlCl_3$-$SbCl_3$-n-BuPyCl System

Samples of the $AlCl_3$-$SbCl_3$-n-BuPyCl melts were obtained from the laboratory of Dr. G. P. Smith at Oak Ridge National Laboratory. Since the liquidus temperature of the two compositions studied, 19.0-60.0-21.0 and 21.0-60.0-19.0 mole %, is below 25°C, we have performed no phase diagram measurements. The results of our specific conductivity measurements are listed in Tables 50 and 51, and shown in Figure 20. The conductivity data for the 25.0-75.0 mole % $AlCl_3$-$SbCl_3$ melt, which has approximately the same $AlCl_3$ to $SbCl_3$ mole ratio as the two ternary n-BuPyCl melts, are shown for comparison in the same figure.

The addition of n-BuPyCl to the $AlCl_3$-$SbCl_3$ melt has a very pronounced effect on its specific conductivity. In the low temperature region, below ca. 100°C, the conductivity vs. temperature plots become increasingly non-linear. Also, the specific conductivity of the $AlCl_3$-$SbCl_3$-n-BuPyCl ternary melts is ca. 40% lower than the conductivity of the corresponding 25.0-75.0 mole % $AlCl_3$-$SbCl_3$ binary melt at the same temperature.

From the practical point of view, however, the lowering of the liquidus temperatures in the $AlCl_3$-$SbCl_3$-n-BuPyCl melts is offset by the large decrease in the specific conductivity compared to the $AlCl_3$-$SbCl_3$ melts. Therefore, no further measurements were performed on this system.

TABLE 50

SPECIFIC CONDUCTIVITY DATA FOR $AlCl_3$-$SbCl_3$-n-BuPyCl SYSTEM AT 1.0 KHz

COMPOSITION: 19.0-60.0-21.0 (Mole %)

Temperature (°C)	Specific Conductivity ($ohm^{-1} cm^{-1}$)
24.4	0.003947
36.5	0.006524
44.3	0.008438
49.2	0.009756
59.3	0.01275
68.2	0.01570
79.1	0.01954
89.7	0.02357
99.8	0.02759
107.8	0.03087
119.8	0.03595
129.8	0.04024
139.9	0.04470
149.9	0.04922
160.8	0.05422

TABLE 51

SPECIFIC CONDUCTIVITY DATA FOR $AlCl_3$-$SbCl_3$-n-BuPyCl SYSTEM AT 1.0 KHz

COMPOSITION: 21.0-60.0-19.0 (Mole %)

Temperature (°C)	Specific Conductivity ($ohm^{-1} cm^{-1}$)
24.4	0.003979
36.8	0.006289
44.2	0.007912
49.3	0.009099
59.3	0.01163
68.2	0.01413
79.0	0.01732
89.7	0.02071
99.8	0.02408
107.4	0.02665
119.9	0.03103
129.7	0.03455
139.9	0.03828
149.8	0.04203
160.8	0.04624

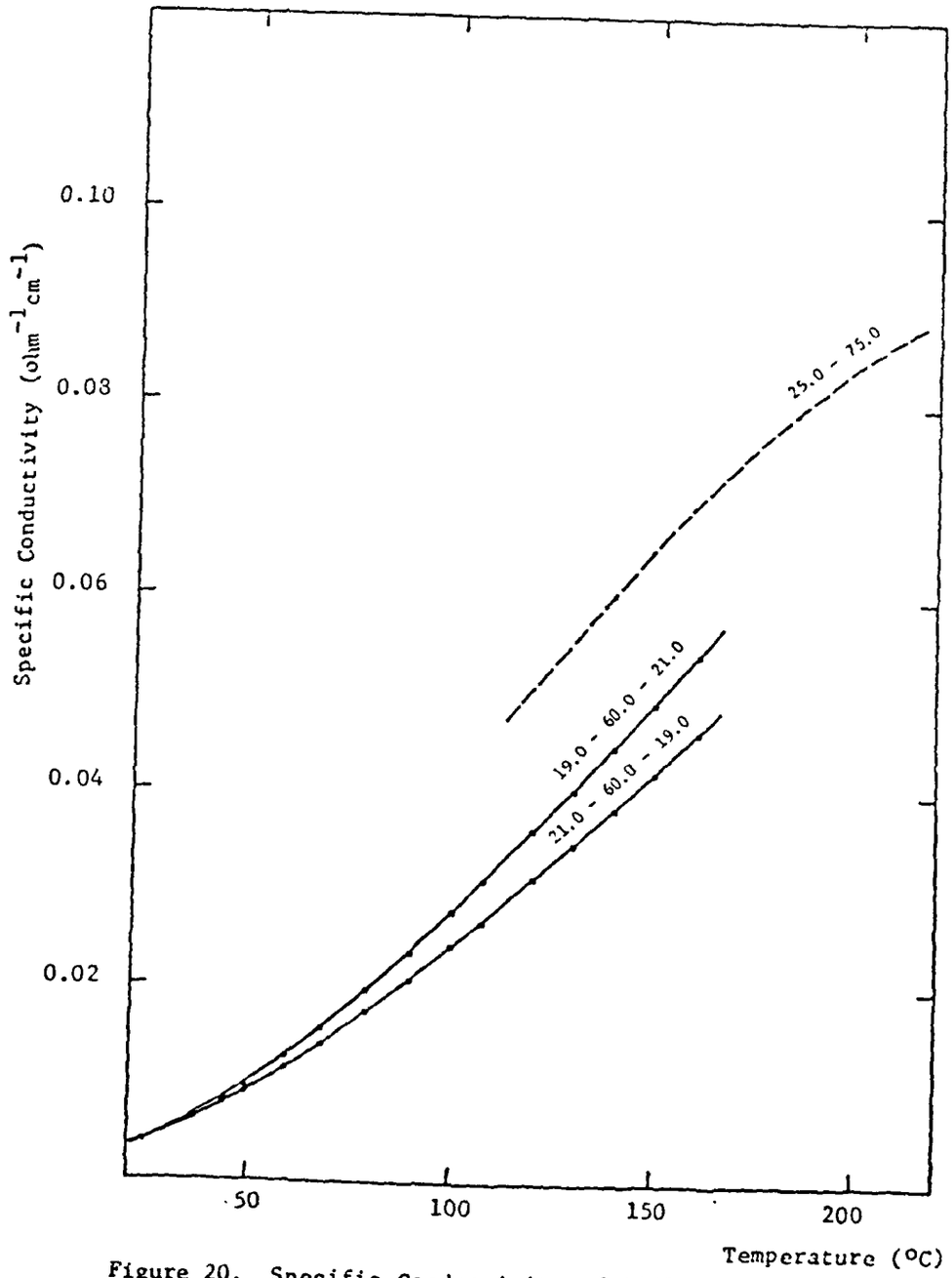

Figure 20. Specific Conductivity of $AlCl_3$-$SbCl_3$-n-BuPyCl System (Full Line) and $AlCl_3$-$SbCl_3$ (Dashed Line). Composition in mole % is indicated on the curves.

3.14 $AlCl_3$-$SbCl_3$-NaCl System

The $AlCl_3$-$SbCl_3$ melts, discussed in Section 3.12 have low liquidus temperatures (>70°C) in the $SbCl_3$ rich composition region and, for molten salt mixtures with molecular constituents only, unexpectedly high specific conductivity (up to 0.1 $ohm^{-1}cm^{-1}$). Thus these melts may be useful in batteries in which $SbCl_3$ is employed as a cathode material. It was of interest to find out whether the addition of NaCl to these melts would significantly increase their specific conductivity without adversely affecting their liquidus temperatures. NaCl is only slightly soluble in $SbCl_3$ (32), and the phase diagram of the $SbCl_3$-NaCl binary system is not available in the literature. Since the liquidus temperatures in the $AlCl_3$-$SbCl_3$ binary system are below 100°C in the composition region with $AlCl_3$ less than 20 mole %, the composition region of the ternary $AlCl_3$-$SbCl_3$-NaCl system of interest for the present project is approximately delineated by $AlCl_3$ < 20 mole % and NaCl < 20 mole %. In addition, two samples with low mole fraction of $SbCl_3$ were also studied.

The results of our liquidus range measurements are listed in Table 52 and Figure 21. The temperatures are reported to 180°C, which was the high temperature limit of the silicone oil in our thermostat bath. The two groups of compositions, with high and low mole fraction of $SbCl_3$ are discussed separately.

The solidus temperature of all but one sample with a high mole fraction of $SbCl_3$ is 70-71°C. This is about the same temperature as in the $AlCl_3$-$SbCl_3$ binary system. The only exception is the 10.0-85.0-5.0 mole % melt with the solidus temperature of 64.9°C, a somewhat unexpected value.

The lowest liquidus temperature in Table 52 is 73.2°C at the composition of 10.0-85.0-5.0 mole % $AlCl_3$-NaCl. This temperature is very close to the melting point of the pure $SbCl_3$. With increasing mole fraction of NaCl, however, the liquidus temperatures increase very steeply. In the melts in which the mole fraction of NaCl is higher than the mole fraction of $AlCl_3$, the liquidus temperatures are above 180°C. Thus the liquidus temperature considerations set a stringent limit on the mole fraction of NaCl, and therefore on the conductivity of the melts for the battery use.

The liquidus temperatures of the two melts with a low mole fraction of $SbCl_3$ are quite high (Table 52). Their solidus temperature, 73.5°C, is *ca*. 40°C lower than the solidus temperature in the low melting region of the $AlCl_3$-NaCl binary system. We do not have sufficient data to locate the minimum in the liquidus temperature surface in this composition region.

TABLE 47

SPECIFIC CONDUCTIVITY DATA FOR $AlCl_3$-$SbCl_3$ SYSTEM AT 1.0 KHz

COMPOSITION: 50.0-50.0 (Mole %)

Temperature (°C)	Specific Conductivity ($ohm^{-1}cm^{-1}$)
181.7	0.06879
191.9	0.07444
192.2	0.07455
197.2	0.07704
201.2	0.07904
202.0	0.07933
210.3	0.08282

TABLE 48

SPECIFIC CONDUCTIVITY DATA FOR $AlCl_3$-$SbCl_3$ SYSTEM AT 1.0 KHz

COMPOSITION: 55.0-45.0 (Mole %)

Temperature (°C)	Specific Conductivity ($ohm^{-1} cm^{-1}$)
183.1	0.06313
186.3	0.06486
189.4	0.0663/
194.4	0.06854
198.3	0.07012
200.6	0.07156
203.4	0.07242
205.2	0.07351
208.4	0.07470
212.8	0.07666
218.0	0.07880

TABLE 52

PHASE DIAGRAM DATA FOR THE $AlCl_3$-$SbCl_3$-NaCl SYSTEM

Composition (Mole %)			Solidus Temperature (°C)	Liquidus Temperature (°C)
$AlCl_3$	$SbCl_3$	NaCl		
5.0	75.0	20.0	70.4	>180
5.0	80.0	15.0	70.4	>180
5.0	85.0	10.0	70.4	>180
5.0	90.0	5.0	70.4	80.6
10.0	70.0	20.0	71.0	>180
10.0	75.0	15.0	71.0	>180
10.0	80.0	10.8	71.0	105.4
10.0	85.0	5.0	64.9	73.2
60.0	10.0	30.0	73.5	147.5
65.0	10.0	25.0	73.5	170.1

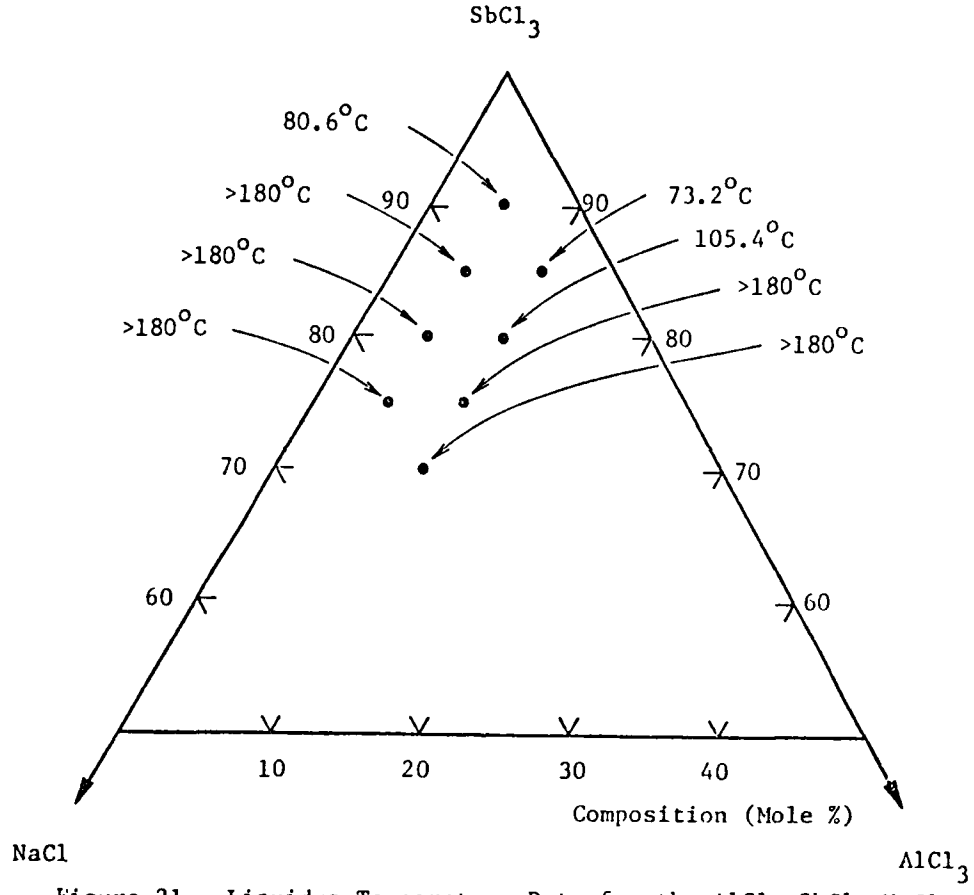

Figure 21. Liquidus Temperature Data for the $AlCl_3$-$SbCl_3$-NaCl System.

Our specific conductivity data for the $AlCl_3$-$SbCl_3$-NaCl melts are shown in Tables 53-55 and Figure 22. The conductivity data for a few $AlCl_3$-$SbCl_3$ melts are also shown for comparison in this figure. In each case the conductivity of the ternary $AlCl_3$-$SbCl_3$-NaCl melt is lower than the conductivity of the binary $AlCl_3$-$SbCl_3$ melt with the same mole fraction of $AlCl_3$ at the same temperature. Thus the addition of NaCl significantly decreases (up to 20%) the conductivity of the $AlCl_3$-$SbCl_3$ melts at low temperatures. In view of the small ionic radius and high ionic mobility of the Na^+ ion, this finding is quite unexpected. However, if the chloride chain conduction is active in addition to the diffusional conduction in the $AlCl_3$-$SbCl_3$ melts, as discussed in Section 3.12, the effect of the addition of NaCl is easily understood. By reacting with Al_2Cl_6, NaCl will suppress Reaction 5, and thus lower the concentration of $SbCl_2^+$ species required for the chloride chain conduction. The high ionic mobility of added Na^+ ions then may not be a sufficient compensation for the reduction in chain conduction, at least at low temperatures. This is also discussed in more detail in the Appendix.

The frequencies at which the most intense peaks of $AlCl_4^-$ and $Al_2Cl_7^-$ ions occur in the Raman spectra of chloroaluminate melts (350 and 313 cm^{-1}) are obscured in the melts with a high mole fraction of $SbCl_3$ by the broad, intense peak of $SbCl_3$. The literature data indicate, however, that the ratio of intensities of the 313 and 350 cm^{-1} peaks in the ternary $AlCl_3$-$SbCl_3$-NaCl melts with a high mole ratio of $AlCl_3$ is approximately the same as in the binary $AlCl_3$-NaCl melts with the same $AlCl_3$ to NaCl mole ratios (31). Our Raman spectrum of the 45.0-45.0-10.0 mole % $AlCl_3$-$SbCl_3$-NaCl melt, Figure 23, shows indication of the presence of the $Al_2Cl_7^-$ and $AlCl_4^-$ ions (shoulders at ca. 320 and 350 cm^{-1}). It was pointed out in Section 3.12 that no Raman evidence was found for the presence of these ions in the binary $AlCl_3$-$SbCl_3$ melts.

In summary, the liquidus temperatures in the $AlCl_3$-$SbCl_3$-NaCl melts in which the mole fraction of NaCl is greater than the mole fraction of $AlCl_3$, are high (>180°C). In the melts in which the mole fraction of NaCl is less than or equal to the mole fraction of $AlCl_3$, however, the liquidus temperatures are low (<110°C). Therefore, only the latter compositions are of interest for battery applications. The addition of NaCl to the $AlCl_3$-$SbCl_3$ melts does not produce the desired increase in the electrical conductivity of the melts. However, NaCl is a necessary constituent in the

TABLE 53

SPECIFIC CONDUCTIVITY DATA FOR $AlCl_3$-$SbCl_3$-NaCl SYSTEM AT 1.0 KHz

COMPOSITION: 5.0-90.0-5.0 (Mole %)

Temperature (°C)	Specific Conductivity ($ohm^{-1} cm^{-1}$)
82.2	0.009469
88.3	0.01016
93.3	0.01072
98.6	0.01132
103.5	0.01186
110.1	0.01259
116.6	0.01329
126.8	0.01438
137.4	0.01545
147.2	0.01643
157.1	0.01738
167.2	0.01833
177.6	0.01924
188.2	0.02010
197.9	0.02086
208.3	0.02160
218.5	0.02228
228.7	0.02289

TABLE 54

SPECIFIC CONDUCTIVITY DATA FOR $AlCl_3$-$SbCl_3$-NaCl SYSTEM AT 1.0 KHz

COMPOSITION: 10.0-85.0-5.0 (Mole %)

Temperature (°C)	Specific Conductivity ($ohm^{-1} cm^{-1}$)
51.4	0.01039
55.9	0.01128
59.6	0.01203
63.4	0.01289
69.9	0.01409
76.3	0.01533
82.2	0.01649
88.2	0.01765
98.2	0.01952
102.2	0.02028
106.5	0.02103
118.5	0.02317
128.9	0.02492
139.6	0.02662
149.8	0.02821
160.2	0.02973
170.4	0.03114
181.0	0.03252
191.2	0.03375
201.2	0.03487
211.6	0.03594
221.5	0.03685
232.2	0.03775

TABLE 55

SPECIFIC CONDUCTIVITY DATA FOR $AlCl_3$-$SbCl_3$-NaCl SYSTEM AT 1.0 KHz

COMPOSITION: 10.0-80.0-10.0 (Mole %)

Temperature (°C)	Specific Conductivity ($ohm^{-1} cm^{-1}$)
107.6	0.02183
108.3	0.02192
113.7	0.02300
118.6	0.02396
124.7	0.02521
130.2	0.02631
134.8	0.02721
145.4	0.02922
155.4	0.03112
165.9	0.03248
175.8	0.03478
186.0	0.03650
196.3	0.03817
206.9	0.03981
217.1	0.04130
226.1	0.04254

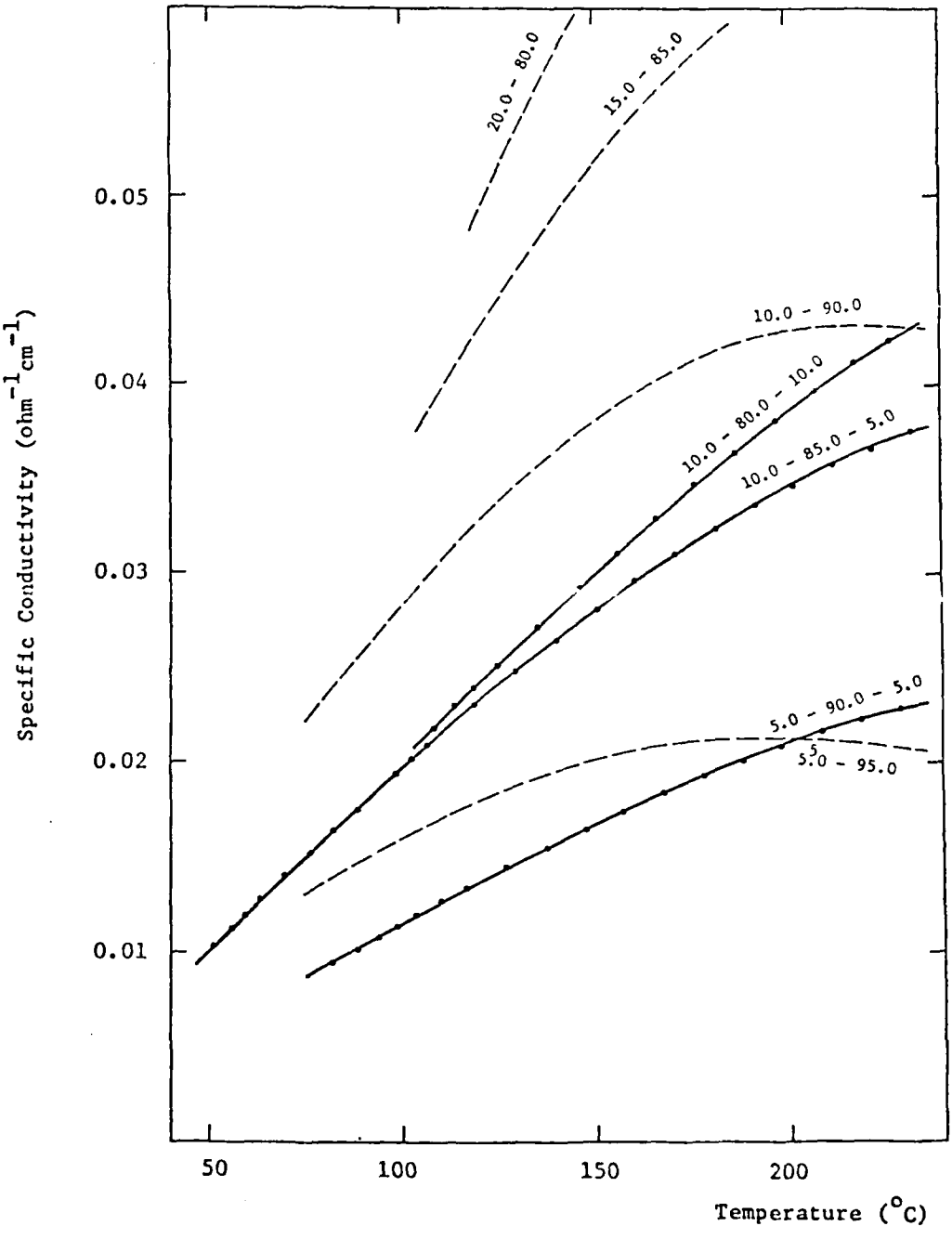

Figure 22. Specific Conductivity of $AlCl_3$-$SbCl_3$-NaCl System (Full Line) and $AlCl_3$-$SbCl_3$ System (Dashed Line). Composition in mole % is indicated on the curves.

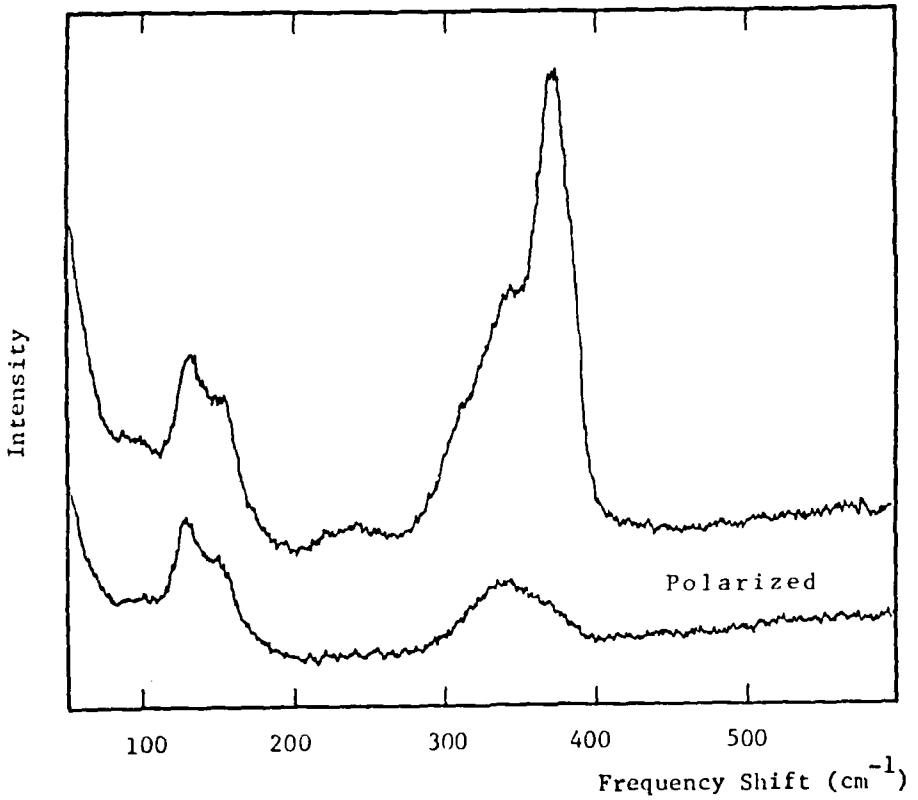

Figure 23. Raman Spectrum of the 45.0-45.0-10.0 Mole % $AlCl_3$-$SbCl_3$-NaCl Melt.

$AlCl_3$-$SbCl_3$ based melts if they are to be used in conjunction with β- or β"-alumina battery separators.

3.15 $FeCl_3$-NaCl System

The phase diagram of the $FeCl_3$-NaCl system, based on the data of Morozov and Toptygin (33), is shown in Figure 24. It is qualitatively similar to the phase diagram of the $AlCl_3$-NaCl system, shown for comparison in the same figure. In both systems a compound with 1:1 stoichiometry is formed in the solid phase, $NaFeCl_4$ and $NaAlCl_4$, respectively, and only one eutectic point exists in the acidic composition region in each case. However, the eutectic composition in the $FeCl_3$-NaCl system is close to 51 mole % $FeCl_3$, i.e., it is shifted by about 10 mole % from the eutectic composition in the $AlCl_3$-NaCl system. Also, the eutectic temperature in the $FeCl_3$-NaCl system is relatively high (156°C) compared to that of 115°C in the $AlCl_3$-NaCl system. As a result of these two differences, the liquidus temperature in the $FeCl_3$-NaCl melts is about 80°C higher than the liquidus temperature of the corresponding $AlCl_3$-NaCl melts in the 60 to 80 mole % region.

Our conductivity data for the $FeCl_3$-NaCl system are listed in Tables 56 to 59, and shown in Figure 25. The specific conductivity vs. temperature plots are linear and similar to the conductivity plots for the $AlCl_3$-LiCl-NaCl melts, which are shown for comparison in Figure 25. However, the specific conductivity of the $FeCl_3$-NaCl melts is higher than the specific conductivity of the corresponding $AlCl_3$-LiCl-NaCl melts. Thus, the conductivity of the 52.0-48.0 mole % $FeCl_3$-NaCl melt is ca. 10% higher than the conductivity of the 52.0-24.0-24.0 mole % $AlCl_3$-LiCl-NaCl melt at the same temperature. This difference increases to ca. 16% for the 56.0-44.0 mole % melt, and becomes as high as ca. 25% for the 64.0-36.0 mole % $FeCl_3$-NaCl melt when its conductivity is extrapolated to lower temperatures.

The reproducibility of our conductivity measurements on the $FeCl_3$-NaCl melts was not very good. The platinum electrodes in the conductivity cells were attacked by the melt. This problem, encountered in all our measurements on the melts containing ferric chloride, will be discussed in more detail in Section 3.16.

The $FeCl_3$-NaCl melts appear to be promising only for batteries in which $FeCl_3$ is used as a cathode material. The important drawback of these melts is their high liquidus temperature. This drawback was dealt with by introducing lithium chloride as a third component into the $FeCl_3$-NaCl system. The

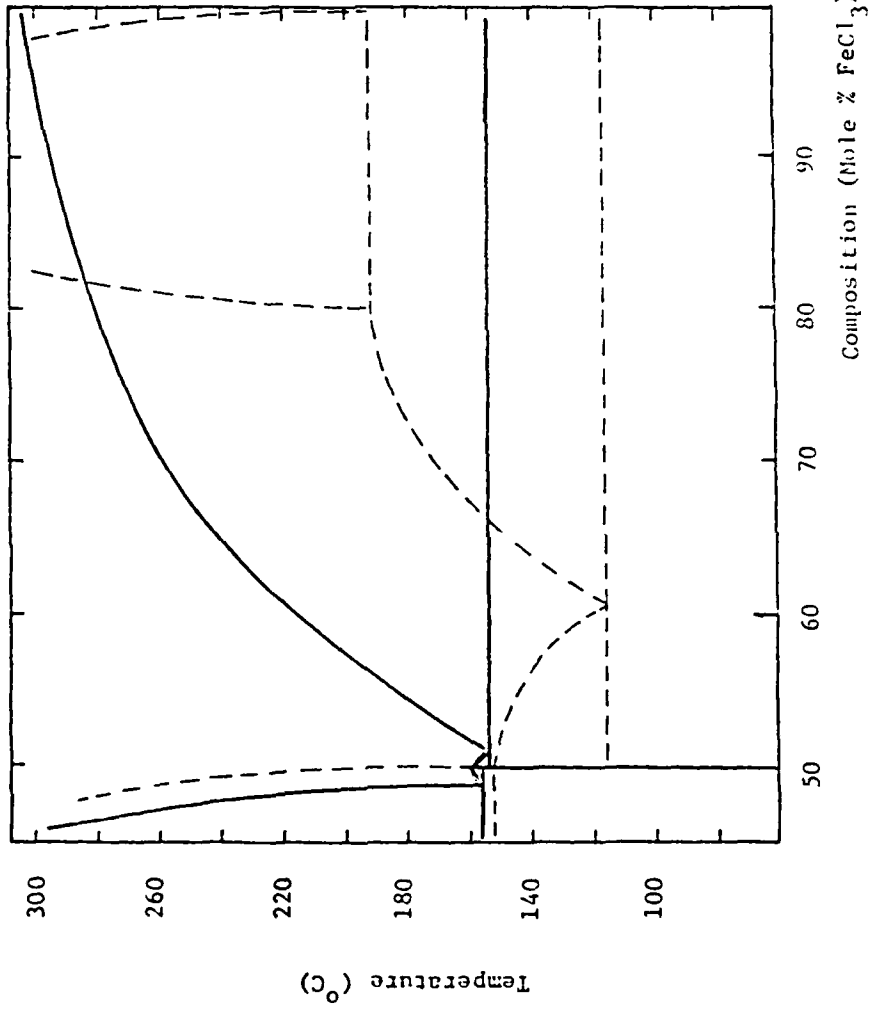

Figure 24. Phase Diagrams of the $FeCl_3$-NaCl System (Full Line) and $AlCl_3$-NaCl System (Dashed Line).

TABLE 56

SPECIFIC CONDUCTIVITY DATA FOR $FeCl_3$-NaCl SYSTEM AT 1.0 KHz

COMPOSITION: 52.0-48.0 (Mole %)

Temperature (°C)	Specific Conductivity ($ohm^{-1}cm^{-1}$)
182.8	0.4318
193.6	0.4611
204.2	0.4901
213.4	0.5157
223.2	0.5420
233.6	0.5682
244.0	0.5953
253.6	0.6196
263.7	0.6477
273.2	0.6686
286.0	0.6997
298.2	0.7290
310.4	0.7579
320.2	0.7794
330.1	0.7986
337.1	0.8148
348.2	0.8389

TABLE 57

SPECIFIC CONDUCTIVITY DATA FOR $FeCl_3$-NaCl SYSTEM AT 1.0 KHz

COMPOSITION: 54.0-46.0 (Mole %)

Temperature (°C)	Specific Conductivity ($ohm^{-1}cm^{-1}$)
236.7	0.5462
247.1	0.5715
258.3	0.5984
267.4	0.6201
277.2	0.6428
286.4	0.6635
297.7	0.6895
305.7	0.7072
315.8	0.7309
325.0	0.7524
331.7	0.7654
342.7	0.7869

TABLE 58

SPECIFIC CONDUCTIVITY DATA FOR $FeCl_3$-NaCl SYSTEM AT 1.0 KHz

COMPOSITION: 56.0-44.0 (Mole %)

Temperature (°C)	Specific Conductivity ($ohm^{-1}cm^{-1}$)
232.0	0.4789
249.0	0.5184
260.2	0.5428
276.4	0.5786
289.2	0.6015
302.4	0.6277
308.7	0.6406
316.2	0.6551
326.2	0.6746
333.1	0.6879
341.5	0.7070
346.8	0.7156
350.8	0.7261

TABLE 59

SPECIFIC CONDUCTIVITY DATA FOR $FeCl_3$-NaCl SYSTEM AT 1.0 KHz

COMPOSITION: 64.0-36.0 (Mole %)

Temperature (°C)	Specific Conductivity ($ohm^{-1}cm^{-1}$)
286.8	0.4443
297.0	0.4612
307.4	0.4779
320.2	0.4986
331.6	0.5177
341.9	0.5311
350.0	0.5436

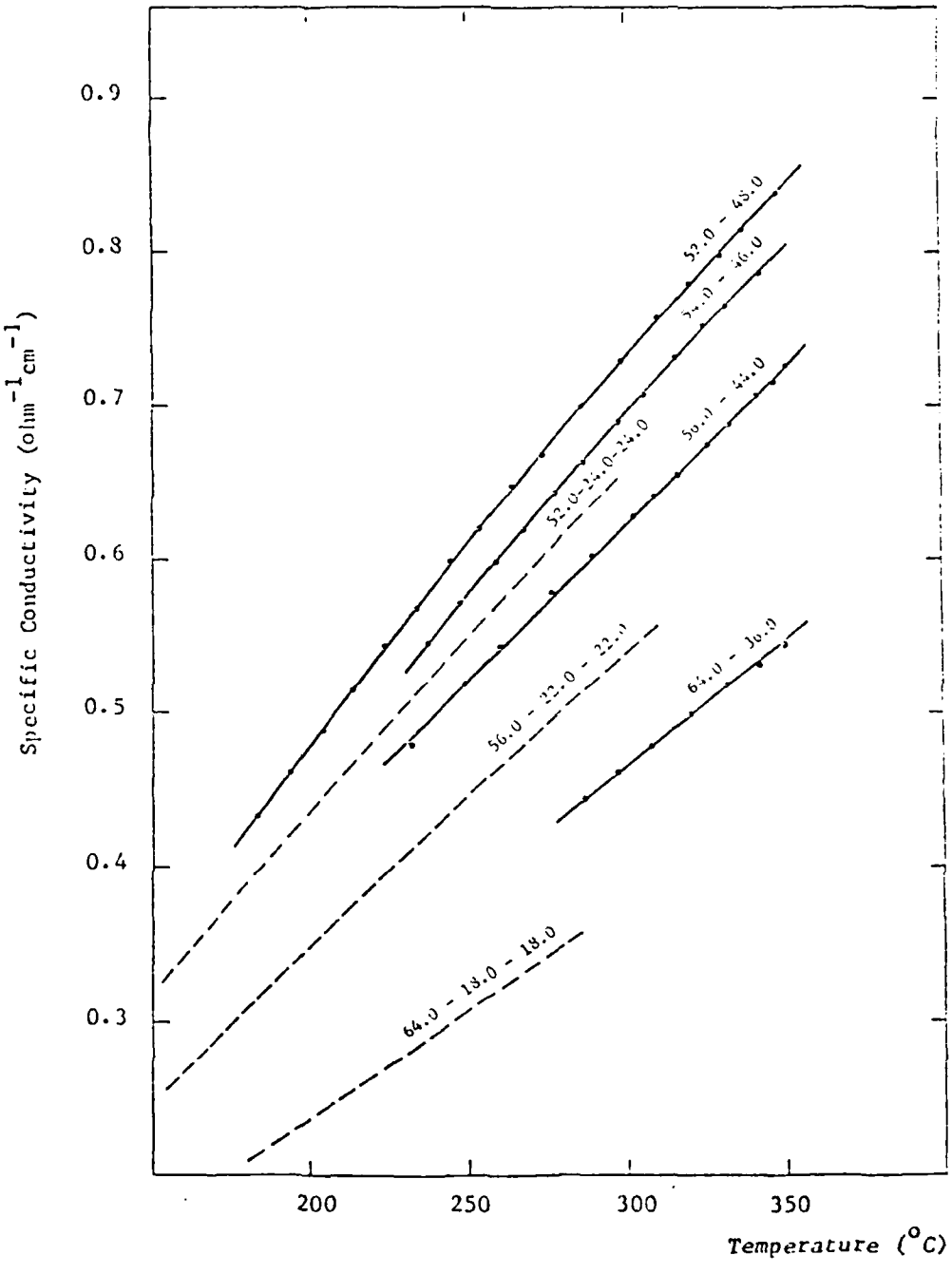

Figure 25. Specific Conductivity of $FeCl_3$-NaCl System (Full Line) and $AlCl_3$-LiCl-NaCl System (Dashed Line).
Composition in mole % is indicated on the curves.

$FeCl_3$-LiCl-NaCl ternary salt system is discussed in the following section.

3.16 $FeCl_3$-LiCl-NaCl System

The problem with impurities in the ferric chloride, brought up in the previous section, was even more evident during our study of the $FeCl_3$-LiCl-NaCl system. Since the conductivity measurements on these melts were extended to lower temperatures than in the case of $FeCl_3$-NaCl melts, the freezing out of the impurities in the conductivity cells was considerably more pronounced. As a consequence, not only the composition of the melt was changing, but the deposition of the solid phase in the conductivity cell was also effectively changing the cell constant during the measurement. We speculate that the solid deposits may have been iron(III) oxychloride or $FeCl_2$. Since the $FeCl_3$ used for the preparation of these melts was distilled under vacuum in sealed Pyrex tubes, the $FeCl_2$ possibly present in the starting material was not expected to distill over in appreciable concentrations at the temperature below the boiling point of $FeCl_3$. Our problem, however, may have been caused by the equilibrium:

$$2FeCl_3 \rightleftarrows 2FeCl_2 + Cl_2 \qquad (6)$$

possibly taking place either in the vapor phase during the distillation of $FeCl_3$, or in the prepared $FeCl_3$-LiCl-NaCl melt in the conductivity cell. The etching of the platinum electrodes during the conductivity measurements seemed to indicate the latter possibility. In subsequent distillations we have indeed observed evidence for the formation of gaseous chlorine during the vacuum distillation of $FeCl_3$. After unsuccessful attempts to improve the purity of $FeCl_3$ by distilling it under argon in the presence of chlorine, we abandoned the distillation route. For the later measurements we used instead the high purity anhydrous $FeCl_3$ (Cerac, 99.9% metals purity, sealed under argon) as received. To minimize the effect of the decomposition of $FeCl_3$ during the measurement, a newly built capillary conductivity cell with a large melt volume and a reduced vapor volume was used, and the 50.0-25.0-25.0 mole % $FeCl_3$-LiCl-NaCl melt was prepared directly in the new cell. After the completion of the measurements, the composition of the melt was changed to 52.0-24.0-24.0 mole % by adding the appropriate amount of $FeCl_3$ into the cell. This procedure minimized the amount of handling of molten $FeCl_3$ and $FeCl_3$ containing melts, and was expected to reduce the loss of chlorine.

Due to the presence of the solid impurities during the visual determination of the liquidus range of the FeCl3-LiCl-NaCl melts, it was difficult to

establish their liquidus temperatures. The DSC measurements, on the other hand, were not practical because of the attack of $FeCl_3$ on the aluminum sample pans. Therefore, no definite phase diagram data are given in this report. However, the liquidus temperatures were estimated on the basis of our visual determinations to be 40 to 50°C lower than in the $FeCl_3$-NaCl system at the equivalent compositions. The eutectic temperature in the $FeCl_3$-LiCl-NaCl system is therefore estimated to be in the 105-115°C range. This is reasonably close to the literature value for the eutectic temperature of the $FeCl_3$-LiCl-KCl system which is as low as 109-110°C (34,35).

The results of our electrical conductivity measurements are listed in Tables 60 to 62 and shown in Figure 26. While the values for the 50.0-25.0-25.0 and 52.0-24.0-24.0 mole % melts, prepared with the $FeCl_3$ from Cerac are reasonably consistent with the values for the 56.0-22.0-22.0 mole % melt, prepared with the distilled $FeCl_3$ from Alfa-Ventron, the reproducibility of the reported data is still not quite satisfactory. For example, the data obtained below 220°C for the 56.0-22.0-22.0 mole % melt were not reproducible and had to be discarded. The specific conductivity *vs.* temperature plot for the 56.0-22.0-22.0 mole % melt is virtually identical to the conductivity plot for the 56.0-44.0 mole % $FeCl_3$-NaCl melt. The specific conductivity of the $FeCl_3$-LiCl-NaCl melt is, therefore, *ca.* 10% higher than the conductivity of the 56.0-22.0-22.0 mole % $AlCl_3$-LiCl-NaCl melt at the same temperature (Figure 25).

In summary, the liquidus temperatures of the $FeCl_3$-LiCl-NaCl system appear to be in approximately the same range as the liquidus temperatures of the $AlCl_3$-NaCl system. The specific conductivity of the $FeCl_3$-LiCl-NaCl system competes favorably with the conductivity of the $AlCl_3$-NaCl system. Moreover, ferric chloride is relatively inexpensive. Based on our preliminary results, therefore, the $FeCl_3$-LiCl-NaCl system is quite promising for batteries in which $FeCl_3$ is used as a cathode material. However, this system clearly requires more study. A high purity $FeCl_3$, prepared in a large scale synthesis from pure iron and gaseous chlorine in a closed system, is a prerequisite for obtaining both more precise and more extensive data for this system. Due to the time limitations such synthesis was not attempted.

3.17 $GaCl_3$-NaCl System

The phase diagram of the $GaCl_3$-NaCl system, based on the data of Fedorov and Yakunina (36) is shown in Figure 27. The most conspicuous difference

TABLE 60

SPECIFIC CONDUCTIVITY DATA FOR $FeCl_3$-LiCl-NaCl SYSTEM AT 1.0 KHz

COMPOSITION: 50.0-25.0-25.0 (Mole %)

Temperature (°C)	Specific Conductivity ($ohm^{-1}cm^{-1}$)
129.8	0.3340
134.5	0.3479
139.0	0.3607
144.3	0.3754
147.4	0.3833
155.2	0.4052
159.7	0.4162
166.2	0.4361
171.4	0.4537
181.7	0.4814
189.9	0.5030
201.7	0.5343
212.3	0.5616
225.2	0.5964
232.5	0.6127
242.5	0.6368
252.7	0.6586

TABLE 61

SPECIFIC CONDUCTIVITY DATA FOR $FeCl_3$-LiCl-NaCl SYSTEM AT 1.0 KHz

COMPOSITION: 52.0-24.0-24.0 (Mole %)

Temperature (°C)	Specific Conductivity ($ohm^{-1}cm^{-1}$)
137.9	0.3278
142.8	0.3402
147.6	0.3531
152.4	0.3654
162.6	0.3921
171.4	0.4150
181.9	0.4415
191.8	0.4615
201.4	0.4871
213.3	0.5135
223.1	0.5366
233.0	0.5595
245.0	0.5845
254.4	0.6072

TABLE 62

SPECIFIC CONDUCTIVITY DATA FOR $FeCl_3$-LiCl-NaCl SYSTEM AT 1.0 KHz

COMPOSITION: 56.0-22.0-22.0 (Mole %)

Temperature (°C)	Specific Conductivity ($ohm^{-1}cm^{-1}$)
226.6	0.4681
236.4	0.4911
246.2	0.5126
256.0	0.5363
265.9	0.5569
275.6	0.5754
302.8	0.6380
312.0	0.6572
322.8	0.6766

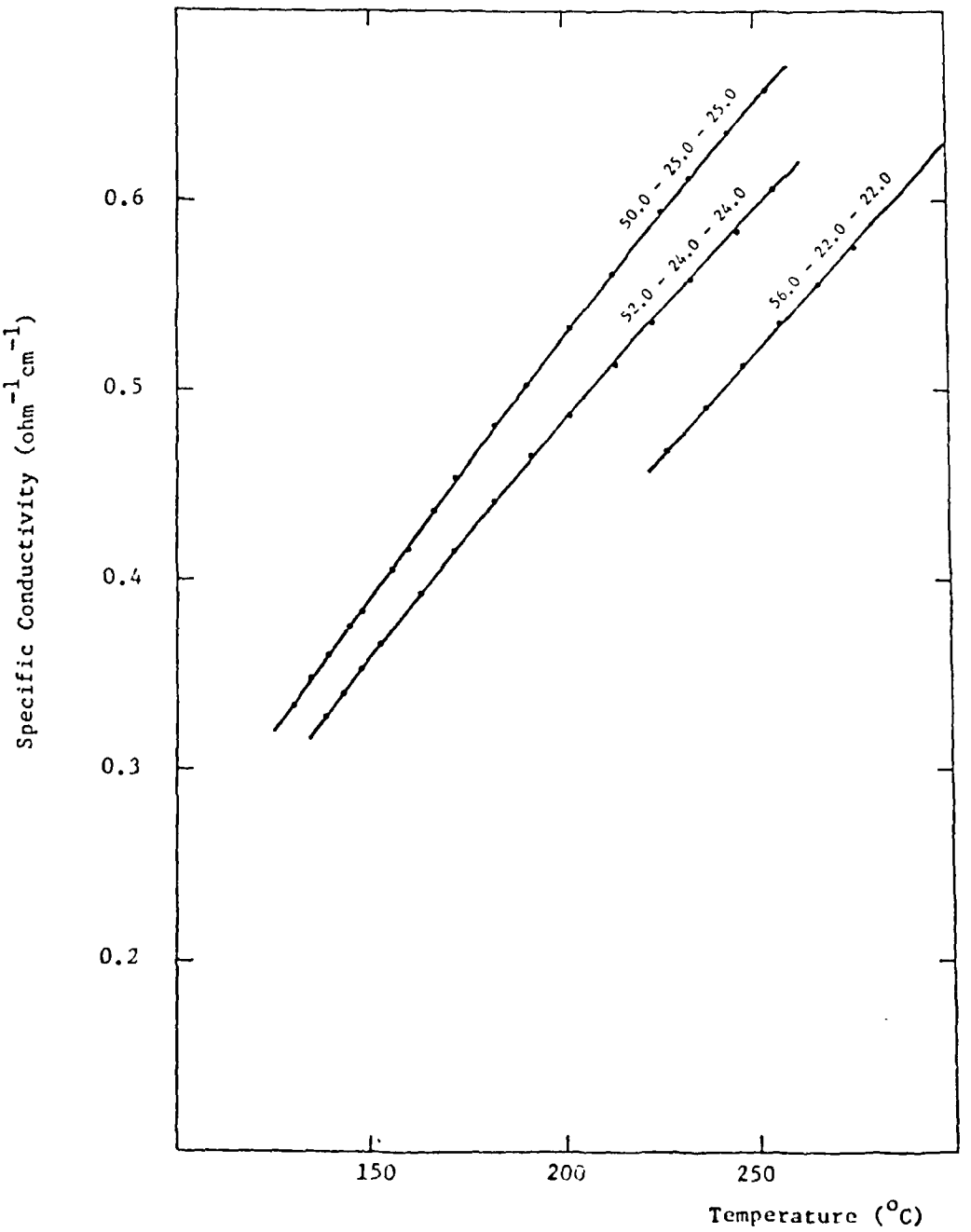

Figure 26. Specific Conductivity of $FeCl_3$-LiCl-NaCl System. Composition in mole% is indicated on the curves.

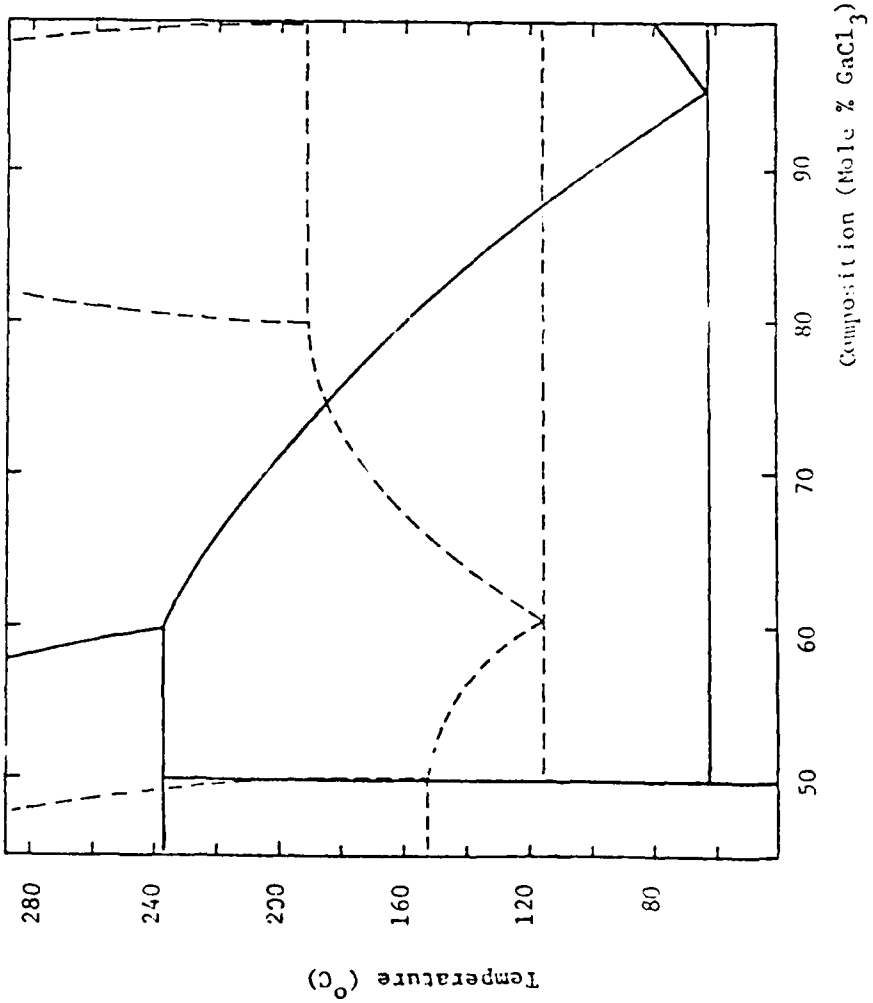

Figure 27. Phase Diagrams of the $GaCl_3$-NaCl System (Full Line) and $AlCl_3$-NaCl System (Dashed Line).

between this phase diagram and the phase diagram of the $AlCl_3$-NaCl system, shown in the same figure, is that the 1:1 compound, $NaGaCl_4$, melts incongruently (solidus temperature 238°C, liquidus temperature ca. 450°C). The other important difference is the very low eutectic temperature of 62°C in the $GaCl_3$-NaCl system. However, due to the very low melting point of pure $GaCl_3$ compared to $NaGaCl_4$, the eutectic composition is displaced to 95 mole % $GaCl_3$. As a consequence, the liquidus temperatures in this system are higher than in the $AlCl_3$-NaCl system in the melts with less than ca. 74 mole % $GaCl_3$. In the 50 to 65 mole % $GaCl_3$ region this difference is as high as 70°C or more. The low melting compositions of the $GaCl_3$-NaCl melts are between 90 and 100 mole % $GaCl_3$, i.e., in the region where the volatility, as well as the acidity of the melts, is quite high.

Our specific conductivity data for the $GaCl_3$-NaCl system are listed in Tables 63 to 65 and shown in Figure 28. The conductivity vs. temperature plots are linear below 200°C. The specific conductivity of the 70.0-30.0 mole % $GaCl_3$-NaCl melt is 15 to 20% higher than the conductivity of the 68.0-24.0-8.0 mole % $AlCl_3$-LiCl-NaCl melt, which has a comparable content of $AlCl_3$. The conductivities for the $GaCl_3$-KCl, $GaCl_3$-RbCl and $GaCl_3$-CsCl systems, which are available in literature (37), are slightly lower. The substantial decrease of the conductivity in the melts with 80.0 and 90.0 mole % $GaCl_3$ reflects a drop in the concentration of Na^+ ions, which are presumably charge carriers in these melts.

Only high purity $GaCl_3$ is commercially readily available at present and its cost is high. Perhaps the more important drawback, however, is the fact that the low melting (<100°C) region of $GaCl_3$-NaCl melts is the narrow region above ca. 90 mole % $GaCl_3$. This is the region of low specific conductivity as well as of high volatility, both undesirable melt properties from the battery use standpoint.

3.18 Battery Electrodes

The compatibility of two electrode materials, LiAl alloy and TiS_2, with the chloroaluminate melts has been studied. The LiAl alloy was of interest as a battery anode to be used without a separator in low temperature molten molten batteries. TiS_2, which has recently received much attention as a battery cathode in nonaqueous solvents (38), has not been studied to date in molten chloroaluminates.

Metallic lithium cannot be used without a separator as an anode in a

TABLE 63

SPECIFIC CONDUCTIVITY DATA FOR $GaCl_3$-NaCl SYSTEM AT 1.0 KHz

COMPOSITION: 70.0-30.0 (Mole %)

Temperature (°C)	Specific Conductivity ($ohm^{-1}cm^{-1}$)
158.1	0.1626
165.3	0.1730
172.0	0.1824
179.5	0.1933
186.1	0.2029
193.7	0.2134
200.5	0.2239
211.5	0.2397
219.2	0.2514
227.6	0.2647
237.0	0.2790

TABLE 64

SPECIFIC CONDUCTIVITY DATA FOR $GaCl_3$-NaCl SYSTEM AT 1.0 KHz

COMPOSITION: 79.6-20.4 (Mole %)

Temperature (°C)	Specific Conductivity ($ohm^{-1} cm^{-1}$)
145.9	0.0946
153.0	0.1009
160.6	0.1075
166.8	0.1130
175.4	0.1206
182.2	0.1265
189.9	0.1332
201.4	0.1428
209.0	0.1503
217.5	0.1584
225.7	0.1668

TABLE 65

SPECIFIC CONDUCTIVITY DATA FOR $GaCl_3$-NaCl SYSTEM AT 1.0 KHz

COMPOSITION: 90.0-10.0 (Mole %)

Temperature (°C)	Specific Conductivity ($ohm^{-1} cm^{-1}$)
110.8	0.02618
118.6	0.02859
125.3	0.03075
132.2	0.03292
138.7	0.03498
145.4	0.03706
151.5	0.03902
163.7	0.04174
170.1	0.04368
175.0	0.04533
182.3	0.04789
190.4	0.05063
197.7	0.05326
206.1	0.05689
211.1	0.05886
220.9	0.06328

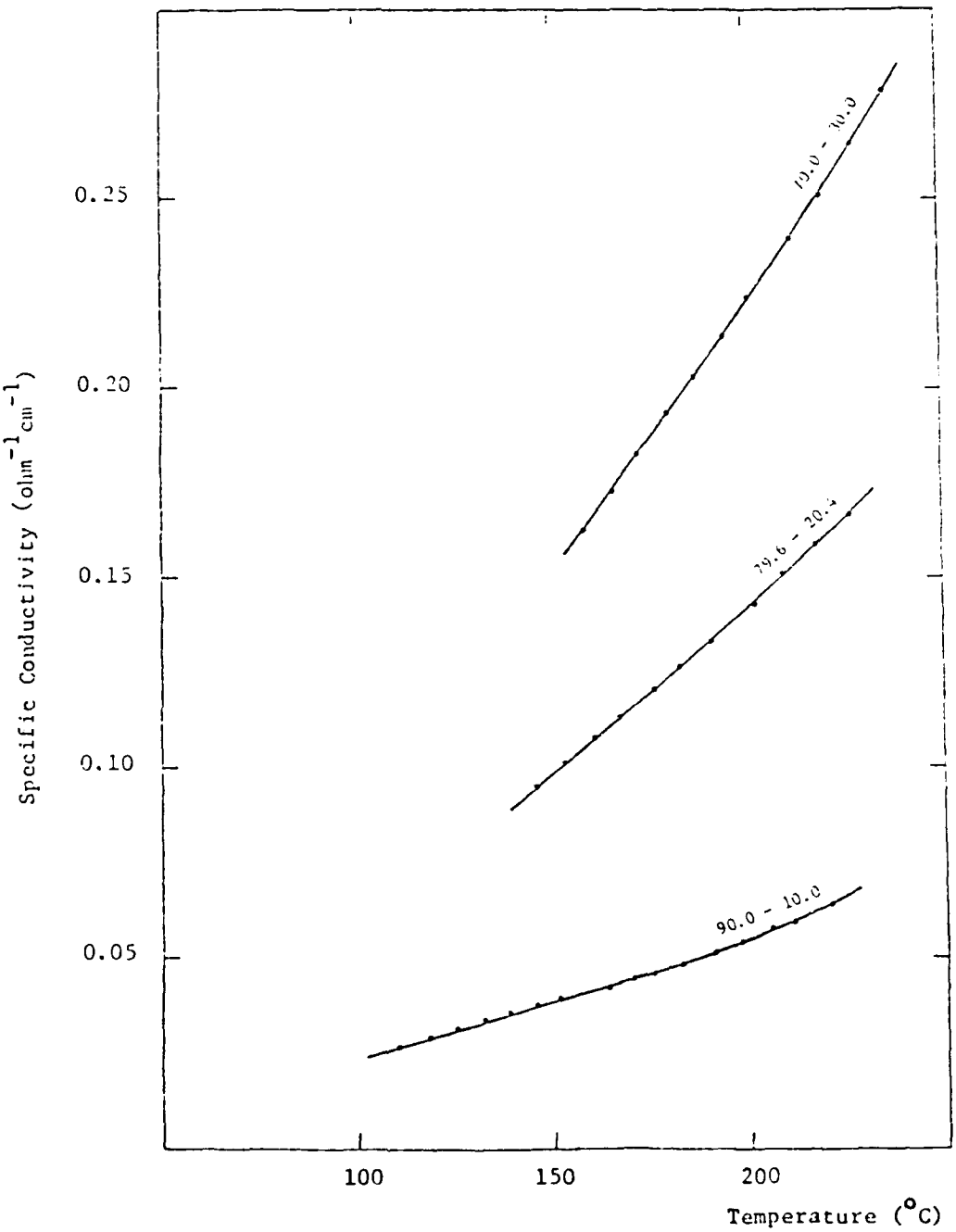

Figure 28. Specific Conductivity of $GaCl_3$-NaCl System. Composition in mole % is indicated on the curves.

molten salt battery which employs a chloroaluminate melt as a solvent. Placed in contact with the melt, it reacts with it to reduce the aluminum(III) to metal according to the reaction:

$$3Li(0) + Al(III) \rightarrow 3Li(I) + Al(0) \qquad (7)$$

Therefore, lithium has to be separated from the chloroaluminate melt with a solid ionic conductor.

The aim of our experiments was to establish whether the reaction of the LiAl alloy with the chloroaluminate melts may be sufficiently slow to allow the use of this alloy without a separator. Both the ternary $AlCl_3$-LiCl-NaCl melts and the binary $AlCl_3$-NaCl melts were employed. A slightly acidic composition (52 mole % $AlCl_3$) and a very acidic composition (72 mole % $AlCl_3$) of each type of melt were used as the two limiting cases. The LiAl alloy samples, 56 atomic % Li(KDI-Score), ca. 1/4" in size, were sealed with 6-8 g of each melt in evacuated Pyrex tubes, and digested with constant agitation for 7 days at 160°C for slightly acidic melts and at 185°C for very acidic melts. The melts were subsequently subjected to thermal analysis. The results of the analysis as well as the visual observations made on the samples and melts are reported in Table 66.

As soon as the alloy samples came in contact with the molten chloroaluminate phase, the formation of aluminum dendrites and a change in the appearance of the alloy samples were observed. Lithium from the alloy was apparently dissolving, and the aluminum was plating out. The results of the thermal analysis of the melts with the Li-Al alloy (Table 66) confirmed the above observations. The solidus temperature of both $AlCl_3$-LiCl-NaCl ternary melts increased after digestion from 86°C to 92-93°C. The liquidus temperature of the 52-24-24 mole % melt increased to ca. 127°C. This shows that the loss in $AlCl_3$ and the gain in LiCl has shifted the composition of the melt into the basic region of the phase diagram ($AlCl_3$ < 50 mole %). The liquidus temperature of the 72-14-14 mole % melt decreased to 131°C, which is consistent with the shift of the melt composition towards lower $AlCl_3$ mole fraction. The binary $AlCl_3$-NaCl melts digested with the LiAl alloy exhibit the same behavior. The solidus temperature of both the 52-48 and 72-28 mole % melts increased from ca. 111°C to 136°C. The liquidus temperature of the 52-48 mole % melt increased from 153°C to 171°C, which is again in the basic composition region of the phase diagram ($AlCl_3$ < 50 mole %). To understand why the liquidus temperature of the 72-28 mole % melt increased from ca. 148°C to 155°C, while at the same time the melt became more basic, it should

TABLE 66

THERMAL ANALYSIS DATA FOR CHLOROALUMINATE MELTS DIGESTED WITH LiAl ALLOY

Melt Composition (Mole %)			Solidus Temperature	Liquidus Temperature	Comments	
$AlCl_3$	LiCl	NaCl	(°C)	(°C)	Solid Sample	Melt
52.0	24.0	24.0	92	127	Al dendrites Edges and corners rounded	Clear
72.0	14.0	14.0	93	131	Al dendrites Edges and corners rounded	Clear
52.0	-	48.0	136	171	Al dendrites Edges and corners rounded	Clear
72.0	-	28.0	136	155	Al dendrites Edges and corners rounded	Clear

be noted that with the dissolution of lithium, the binary $AlCl_3$-NaCl melt system was transformed into the ternary $AlCl_3$-LiCl-NaCl melt system, and the eutectic composition of this new system is shifted towards lower mole fraction of $AlCl_3$.

The use of TiS_2 as a solid battery cathode is based on the redox reaction

$$xNa^+ + TiS_2 + e \underset{\text{oxidation}}{\overset{\text{reduction}}{\rightleftharpoons}} Na_xTiS_2 \qquad (8)$$

Na_xTiS_2 ($o < x \leq 1$), formed in the above reaction, is a solid intercalation compound in which Na^+ ions are inserted between the TiS_2 layers without a radical change of the existing layer structure of TiS_2. The open circuit voltage of a typical room temperature Na-TiS_2 cell with a nonaqueous electrolyte is ca. 2.2 V, and the theoretical energy density is 144 W-hr/kg (38). The energy density increases to 480 W-hr/kg when lithium is substituted for sodium as the anode. This increase is due to the extended range of values of x in Li_xTiS_2 for which the reaction (8) is reversible (38).

Two grades of TiS_2 were used in our study. The material from Alfa-Ventron (99.5 %, dull black appearance) was treated before use with sulfur vapor at 420°C for 14 days in a sealed, evacuated Pyrex tube. The excess sulfur was subsequently distilled off through a glass frit into a separate section of the same reaction tube. The TiS_2 from Cerac (99.8 %, battery grade, sealed under nitrogen, metallic bronze appearance) was used as received. A powdered sample of each grade of TiS_2 was tested for the reactivity towards chloroaluminate melts by digesting overnight at 150°C with an excess of a 63.0-37.0 mole % $AlCl_3$-NaCl melt in a sealed, evacuated Pyrex tube. Both melt samples became quickly yellow-brown in color, and when the two melt tubes were removed from the furnace for inspection, a bright yellow product distilled off and deposited on the walls of the cooler section of the melt tubes. Upon cooling to room temperature, samples of the yellow solid were removed for identification.

The Raman spectra of the two solid samples were similar, and therefore only one is shown in Figure 29. In addition to the six peaks of the solid Al_2Cl_6 (a strong peak at 307 cm^{-1}, medium intensity peak at 170 cm^{-1}, and weak peaks at 117, 200, 257 and a very broad 380-400 cm^{-1}), the spectrum shows two new peaks of unknown origin: a strong peak at 460 cm^{-1} and a less prominent peak at 95 cm^{-1}. The spectrum of the other sample exhibits

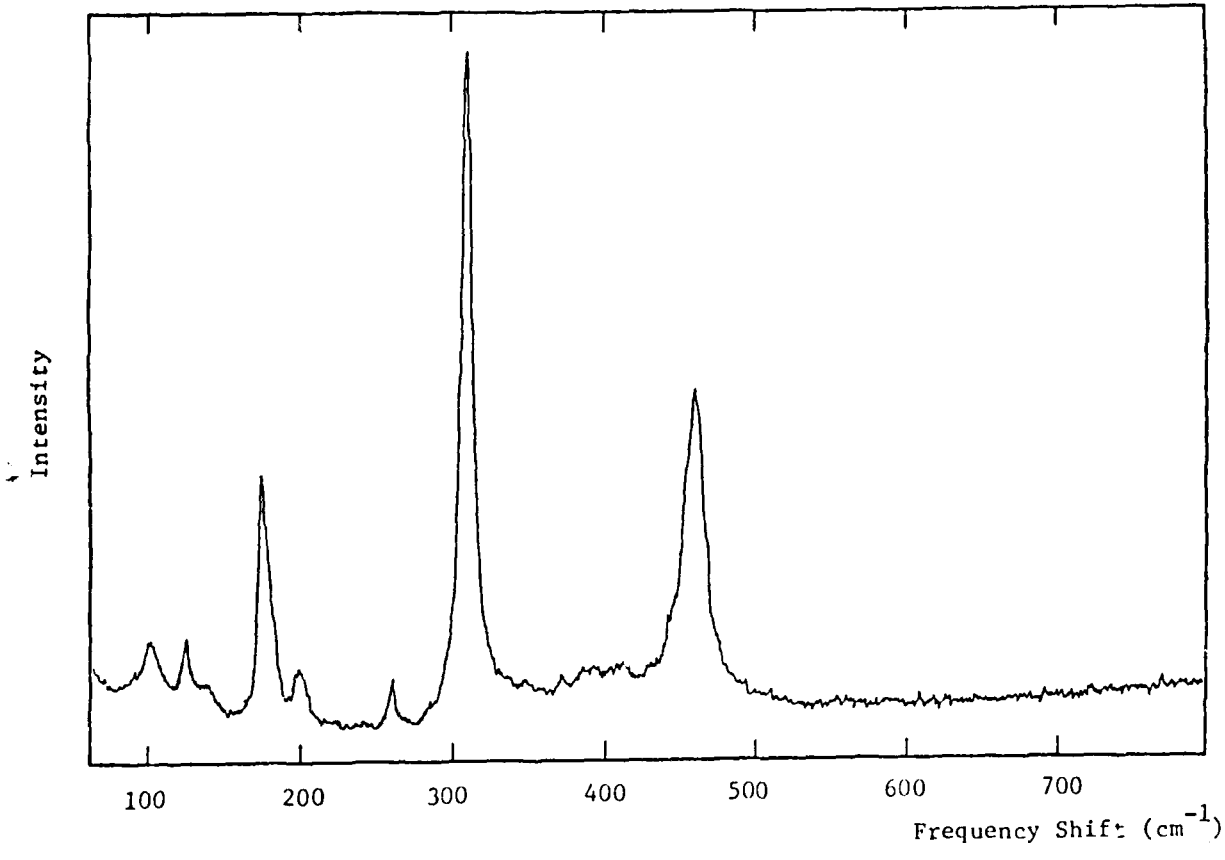

Figure 29. Raman Spectrum of the Volatile Component of the TiS_2 - $AlCl_3$-NaCl 63.0-37.0 Mole % Melt Mixture.

the same peaks, with approximately the same intensity ratio of the 460 and 95 cm^{-1} peaks, but with a different intensity ratio of the 460 cm^{-1} peak and the Al_2Cl_6 peaks. This difference indicates that the yellow substance does not form a stoichiometric adduct with Al_2Cl_6. Neither spectrum shows any evidence for the presence of the $Al_2Cl_7^-$ or $AlCl_4^-$ ions, since their most intense peaks in the solid alkali chloroaluminate salt mixtures, at 317 and 347 cm^{-1}, are absent. This indicates that the yellow solid is probably not an ionized compound. The spectra also show no evidence of $TiCl_4$ (the most intense peak at 388 cm^{-1}), or elemental sulfur S_8 (at 218 cm^{-1}). The TiS_2 itself has no volatility under our experimental conditions. The yellow substance may possibly be a titanium sulfochloride, but the available Raman data are not sufficient for positive identification. Our experiments, however, have established that TiS_2 reacts with the $AlCl_3$-NaCl melts.

3.19 Battery Separators

Our study of the effect of chloroaluminate melts on Nafion, an $-OSO_3^-$ substituted fluorocarbon polymer of interest as a potential low temperature molten salt battery separator, and on Teflon, a battery seal material, is described in this section. The effect of the $AlCl_3$-LiCl-NaCl melts on the β"-alumina separator is discussed in the following section together with the other aspects of the

$$Na/\beta"\text{-alumina}/SCl_3^+ \text{ in } AlCl_3\text{-LiCl-NaCl}$$

battery.

Nafion film (DuPont), 0.020" thick, and Teflon rod, 1/4" diameter, were digested for 7 days with the samples of ternary $AlCl_3$-LiCl-NaCl melts and binary $AlCl_3$-NaCl melts. Both the slightly acidic (52 mole % $AlCl_3$) melts at 160°C, and very acidic (72 mole % $AlCl_3$) melts at 185°C were used. The experimental details for these experiments are the same as in Section 3.18. The results of the thermal analysis performed on the melts after the experiments are shown in Table 67.

Nafion appeared to withstand the exposure to the $AlCl_3$-NaCl binary melts considerably better than to the $AlCl_3$-LiCl-NaCl ternary melts. The solidus and liquidus temperatures of the two binary melts digested with Nafion did not change from the corresponding values for the melts with Teflon. However, the 72 mole % $AlCl_3$ melt was more strongly discolored of the two. The effect of the two ternary melts on Nafion was more drastic. The solidus temperature of the 52-24-24 mole % melt with Nafion was lower by 10°C than the solidus

TABLE 67

THERMAL ANALYSIS DATA FOR CHLOROALUMINATE MELTS DIGESTED WITH NAFION AND TEFLON

Melt Composition (Mole %)			Solid Sample	Solidus Temperature (°C)	Liquidus Temperature (°C)	Comment	
$AlCl_3$	LiCl	NaCl				Solid Sample	Melt
52.0	24.0	24.0	Nafion	76	111	Lightly discolored	Lightly discolored
52.0	24.0	24.0	Teflon	86	110	Unchanged	Clear
52.0	-	48.0	Nafion	113	153	Lightly discolored	Lightly discolored
52.0	-	48.0	Teflon	109	153	Unchanged	Clear
72.0	14.0	14.0	Nafion	73	151-160	Decomposing	Strongly discolored Turbid
72.0	14.0	14.0	Teflon	86	?	Light gray	Clear
72.0	-	28.0	Nafion	112	149	Discolored	Lightly discolored
72.0	-	28.0	Teflon	111	148	Very light gray	Clear

temperature of the same melt with Teflon (or the pure melt), and by 13°C for the 72-14-14 mole % melt. In the last case Nafion was clearly disintegrating.

It is clear that Nafion cannot withstand the effect of strongly acidic $AlCl_3$-LiCl-NaCl ternary melts at the temperature studied for an extended period of time. It is not clear, however, to what extent the physical properties of Nafion, particularly its electrical conductivity, change by the exposure to the basic melts. Since the $-OSO_3^-$ functional groups in Nafion are readily hydrated, hydration water may be contributing to the problem. A pretreatment of Nafion may improve its resistance towards the binary $AlCl_3$-NaCl melts.

Teflon did not appear to be affected by the 52 mole % $AlCl_3$ melts, and judging by its light discoloring and by the thermal analysis results, was affected very little by the 72 mole % AlCl melts. This indicates that Teflon will probably be able to withstand the effect of chloroaluminate melts at the temperatures used in our experiments for considerably longer periods as well.

3.20 Cell Na/β"-alumina/SCl_3^+ in $AlCl_3$- LiCl-NaCl

The Na/S(IV) cell (3) employs SCl_3^+ dissolved in an $AlCl_3$-LiCl-NaCl melt as a cathode and molten sodium as an anode:

Na/β"-alumina/SCl_3^+ in $AlCl_3$-LiCl-NaCl.

The electrochemical reactions in this cell are schematically represented as

$$Na(I) + e \underset{\text{Discharge}}{\overset{\text{Charge}}{\rightleftharpoons}} Na \qquad (9)$$

$$S \underset{\text{Discharge}}{\overset{\text{Charge}}{\rightleftharpoons}} S(IV) + 4e \qquad (10)$$

To prevent the reduction of Al(III) to metal by sodium, β"-alumina, a solid Na^+ ion conductor, is used as a separator between the molten sodium anode and the chloroaluminate melt. The potential of the Na/β"-alumina electrode in the 63.0-37.0 mole % $AlCl_3$-NaCl melt vs. the Al(III)/Al reference electrode in the NaCl saturated $AlCl_3$-NaCl melt is -1.60 V at 250°C, and the potential of the S(IV)/S_2^{2+} electrode in the 63.0-37.0 mole % $AlCl_3$-NaCl melt vs. the same reference electrode at the same temperature is +2.57 V (3). Therefore, the open circuit voltage of the Na/S(IV) cell at 250°C is 4.2 V. The theoretical energy density of the cell that uses $AlCl_3$-NaCl solvent melt is 666 Wh/kg if the cathode is discharged to the S^{2-} state instead of S(0).

The usual operating temperature range of the Na/S(IV) cell, which employs an $AlCl_3$-NaCl melt as the cathode solvent, is 180-250°C. By substituting an $AlCl_3$-LiCl-NaCl ternary melt for the binary $AlCl_3$-NaCl melt as the cathode solvent, it is possible to lower the low temperature limit of this cell from ca. 160°C to as low as 120°C. This requires the composition of the $AlCl_3$-LiCl-NaCl melt to be close to 50-25-25 mole % in the fully discharged state, and the concentration of $AlCl_3$ not to exceed ca. 60 mole % in the fully charged state (cf. Figure 5). This change of the melt composition during the charging of the cell is due to the transport of the current carrier Na^+ ions through the β"-alumina separator and the subsequent reduction of Na^+ to the metal. The mole ratio of sulfur to chloroaluminate melt, therefore, has to be adjusted so that the concentration of $AlCl_3$ in the cathode melt does not exceed 60 mole % in the fully charged state.

The design of the Na/S(IV) cell is shown in Figure 30. It closely parallels the design of our cell developed for DOE (University of California Subcontract 4502810). The β"-alumina separator was sealed to the Pyrex cell body using Corning 7052 glass - uranium glass graded seal. Tungsten wires were employed as current collectors in both electrode compartments. An aluminum reference electrode was separated from the cathode melt by a thin Pyrex membrane. The construction of the cell is described in more detail elsewhere (3). Three cells of identical design were tested.

Our first cell employed a β-alumina separator tube, 10 mm O.D. and 60 mm long (obtained from Dr. A. Pelton, University of Montreal). Its maximum theoretical coulombic capacity was 1.5 Ah. The cell was baked under vacuum at 350°C for 14 days, and sodium metal (DuPont, reagent grade), filtered in vacuum through Pyrex wool, was introduced into the anode compartment. To improve the wetting of the separattor by sodium, the baking was continued for three days before adding the cathode mixture, which consisted of elemental sulfur and the 50.6-24.7-24.7 mole % $AlCl_3$-LiCl-NaCl melt. The open circuit voltage of the cell in the discharged state, at the beginning of the first charging cycle was 3.55 V at 150°C. The charging current density was 1.5 mA/cm of β-alumina. Before the end of the first charging cycle, the β-alumina separator shorted out, and the testing of the cell had to be terminated. The cause of the separator failure was not clear.

The second cell employed a larger β"-alumina separator tube, 15 mm O.D. and 200 mm long (Cerametec). This cell had a theoretical coulombic capacity of 4.5 Ah. It was baked out in the same way as the first cell and loaded

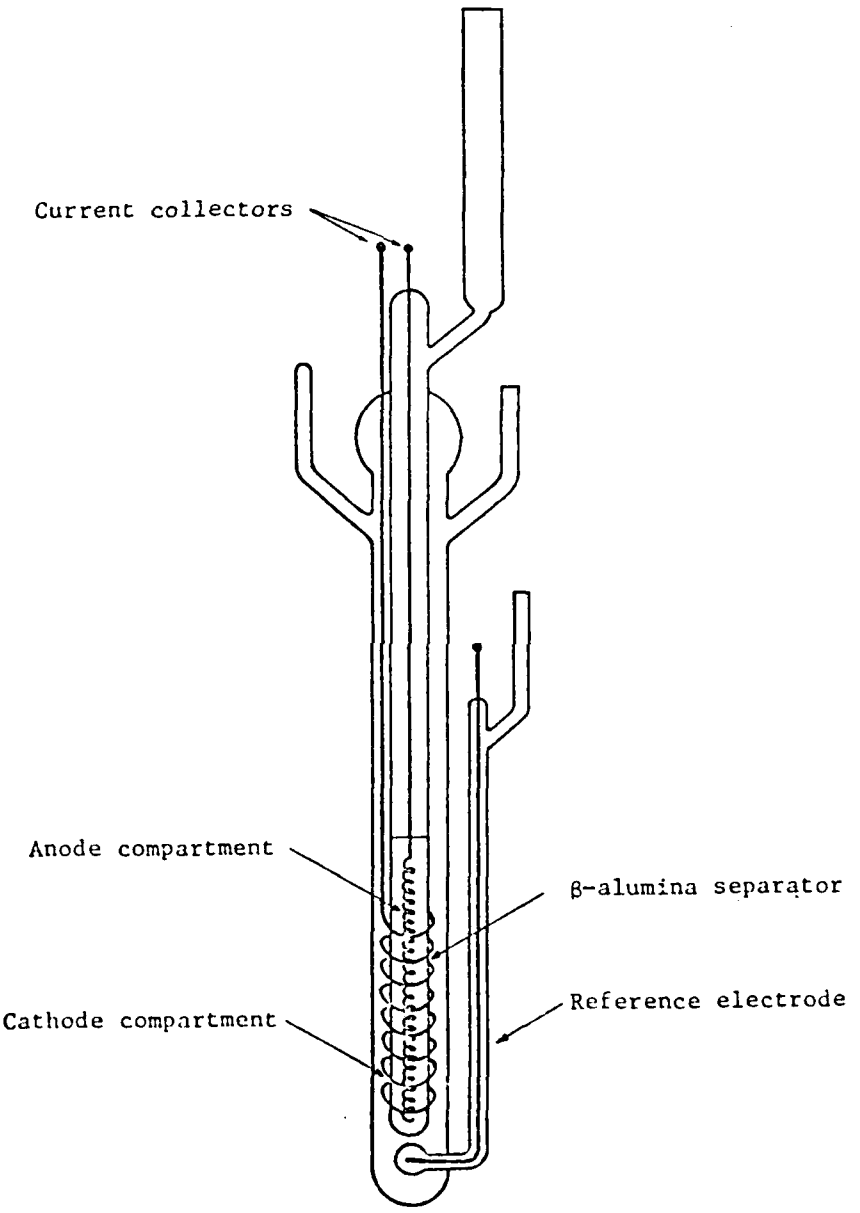

Figure 30. Low Temperature molten salt cell.

with the filtered sodium metal and the sulfur-50.6-24.7-24.7 mole % $AlCl_3$-LiCl-NaCl melt mixture. Its open circuit voltage in the discharged state, before the beginning of the first charging cycle, was 3.35 V at 225°C. The charging current density was 1 mA/cm^2.

The second cell also shorted out well before the end of the first charging cycle. The β"-alumina - Corning 7052 glass seal and the Corning 7052 glass itself showed a network of very fine cracks. The mechanical strength of the Corning 7052 glass, removed from the battery, appeared to be very low.

The third cell, in contrast to the previous two, was prepared in the charged state. The cell employed a β"-alumina separator tube, 13.8 mm O.D. and 170 mm long (from British Rail), and had a theoretical coulombic capacity of 3.04 Ah. It was loaded with a mixture of SCl_3AlCl_4 and the 60.0-32.3-7.7 mole % $AlCl_3$-LiCl-NaCl melt. The theoretical composition of the solvent melt in the cell discharged to the S(0) state was 50.6-24.7-24.7 mole % $AlCl_3$-LiCl-NaCl. In order to avoid the contact between the cathode melt and the Corning 7052 sealing glass, which had sustained damage in the previous cell, the melt level in the third cell was well below the β"-alumina-glass seal.

The open circuit voltage of the third cell was 4.02 V at 120°C. To condition the β"-alumina to the Li^+ ions, the cell was maintained at this temperature for 72 hours before initiating the discharge. It was discharged at current densities of 0.1 to 3.0 mA/cm^2 at temperatures from 120 to 180°C. No problems were observed during the discharge. Once again, however, the β-alumina separator failed during the first charging cycle, and the cell shorted out. The examination of the β"-alumina tube revealed several cracks and numerous small damage spots. Some damage of the cell Pyrex body was also apparent.

Our results clearly indicate that β"-alumina in the Na/SCl_3^+ cell which contains LiCl as a component of the cathode melt, is cracked by the charging process. No similar problems have been encountered with β"-alumina in Na/SCl_3^+ cells which utilize the $AlCl_3$-NaCl binary melt as the cathode solvent (3). On the other hand, the same problem has been reported for cells which employ molten $LiNO_3$ as the cathode (39). Therefore, the problem is clearly due to the presence of LiCl in our cell, i.e., to the diffusion of Li^+ ions through the β"-alumina separator and/or the reduction of Li^+ to Li(0) on the β"-alumina-molten sodium interface. It is known, however, that it is possible to exchange Na^+ ions in the β"-alumina by Li^+ ions (40). Thus the damage is probably caused by the lithium metal formed during the charging of the cell and not by the diffusion of the Li^+ ions.

3.21 Thermal Cell Na/Nafion/SCl_3^+ in $AlCl_3$-LiCl-NaCl

The cell Na/β"-alumina/SCl_3^+ in $AlCl_3$-LiCl-NaCl cannot be successfully charged due to the attack of lithium on the β"-alumina separator (Section 3.20). This cell, however, still can be used as a primary molten salt (thermal) cell. Its discharge current density is limited by the polarization at the β"-alumina/melt and/or β"-alumina/sodium interfaces, and by the resistivity of β"-alumina itself. Thus a thermal cell which employs another separator may be attractive.

Nafion is reasonably compatible with binary $AlCl_3$-NaCl melts containing 50-70 mole % AlCl, as well as with ternary $AlCl_3$-LiCl-NaCl melts which are not excessively acidic, i.e., which contain considerably less than 70 mole % $AlCl_3$ (Section 3.19). Since Nafion is a Teflon based polymer, and since Teflon reacts with molten sodium at sufficiently high temperatures (>250°C), the reactivity of Nafion towards molten sodium was also of concern. Our tests have indicated that Nafion is able to withstand the attack of molten sodium at temperatures below 150°C for at least 24 hours, which is a sufficiently long time for thermal cell applications.

The design of the thermal cell Na/Nafion/SCl_3^+ in $AlCl_3$-LiCl-NaCl melt is shown in Figure 31. The cell body was constructed of Pyrex O-ring joints with a tungsten wire current collector sealed in each electrode compartment. A 0.020" thick Nafion film (DuPont), dried under vacuum at 150°C for 7 days before use, was sealed between the two electrode compartments with the aid of a Teflon O-ring. The cell was held together with a screw clamp (not shown in the figure). Sodium, SCl_3AlCl_4 and the $AlCl_3$-LiCl-NaCl melt were introduced into the cell, and the cell was sealed under vacuum.

Two thermal cells prepared as described above have been tested. In the first cell, an air leak occurred in the anode compartment before the operating temperature of 140°C was reached. The cell never approached its expected open circuit voltage of 4.0-4.2 V. Its voltage remained very low and unstable, never exceeding 0.9 V. Upon terminating the experiment, it was found that the sodium surface was coated with an oxide layer, and therefore sodium never established good contact with Nafion. It was not clear, however, whether the Nafion surface was chemically attacked by sodium as well.

The open circuit voltage of the second cell was also below the expected value of 4.0-4.2 V, as well as strongly time dependent. After the cell reached its operating temperature of 140°C, its voltage was 3.12 V, steadily decreasing to 1.32 V and finally, after one hour, to 0.20 V. After 20 hours,

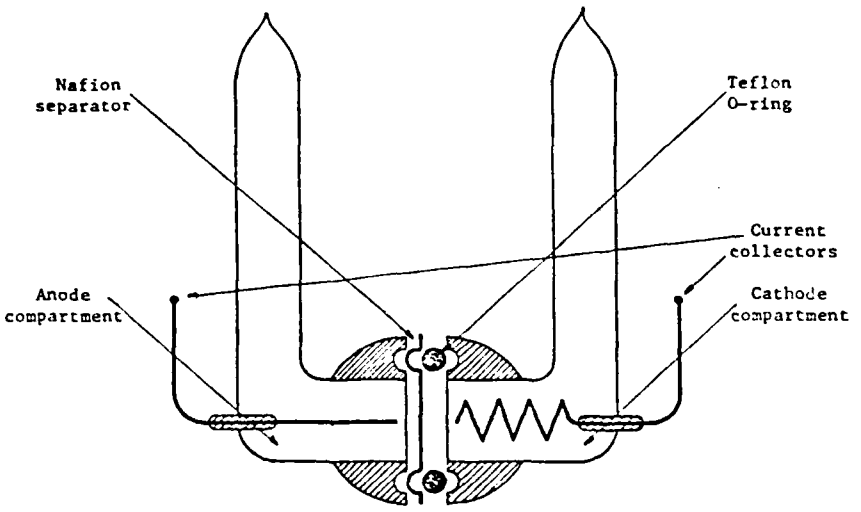

Figure 31. Thermal Cell Na/Nafion/SCl_3^+ in $AlCl_3$-LiCl-NaCl.

however, the cell open circuit voltage was as high as 3.70 V. The cell polarization stayed so high, however, that it was impossible at any time during the experiment to discharge the cell at currents even as low as 0.1 mA/cm^2. No sealing problems and no formation of sodium oxide were encountered in the second experiment, and the examination of the Nafion surface after the experiment revealed that sodium was in good contact with Nafion. Therefore, the variable open circuit voltage and the high resistivity of Nafion indicate that the Nafion surface was probably chemically attacked by the molten sodium.

Based on our preliminary results, Nafion does not appear to be promising for use as a separator in the Na/SCl_3^+ in $AlCl_3$-LiCl-NaCl thermal cell.

3.22 Cyclic Voltammetry of $AlCl_3$-$SbCl_3$-NaCl System

When NaCl is added to the $AlCl_3$-$SbCl_3$ melts, the Cl^- ions from NaCl react with molecular Al_2Cl_6 to form $AlCl_4^-$ and $Al_2Cl_7^-$ ions. Thus the addition of NaCl also indirectly affects the equilibrium between Al_2Cl_6 and $SbCl_3$ (Reaction 5, Section 3.12). Our cyclic voltammetry studies, therefore, were performed on a range of melt compositions, from the saturated $SbCl_3$-NaCl melt ($AlCl_3$=0.0 mole %) to the 10.0-85.0-5.0 mole % $AlCl_3$-$SbCl_3$-NaCl, i.e. over the $AlCl_3$/NaCl mole ratio of 0.0 to 2.0.

The design of our voltammetry cells is shown in Figure 32. Since antimony metal alloys with platinum, only tungsten and glassy carbon electrodes of ~0.1 cm^2 area were utilized as working electrodes. A tungsten wire spiral of ~1.0 cm^2 area was used as a counter electrode. A second tungsten spiral was used as a quasi-reference electrode in the initial series of experiments. Its potential was determined vs. an Al/Al(III) reference electrode which consisted of an aluminum wire immersed in a 63.0-37.0 mole % $AlCl_3$-NaCl melt separated from the $SbCl_3$-containing melt by a thin Pyrex membrane. Since the potential of the quasi-reference electrode was not sufficiently stable during the measurements close to the cathodic limit of the melt, this electrode was subsequently replaced by an antimony reference electrode. All the potentials in this section are reported vs. the Al(III)/Al reference electrode in the 63.0-37.0 mole % $AlCl_3$-NaCl melt. The temperature range studied was from 78 to 220°C, and the scanning rate was from 1 to 200 mV/sec. The results obtained on the tungsten and glassy carbon electrodes were quite similar.

The saturated binary $SbCl_3$-NaCl melt ($AlCl_3$= 0.0 mole %) was the most

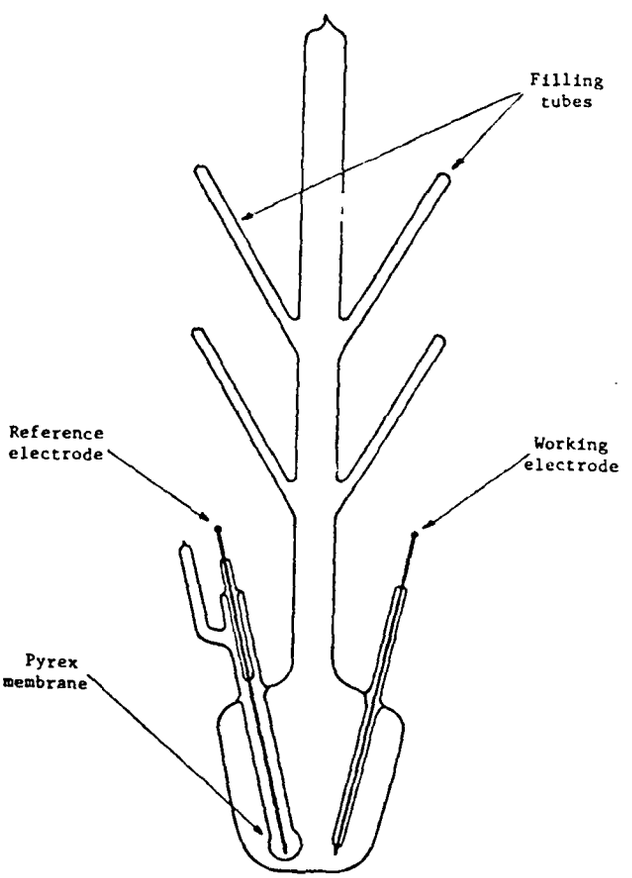

Figure 32. Cyclic Voltammetry Cell.

basic melt studied. The actual composition of the melt was not known. The estimated solubility of NaCl in $SbCl_3$ in the absence of $AlCl_3$ in the temperature range studied, however, is well below 0.5 mole % (32). The cyclic voltammogram of this melt at the tungsten electrode is shown in Figure 33A. The cathodic region of this melt at the same electrode is shown in more detail in Figure 33B, and the anodic region of this melt on the glassy carbon electrode in Figure 33C. The scan rates are noted in the figure captions.

The potential of the antimony electrode in the saturated melt is +600 mV vs. the Al(III)/Al reference electrode. The reduction of Sb(III) occurs at +520 mV. On oxidation, the antimony stripping wave is followed by a broad wave with the position dependent on the scanning rate and temperature. The anodic behavior of the melt is highly irreversible. A broad wave at ~+1700 mV is observed before the anodic limit of the melt is reached at ~+1850 mV. Either, or both, of the processes,

$$Sb(III) \rightarrow Sb(V) + 2e \qquad (11)$$

or

$$Cl^- \rightarrow 1/2Cl_2 + e \qquad (12)$$

is probably taking place here.

The cyclic voltammogram of the 5.0-90.0-5.0 mole % $AlCl_3$-$SbCl_3$-NaCl melt at the tungsten electrode is shown in Figure 34A. The potential of the antimony electrode in this melt is +830 mV vs. the Al(III)/Al reference electrode. A new reduction wave at +680 mV is observed in this melt. This wave, shown in more detail in Figure 34B, does not appear in the saturated melt. Thus it is tentatively assigned to the reduction of Sb(III) associated with $AlCl_3$. The corresponding stripping wave is observed at +1040 mV.

When the cyclic voltammetric scan of the 5.0-90.0-5.0 mole % $AlCl_3$-$SbCl_3$-NaCl melt is reversed at a less negative potential, it becomes apparent that the stripping of antimony is considerably more complex (Figure 34C). Three distinct stripping waves at +630, +670 and +730 mV, as well as another broad oxidation wave at +950 mV are observed in addition to the already described waves. These new features of the voltammogram are difficult to interpret. The simultaneous deposition of aluminum and antimony is unlikely in view of the ~600 mV difference in the reduction potentials of the Al(III) and Sb(III). On the other hand, no alloy of antimony and tungsten has been reported to date in the literature. The presence of the lower oxidation states of antimony, stabilized by $AlCl_3$ (41), may offer a plausible explanation for the number of stripping peaks.

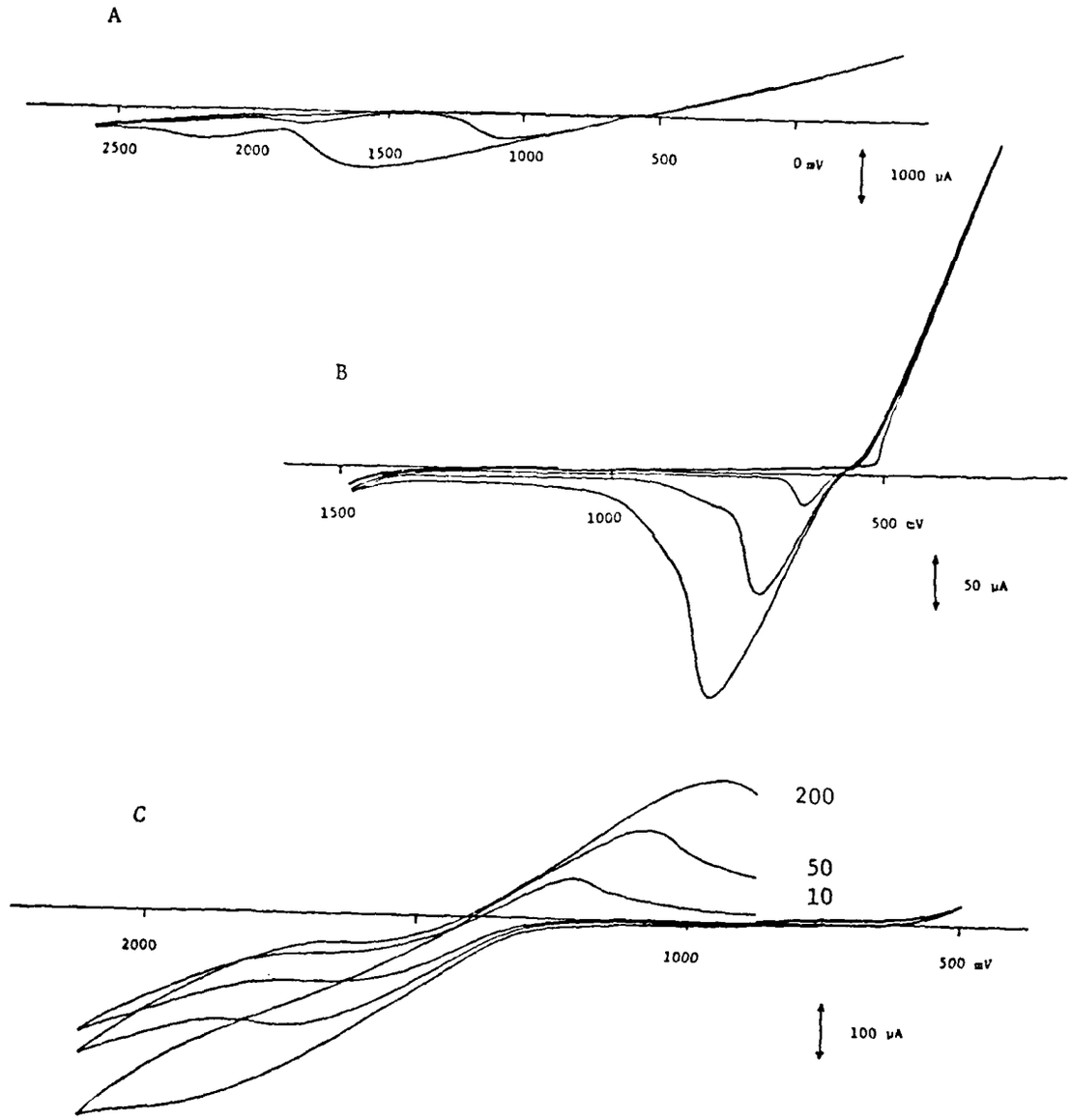

Figure 33. Cyclic Voltammograms of $SbCl_3$-NaCl Saturated Melt. Electrodes: tungsten (A,B) and glassy carbon (C). Scanning rate: 50 mV/sec (A,B) and 10, 50 and 200 mV/sec (C). Temperature: 140°C.

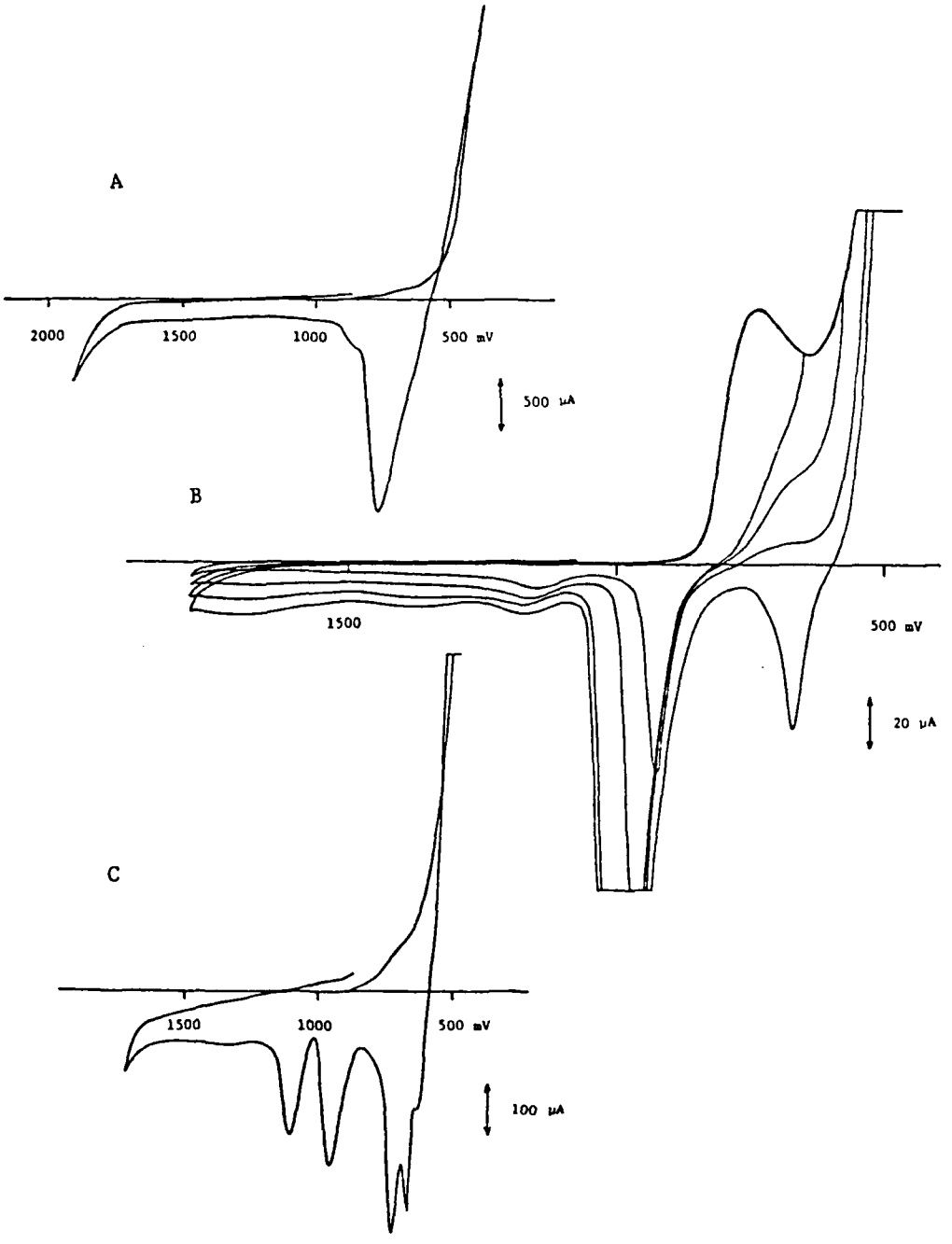

Figure 34. Cyclic Voltammograms of 5.0-90.0-5.0 Mole % $AlCl_3$-$SbCl_3$-NaCl Melt.
Electrode: tungsten. Scanning rate 50 mV/sec.
Temperature: 200°C (A,C) and 118°C (B).

The potential of the antimony electrode in the 10.0-85.0-5.0 mole % $AlCl_3$-$SbCl_3$-NaCl melt is +980 mV *vs.* the Al(III)/Al reference electrode. This represents a shift of as much as 380 mV compared to the potential of the same electrode in the $SbCl_3$-NaCl saturated melt. The cyclic voltammogram of this melt at the tungsten electrode is shown in Figure 35. It exhibits two reduction waves at +790 and +650 mV before the cathodic limit of this melt is reached. The position of the second wave is reasonably close to the position of the single reduction wave in the 5.0-90.0-5.0 mole % $AlCl_3$-$SbCl_3$-NaCl melt. The corresponding stripping waves are observed at +1160 and +1240 mV.

From the standpoint of the application of the $AlCl_3$-$SbCl_3$-NaCl melts as the cathode material in the Na/Sb(III) cell, the above results may be summed up as follows. It is not clear whether the anodic limit of these melts is due to the chlorine evolution or the oxidation of Sb(III) to Sb(V), *i.e.* whether the Na/Sb(III) cell may be charged to the Sb(V) state or not. The addition of $AlCl_3$ to the $SbCl_3$-NaCl saturated melt results in a positive shift of the antimony electrode potential of 380 mV. Thus the open circuit voltage of the Na/Sb(III) cell is also expected to be dependent on the acidity of the cathode melt, *i.e.* to be higher in the presence of an excess of $AlCl_3$.

3.23 Cell Na/β"-alumina/$AlCl_3$-$SbCl_3$-NaCl

The cell Na/Sb(III) employs molten sodium as an anode and $SbCl_3$ in the form of $AlCl_3$-$SbCl_3$-NaCl melt as a cathode:

$$Na/\beta\text{"-alumina}/AlCl_3\text{-}SbCl_3\text{-NaCl}.$$

The electrochemical reactions in this cell are schematically represented as:

$$Na(I) + e \underset{\text{discharge}}{\overset{\text{charge}}{\rightleftharpoons}} Na \qquad (13)$$

$$Sb \underset{\text{discharge}}{\overset{\text{charge}}{\rightleftharpoons}} Sb(III) + 3e. \qquad (14)$$

Beta"-alumina separator is used to prevent the reduction of Al(III) and Sb(III) by direct contact with molten sodium. This is the same separator which was utilized in our Na/SCl_3^+ cell (Section 3.20). However, the active material $SbCl_3$ is not a solute in the cathode melt, as was the case with SCl_3^+ in the Na/SCl_3^+ cell. $SbCl_3$ is the most abundant component of the cathode melt in our cell, and its mole fraction in the melt determines the liquidus temperature and other properties of the melt. Since β"-alumina is a Na^+ ion conductor, its use requires the presence of NaCl in the cathode

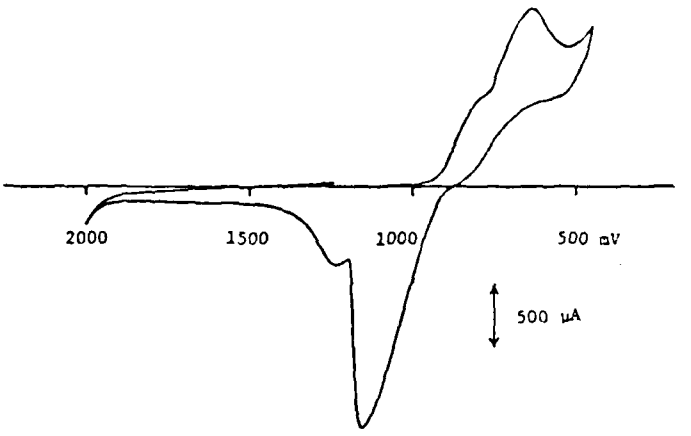

Figure 35. Cyclic Voltammogram of 10.0-85.0-5.0 Mole % $AlCl_3$-$SbCl_3$-NaCl Melt. Electrode: tungsten. Scanning rate: 50 mV/sec. Temperature: 140°C.

melt. Its addition to the $AlCl_3$-SbCl melt does not increase the specific conductivity of the melt, except at temperatures close to the high temperature limit of the melt (Figure 22). The presence of $AlCl_3$ above ~12 mole % in the $AlCl_3$-$SbCl_3$ melt will increase the liquidus temperature of the melt (Figure 17), and thus a high mole fraction of $AlCl_3$ is not desirable in the low temperature Na/Sb(III) cell. The main function of $AlCl_3$ in the melt is to act as a solvent for NaCl, which has only a slight solubility in pure molten $SbCl_3$.

The open circuit voltage of the fully charged Na/Sb(III) cell at 210°C is 3.30 V. The potential of the Sb(III)/Sb electrode in the $AlCl_3$-$SbCl_3$-NaCl melt with the $AlCl_3$/NaCl mole ratio greater than 1.0 vs. the Al(III)/Al reference electrode in the 63-37 mole % $AlCl_3$-NaCl melt at the same temperature is +0.95 V (Section 3.14). The theoretical energy density of this cell is difficult to estimate. Since our cell utilizes $SbCl_3$ as a solvent as well as the active cathode material, its theoretical capacity is determined by the number of moles of NaCl that the melt is able to accommodate before the precipitation of NaCl on the β"-alumina surface causes excessive polarization. This precipitation, in turn, is a function of the discharge current density. Thus the maximum energy density of the Na/Sb(III) cell has to be determined experimentally.

The design of the Na/Sb(III) cell is the same as used for the Na/SCl_3^+ cell. It is shown in Figure 30 and discussed in Section 3.20. The β"-alumina separator tube (from British Rail) was 13.8 mm in diameter and 170 mm long. The composition of the cathode melt in the fully charged state was 20.0-75.0-5.0 mole % $AlCl_3$-$SbCl_3$-NaCl.

The discharge curve of the Na/Sb(III) cell exhibits two plateaus. During the discharge, the cathode melt gains 3 moles of Na^+ for every mole of reduced Sb(III). After 5 mole % of Sb(III) are reduced to the metal, the melt composition becomes 18.2-63.6-18.2 mole % $AlCl_3$-$SbCl_3$-NaCl, i.e. the melt becomes neutral with respect to $AlCl_3$. At that point the cathode potential in the cell decreases by 350 mV from 0.95 V to +0.60 V, and, therefore, the open circuit voltage of the cell decreases from 3.30 V to 2.95 V. This cathode potential decrease is in agreement with the potential decrease of 380 mV predicted by our voltammetry measurements (Section 3.22). The theoretical coulombic capacity of the first plateau in our cell was 1.62 Ah. When the discharge of the cell is continued beyond the end of the first plateau, the precipitation of NaCl will start as the melt becomes saturated

with it. The discharge of the cell can proceed far beyond the neutral point, however, depending on the discharge current density and temperature, i.e. depending on the deposition rate of NaCl on the β"-alumina surface. For example, at 10 mA/cm^2 current density and 210°C the second plateau in our cell is 55-65 % of the first plateau. At this point the cell polarization becomes very high and the cell voltage starts to decrease rapidly. A typical charge-discharge cycle of the Na/Sb(III) cell is shown in Figure 36. On charging, the two plateaus are again observed, as the melt composition changes from saturated to acidic. Overcharging the cell to Sb(V) state is not practical due to the formation of chlorine. The yellow-green color of the melt in the overcharged cell is probably caused by the presence of molecular Cl_2 dissolved in the $AlCl_3$-$SbCl_3$-NaCl melt.

The Na/Sb(III) cell has been extensively studied prior to our work by the ESB Technology Company (42). The ESB cell also employs β"-alumina as the separator and the $AlCl_3$-$SbCl_3$-NaCl melt as the cathode. The main difference between our cell and the ESB cell is in the composition of the two cathode melts. The ESB cell employs in the charged state an amount of $SbCl_3$, equivalent to the theoretical cell capacity, dissolved in the acidic $AlCl_3$-NaCl melt. All the Sb(III) is reduced to metal in this cell in the fully discharged state, and the cathode melt becomes a saturated $AlCl_3$-NaCl melt, with the excess NaCl precipitating in the cathode compartment of the cell. Since in our cell $SbCl_3$ is used both as the active cathode material and as a component of the solvent melt, only a fraction of Sb(III) is reduced to metal in the fully discharged state. This difference in the cathode melt composition of the two cells has several consequences.

The discharge voltage of our cell throughout the most of its operating range is 350 mV higher than the discharge voltage of the ESB cell at the same current density, even though the open circuit voltage of the two fully charged cells is the same. For example, at the discharge current density of 10 mA/cm^2 and at 210°C, the discharge voltage of our cell is 2.95 V, compared to 2.60 V for the ESB cell. In effect, most of the operating region of the ESB cell corresponds to the second plateau of our cell. This is schematically illustrated in Figure 37. It should be noted that since the horizontal axis in this figure is on a relative scale, the figure does not compare the actual coulombic capacities of the two cells.

Our cell can be operated in the 120-220°C temperature range, which is considerably lower than the typical temperature range of the ESB cell

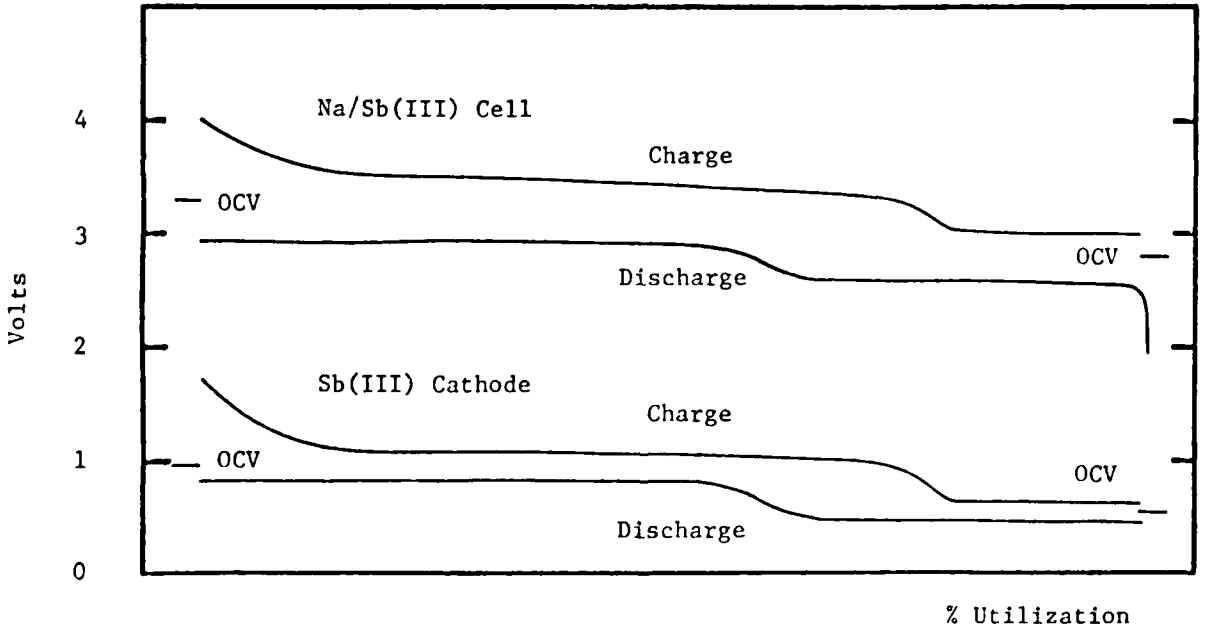

Figure 36. Typical Charge-Discharge Cycle for Na/β"-alumina/$AlCl_3$-$SbCl_3$-NaCl Cell.
Current density: 10 mA/cm^2; Temperature: 210°C.

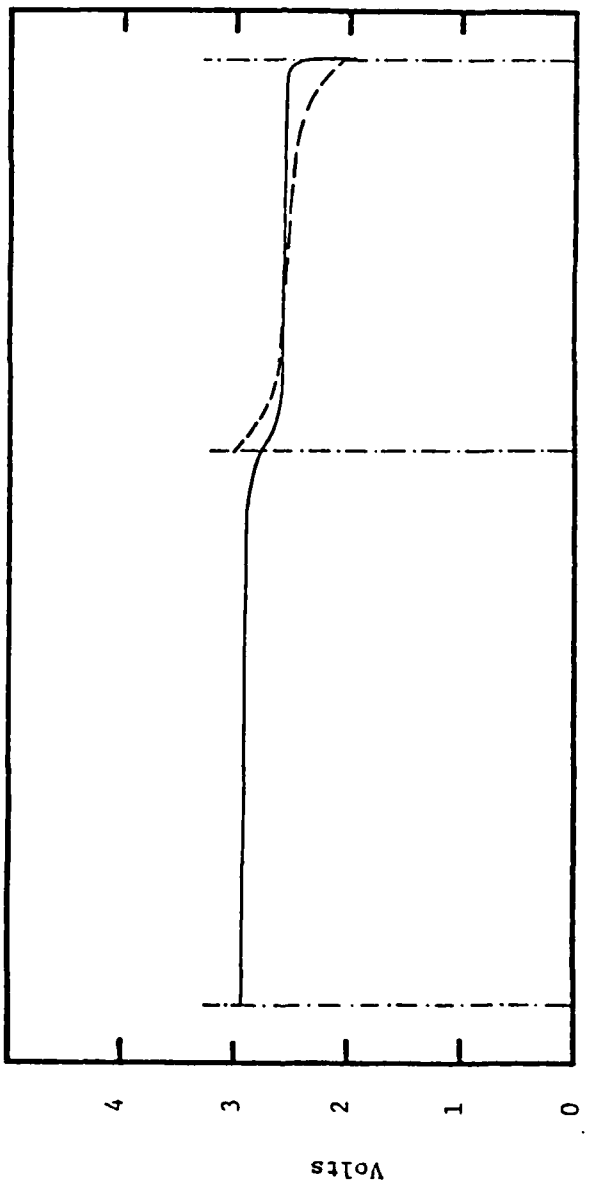

Figure 37. Schematic Comparison of Discharge Plateaus of Present Na/Sb(III) Cell (Full Line) and ESB Cell (Dashed Line). Current density: 10 mA/cm^2; temperature: 210°C.

(210-220°C). This is the result of the lower liquidus temperatures of the $SbCl_3$-rich cathode melt in our cell.

The discharge voltage in our cell does not decrease appreciably with the degree of discharge in either of the two plateaus. This is due to the excess of $SbCl_3$ present in our cathode melt even in the discharged state.

The coulombic discharge capacity of the first plateau of our cell is approximately independent of the discharge current density since the cathode melt is acidic throughout the first plateau, and therefore the solubility of NaCl in the melt does not pose a problem. In the ESB cell, however, in which the cathode melt is saturated with NaCl throughout most of the operating range, the polarization due to the precipitation of NaCl on the β"-alumina surface determines the cell capacity. Thus the coulombic discharge capacity of the ESB cell will decrease at higher current densities (cf. Figure 4-11 in (42)).

3.24 Cell $Na/\beta"$-alumina/SCl_3^+ in $FeCl_3$-LiCl-NaCl

The $FeCl_3$-LiCl-NaCl melts cannot be used as the cathode solvent melt in rechargeable cells which employ β- or β"-alumina as a separator. As discussed in Section 3.20, the analogous cell $Na/\beta"$-alumina/SCl_3^+ in $AlCl_3$-LiCl-NaCl, which utilizes $AlCl_3$ instead of $FeCl_3$ can be successfully discharged. It cannot be charged, however, since the β"-alumina is attacked by the lithium metal formed by the reduction of Li^+ ions during the charging of the cell. This results in the failure of the β"-alumina separator. The same problem has been also encountered in the cells which employ molten $LiNO_3$ as the cathode (39), and will be encountered in any cell which employs a lithium salt as a constituent of the cathode melt, including the $FeCl_3$-LiCl-NaCl melt studied in this project. If LiCl is eliminated as a constituent of the $FeCl_3$-LiCl-NaCl cathode melts, however, the resulting binary $FeCl_3$-NaCl melts fall outside the scope of the present project due to high liquidus temperatures. Other $FeCl_3$-based melts may have a potential for the rechargeable cell use. Other Na^+-ion conductors which are stable in the presence of lithium may be available in the future.

4. CONCLUSIONS

Based on the results of our study of eighteen molten salt systems presented in this report, four low temperature molten salt systems emerge as the most promising solvents for battery applications: $AlCl_3$-LiCl-NaCl, $AlCl_3$-$SbCl_3$-NaCl, $FeCl_3$-LiCl-NaCl and, possibly, $AlCl_3$-Me_4NCl-NaCl.

The addition of LiCl to the binary $AlCl_3$-NaCl melts, the most widely used of the chloroaluminate melts, significantly lowers the liquidus temperature of these melts. The specific conductivity of the $AlCl_3$-LiCl-NaCl melts is not substantially lower than the conductivity of the $AlCl_3$-NaCl melts. However, the β"-alumina separator in the cells which employ an $AlCl_3$-LiCl-NaCl melt consistently failed during the charging of these cells. This failure appears to be due to the attack of lithium metal on the β"-alumina separator. Thus our results show that although the cell, Na/β"-alumina/SCl_3^+ in $AlCl_3$-LiCl-NaCl, can be discharged, it cannot be successfully charged. Until an alternate separator, compatible with the the lithium metal, is developed, the $AlCl_3$-LiCl-NaCl melts do not hold promise for use as cathode solvent melts in the rechargeable molten salt cells. They can be employed, however, in the primary (thermal) cells which utilize the β"-alumina or some other separator.

The $AlCl_3$-$SbCl_3$-NaCl system is promising for use in batteries which employ $SbCl_3$ as a cathode material. The liquidus temperatures in this system are low. The specific conductivity of the $AlCl_3$-$SbCl_3$-NaCl system is substantially lower than the conductivity of the $AlCl_3$-NaCl system, as the addition of NaCl to the $AlCl_3$-$SbCl_3$ does not produce the desired increase in the conductivity of these melts. The Na^+ ion, however, is still a necessary constituent of these melts when they are to be employed with the β"-alumina separators. Our results for the cell, Na/β"-alumina/$AlCl_3$-$SbCl_3$-NaCl demonstrate that this cell has a higher voltage by 350 mV as well as a flatter discharge plateau as a function of percent discharge, and is capable of operating at a lower temperature than the ESB cell which utilizes the same constituents. This is due to our use of $SbCl_3$ as the most abundant component of the cathode melt and to the operation of our cell at more acidic cathode melt compositions.

The specific conductivity of the two $FeCl_3$-based molten salt systems is higher than the conductivity of the $AlCl_3$-LiCl-NaCl system. The liquidus temperatures in the $FeCl_3$-LiCl-NaCl system, the lower melting of the two $FeCl_3$-containing systems, appear to be in the same range as the liquidus

temperatures in the $AlCl_3$-NaCl melts. The $FeCl_3$-LiCl-NaCl system, therefore, appeared to be quite promising for use in batteries which employ $FeCl_3$ as the cathode material. Due to the incompatibility of β"-alumina with lithium, however, the $FeCl_3$-LiCl-NaCl melts do not hold promise for use as cathode melts in the rechargeable cells which employ β"-alumina as the separator.

Based on the low liquidus temperatures and the chemical stability of the $AlCl_3$-Me_4NCl-NaCl system, this is probably the most promising system of the $AlCl_3$-R_4NCl type. The decision of the sponsoring agency, however, was to terminate the study of this molten salt system.

REFERENCES

1. For an overview of advanced batteries, see D. W. Murphy, J. Broadhead and B. C. H. Steele, eds., Materials for Advanced Batteries, Plenum Press, 1980.

2. D. M. Ryan and L. C. Bricker, Report AFAPL-TR-77-12, April 1977.

3. G. Mamantov, R. Marassi, M. Matsunaga, Y. Ogata, J. P. Wiaux, and E. J. Frazer, J. Electrochem. Soc., 127, 2319 (1980).

4. G. J. Janz, C. B. Allen, N. P. Bansal, R. M. Murphy and R. P. T. Tomkins, Report NSRDS-NBS61, Part 2, April 1979.

5. G. Mamantov and R. A. Osteryoung, in Characterization of Solutes in Non-aqueous Solvents, G. Mamantov, ed., Plenum Press, N.Y., 1978.

6. H. L. Chum, V. R. Koch, L. L. Miller and R. A. Osteryoung, J. Amer. Chem. Soc., 97, 3264 (1975).

7. V. R. Koch, L. L. Miller and R. A. Osteryoung, J. Amer. Chem. Soc., 98, 5277 (1976).

8. C. L. Hussey, J. C. Nardi, L. A. King, and J. K. Erbacher, J. Electrochem. Soc., 124, 1451 (1977); C. L. Hussey, private communcation.

9. R. A. Carpio, L. A. King, R. E. Lindstrom, J. C. Nardi, and C. L. Hussey, J. Electrochem. Soc., 126, 1644 (1979).

10. G. J. Janz, C. B. Allen, J. R. Downey, Jr., and R. P. T. Tomkins, ERDA Report TID 27163-P1 and P2, July 1976.

11. P. V. Clark, Report SC-R-68-1680, vol. 1 and 2, 1968.

12. W. P. Brennan, B. Miller, and J. C. Whitewell, Proc. 2nd Symp. Analytical Calorimetry R. S. Porter, ed., Plenum Press, New York, 1970.

13. J. L. McNaughton and C. T. Mortimer, in IRS, Physical Chemistry, Series 2, Vol. 10, Butterworths, London, 1975, reprinted by the Perkin Elmer Co.

14. E. Pella and M. Nebuloni, J. Thermal Anal., 3, 229 (1971).

15. J. Kendall, E. D. Crittenden, and H. K. Miller, J. Amer. Chem. Soc., 45, 976 (1923).

16. E. M. Levin, J. F. Kinney; R. D. Wells, and J. T. Benedict, J. Res. Nat. Bur. Stand., 78A, 505 (1974).

17. G. Jones and B. C. Bradshaw, J. Amer. Chem. Soc., 55, 1790 (1933).

18. R. A. Carpio, personal communication.

19. R. A. Carpio, F. C. Kibler, Jr., L. A. King, W. Brokne:, K. Tørklep and H. A. Øye, Ber. Bunsenges. Phys. Chem., 85, 31 (1981).

20. R. A. Robinson and R. H. Stokes, Electrolyte Solutions, 2nd ed., Butterworths, London, 1970.

21. R. Midorikawa, J. Electrochem. Soc. Japan, 23, 72, 127 (1955).

22. M. D. Pyatunin, A. V. Storonkin and I. V. Vasil'kova, Vestnik Leningrad. Univ., Ser. Fiz. Khim., 165 (1973).

23. M. A. Kuvakin, L. I. Talanova, and A. I. Kulikova, Russ. J. Inorg. Chem., 18, 602 (1973).

24. C. T. H. M. Cronenberg and J. W. Van Spronsen, Z. Anorg. Allg. Chem., 354, 103 (1967).

25. V. I. Mikheeva, S. M. Arkhipov, and T. V. Revzina, Russ. J. Inorg. Chem., 13, 884 (1968).

26. E. Ya. Gorenbein, Zhur. Obshch. Khim., 18, 1427 (1948); 19, 1978 (1949).

27. J. A. Plambeck, J. Chem. Eng. Data, 12, 77 (1967).

28. J. C. Goodrich, F. M. Goyan, E. E. Morse, R. G. Preston, and M. B. Young, J. Am. Chem. Soc., 72, 4411 (1950); T. R. Griffiths, J. Chem. Eng. Data, 8, 568 (1963); M. B. Reynolds and C. A. Kraus, J. Am. Chem. Soc., 70, 1709 (1948).

29. Handbook of Chemistry and Physics, 57th edition, Cleveland, 1977, p. C-105.

30. L. A. Nisel'sen, Z. N. Orshanskaya and K. V. Tret'yakova, Zh. Neorg. Khim., 19, 1060 (1974).

31. R. Huglen, G. Mamantov, G. M. Begun and G. P. Smith, J. Raman Spectr., 9, 188 (1980).

32. Gmelin's Handbuch der Anorganischen Chemie, 8 Aufl. Bd. 18B (Antimon), 1949.

33. I. S. Morozov and D. Ya. Toptygin, Zhur. Neorg. Khim., 2, 1233 (1957).

34. A. V. Storonkin, I. V. Vasil'kova, and M. D. Pyatunin, Rus. J. Phys. Chem., 47, 25 (1973).

35. M. D. Pyatunin, A. V. Storonkin, and I. V. Vasil'kova, Vestnik Leningrad Univ., Ser. Fiz Khim., 165 (1973).

36. P. I. Fedorov and V. M. Yakunina, Russ. J. Inorg. Chem., 8, 1099 (1963).

37. V. N. Arbekov and E. S. Petrov, Izv. Sibirsk. Otd. ANSSSR, Ser. Khim. Nauk, 133 (1968).

38. G. H. Newman and L. P. Klemann, J. Electrochem. Soc., 127, 2097 (1980).

39. M. F. Roche, Fifth U.S. DOE Battery and Electrochemical Contractors' Conference, Arlington, Virginia, December 1982, Abstracts, p. 285.

40. Y.-F, Y. Yao and J. T. Kummer, J. Inorg. Nucl. Chem., 29, 2453 (1967).

41. M. Sorlie and G. P. Smith, J. Inorg. Nucl. Chem., 43, 931 (1981).

42. ESB Technology Company, Development of the Sodium - Antimony Trichloride Battery For Utility Applications, Final Report, Yardley, Pennsylvania, February 1980.

APPENDIX

Reprinted from The Journal of Physical Chemistry, 1982, 86, 4598.

Electrical Conductivity of Molten Mixtures of Antimony(III) Chloride–Aluminum Chloride and Antimony(III) Chloride–Aluminum Chloride–Sodium Chloride

Cedomir Petrovic, Gleb Mamantov,*[1a]

Department of Chemistry, University of Tennessee, Knoxville, Tennessee 37996-1600

Morten Sorlie,[1b] M. H. Lietzke, and G. Pedro Smith*

Chemistry Division, Oak Ridge National Laboratory, Oak Ridge, Tennessee 37830 *(Received: April 22, 1982; In Final Form: July 21, 1982)*

The electrical conductivity of $SbCl_3$–$AlCl_3$ mixtures was measured for melts containing 2.5–60.0 mol % $AlCl_3$ at temperatures ranging from 81–224 °C for 2.5 mol % $AlCl_3$ to 189–212 °C for 60.0 mol % $AlCl_3$. These data were accurately represented by the empirical equation $\ln \kappa = A_1 - A_2T^{-1} - A_3T^{1/10}$, where κ is the specific conductivity and A_1, A_2, and A_3 are adjustable parameters. For melts containing 2.5–30.0 mol % $AlCl_3$, deviations from Arrhenius behavior were large, and in the range 2.5–10.0 mol % $AlCl_3$ the conductivity passed through a maximum T_m as a function of temperature. At 2.5 mol % $AlCl_3$ the maximum occurred at 180 °C with a specific conductivity of 0.001 07 S cm^{-1}. Isothermal conductivity–composition curves passed through maxima that shifted from 0.042 S cm^{-1} and 25 mol % $AlCl_3$ at 100 °C to 0.092 S cm^{-1} and 35 mol % $AlCl_3$ at 200 °C. Conductivity as a function of temperature up to about 225 °C was measured for $SbCl_3$–$AlCl_3$–NaCl melts containing 5.0–5.0, 10.0–5.0, and 10.0–10.0 mol % $AlCl_3$ and NaCl, respectively. It was found that at low temperatures the addition of NaCl to a $SbCl_3$-rich $SbCl_3$–$AlCl_3$ mixture results in a substantial conductivity decrease. Although the data for $SbCl_3$–$AlCl_3$ melts can be interpreted in terms of a Stokesian diffusional transport mechanism, the $SbCl_3$–$AlCl_3$–NaCl data favor the occurrence of a non-Stokesian chloride-exchange transport process in addition to Stokesian conductivity.

Introduction

The electrical conductivity of molten $SbCl_3$–$AlCl_3$ mixtures responds to changes in composition and temperature in ways that are not commonly found in combination. The individual components melt to form nonconducting molecular liquids,[2] and their binary diagram shows no compound formation.[10,11] Nevertheless, prior investigators found substantial ionic conductivity when up to 10 mol % $AlCl_3$ was added to molten $SbCl_3$ at 100 °C.[3] We extended these measurements to higher temperatures and higher $AlCl_3$ concentrations and found that the conductivity reaches large values. We also found that for melts with 10 mol % $AlCl_3$ or less the conductivity passes through a maximum at moderate temperatures and this maximum occurs at progressively lower temperatures as the $AlCl_3$ content diminishes. Finally, when NaCl is added to melts containing 10 mol % $AlCl_3$ and less, the conductivity decreases substantially despite the small size of the Na^+ ion.

Experimental Section

Antimony(III) chloride (Mallinckrodt, 99% minimum) was purified by melting and mixing with Sb metal in order to reduce any Sb(V), and with Sb_2O_3 to remove some volatile chloride impurities. This was followed by two sublimations at 40 °C. $AlCl_3$ (Fluka, puriss) was purified by sublimation at 120 °C under a dynamic vacuum followed by four to five distillations at 200 °C in evacuated

(1) (a) Analytical Chemistry Division, Oak Ridge National Laboratory (b) Visiting scientist from the University of Tennessee, Knoxville.

(2) Reported values of κ for molten $SbCl_3$ near its melting point span a wide range of values probably because of differing amounts of impurities.[3,9] The least value reported is 8.7×10^{-7} S cm^{-1}. A similar situation holds for molten Al_2Cl_6 for which the least value is 1×10^{-7} S cm^{-1} at 200 °C.[9]

(3) G. Jander and K.-H. Swart, *Z. Anorg. Allg. Chem.*, **299**, 252 (1959).

(4) P. Walden, *Z. Anorg. Allg. Chem.*, **25**, 209 (1900).

(5) Z. Klemensiewicz, *Bull. Int. Acad. Sci. Cracovie*, **6**, 485 (1908); *Z. Phys. Chem.*, **113**, 28 (1924).

(6) Z. Klemensiewicz and Z. Balówna, *Rocz. Chem.*, **10**, 481 (1930); **11**, 683 (1931).

(7) A. G. Davies and E. C. Baughan, *J. Chem. Soc.*, 1711 (1961).

(8) K. Saito, K. Ichikawa, and M. Shimoji, *Bull. Chem. Soc. Jpn.*, **41**, 1104 (1968).

(9) C. R. Boston, S. J. Yosim, and L. F. Grantham, *J. Chem. Phys.*, **51**, 1669 (1969).

(10) J. Kendall, E. D. Crittenden, and H. K. Miller, *J. Am. Chem. Soc.*, **45**, 963 (1923).

(11) L. A. Nisel'son, Z. N. Orshanskaya, and K. V. Tret'yakova, *Russ. J. Inorg. Chem. (Engl. Transl.)*, **19**, 580 (1974).

0022-3654/82/2086-4598$01.25/0

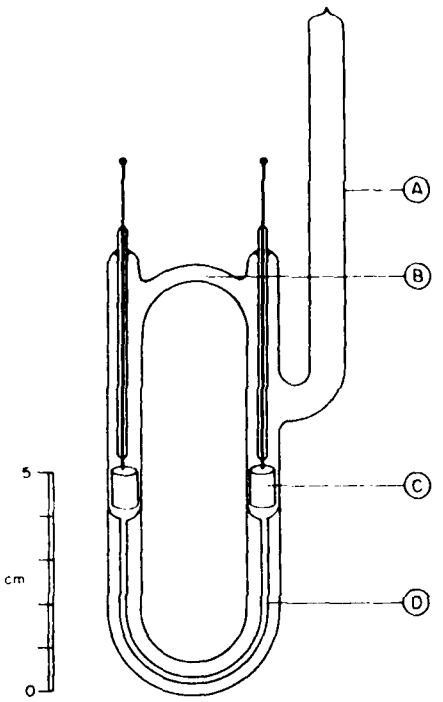

Figure 1. Conductivity cell: (A) filling tube, (B) pressure equalization tube, (C) Pt foil electrodes, (D) capillary.

and sealed Pyrex tubes. Each distillation was terminated with a small pool of undistilled liquid remaining. Both purified compounds were clear, colorless, crystalline materials that melted to give clear, colorless liquids. NaCl (reagent grade) was purified by vacuum drying in the solid state followed by melting and bubbling first HCl and then argon (both high-purity grades) through the melt.

All handling of salts was carried out in an argon-atmosphere glovebox in which both water vapor and oxygen were monitored instrumentally and kept below 1 ppm by continuous circulation of the atmosphere through a purification train. Each sample (6–8 g) was weighed on an analytical balance, then sealed in a Pyrex ampule, melted, and homogenized. The sample was then rapidly frozen to give a uniform solid mixture. In most experiments a complete sample was transferred to the conductivity cell. After evacuation, the filling tube of the cell was sealed off as short as possible so as to reduce the vapor volume. No correction was made or considered necessary for the small change in melt composition due to the fact that the melt and vapor phases have different compositions.

Small-volume capillary conductivity cells with bright platinum foil electrodes were made of Pyrex (Figure 1). They were calibrated at 25 °C with a KCl solution according to the procedure of Jones and Bradshaw.[12] Values of cell constants were between 215 and 265 cm^{-1}, and the measured resistances of the melts were in the 2000–35 000-Ω range. The temperature dependence of the cell constants was calculated to be −0.0007 to −0.000 85 cm^{-1} deg^{-1}, or −0.07% over the 25–240 °C temperature range.

An aluminum block furnace with noninductive cartridge heaters was controlled by a Bayley Model 124 proportional temperature controller. The temperature was measured with a chromel–alumel thermocouple and a Fluke Model 895 differential dc voltmeter. The thermocouple was calibrated against a standard platinum resistance thermometer at the Metrology Laboratory at ORNL. To minimize the temperature readout errors due to the microstructure inhomogeneity effects in the thermocouple, the position of the cell and therefore the immersion depth of the thermocouple in the furnace were always maintained the same. Neither short-term nor long-term thermocouple hysteresis effects were observed during the period in which the present measurements were made.

The conductivity measurements were performed by the conventional ac method. The equipment consisted of a Hewlett-Packard Model 100 CD wide band oscillator, an RC bridge built in the University of Tennessee electronics shop, General Radio precision decade resistors and capacitors, and a Tektronix Model 549 oscilloscope with Type 147 plug-in high-grain amplifier. Using the maximum gain of 10 μV cm^{-1} and minimizing external interference with high- and low-frequency filtering of the signal, we routinely obtained a resolution of 0.003% for the conductivity bridge.

Measurements were performed at a frequency of 1.0 kHz. No frequency dispersion of conductivity was observed within the error limits of the measurements. The overall reproducibility of the measurements was checked by performing independent measurements in two different cells on two separately prepared samples of melt each with the same composition. The difference between the two sets of data was less than the scatter within each data set. The two error-determining factors in the conductivity values reported in this paper were probably the temperature instability of the furnace and the uncertainty in the measurement of the sample temperature.

Results

Arrhenius plots of our experimental results for $SbCl_3$–$AlCl_3$ melts are shown in Figures 2 and 3. For melts containing 2.5 mol % $AlCl_3$ deviations from Arrhenius behavior are very large and the specific conductivity κ passes through a maximum well within the experimental temperature range. As the $AlCl_3$ content increases, these deviations gradually diminish and the conductivity maximum moves progressively toward higher temperatures. At 15 mol % $AlCl_3$ the maximum is at the end of the experimental range. For melts with large $AlCl_3$ contents the experimental range is short but small deviations from Arrhenius behavior are still observed.

These data are represented to within experimental accuracy by the empirical equation

$$\ln \kappa = A_1 - A_2 T^{-1} - A_3 T^{1/10} \qquad (1)$$

where T is in K and the adjustable parameters, listed in Table I, were calculated by the method of least squares.[13]

(12) G. Jones and B. C. Bradshaw, *J. Am. Chem. Soc.*, **55** 1780 (1933).

(13) A variety of functions was found to represent the data to within experimental accuracy but none was superior to eq 1 in any meaningful way. For example, when the exponent 0.1 is replaced with an adjustable parameter, the variance of fit can be reduced slightly but there is no real gain because the residuals obtained are within the range of experimental uncertainty, whether the exponent is allowed to vary or fixed at 0.1. In this connection it is interesting to note that the following form of the empirical Vogel–Tammann–Fulcher (VTF) equation comes close to fitting the data but there is a systematic trend in the residuals that exceeds the probable experimental uncertainty

$$\kappa = A_1 T^{1/2} \exp[-A_2/(T - A_3)]$$

The $T^{1/2}$ term (sometimes omitted) is essential in achieving this nearness of fit. Since the VTF equation is often used to represent empirically the transport properties of glass-forming liquids,[14] and since $SbCl_3$-rich $SbCl_3$–$AlCl_3$ melts are glass-forming liquids, one might infer that we are proposing an improvement over the VTF equation. This is not so. Clearly eq 1 will fail at temperatures near the glass-forming temperature, where the VTF equation usually provides an excellent representation.

TABLE I: Estimates of Parameters from Fitting Data to Eq 1

$SbCl_3$, $AlCl_3$-NaCl, mol %	$A_1/100$	$A_2/1000$	A_3	largest residual, %	temp range, K
97.5-2.5-0	1.0042	4.3207	51.763	0.02	354-497
95.0-5.0-0	1.0244	4.4955	52.279	0.06	355-501
90.0-10.0-0	1.0111	4.6221	51.034	0.2[a]	352-498
85.0-15.0-0	0.9734	4.6413	48.778	0.05	380-508
80.0-20.0-0	0.9762	4.8123	48.620	0.05	393-495
75.0-25.0-0	1.0145	5.1159	50.285	0.1	395-493
70.0-30.0-0	1.0190	5.2762	50.031	0.009	430-489
60.0-40.0-0	1.1383	6.0216	55.907	0.09	442-486
50.0-50.0-0	2.3044	11.131	113.12	0.02	450-479
45.0-55.0-0	0.9996	5.6458	48.961	0.1	452-487
40.0-60.0-0	0.6163	4.0092	31.793	0.1	462-485
90.0-5.0-5.0	0.5964	3.3970	30.412	0.08	354-497
85.0-10.0-5.0	0.7815	4.0186	39.432	0.5	324-501
80.0-10.0-10.0	0.4583	2.9096	23.182	0.07	379-495

[a] All residuals but two are < 0.05%.

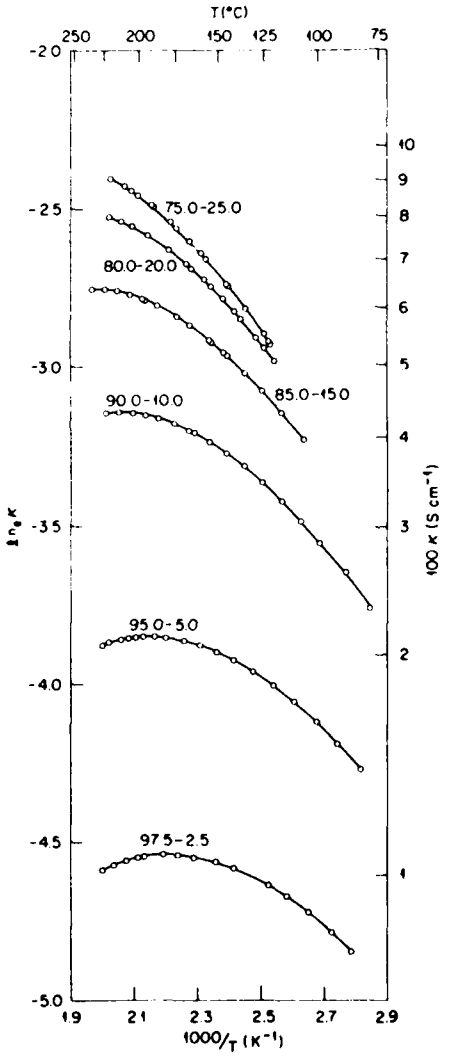

Figure 2. Temperature dependence of the conductivity of $SbCl_3$-$AlCl_3$ melts containing up to 25 mol % $AlCl_3$. Labels on the curves are in the format mol % $SbCl_3$-mol % $AlCl_3$.

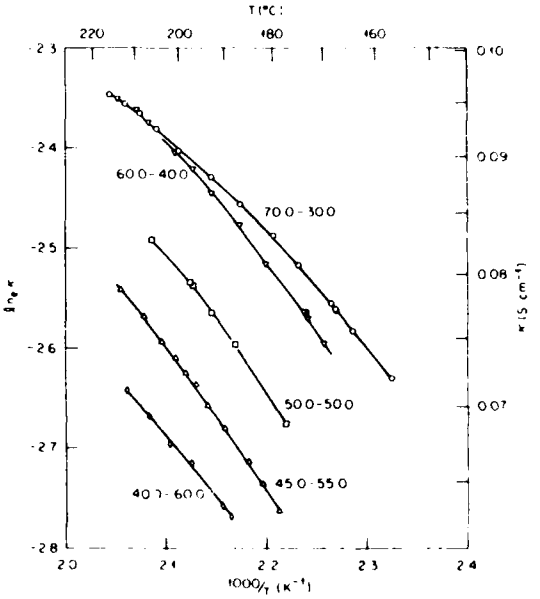

Figure 3. Temperature dependence of the conductivity of $SbCl_3$-$AlCl_3$ melts containing greater than 25 mol % $AlCl_3$. Labels on the curves are in the format mol % $SbCl_3$-mol % $AlCl_3$.

TABLE II: Calculated Coordinates of Maxima for $SbCl_3$-$AlCl_3$ Melts

$AlCl_3$, mol %	100κ, S cm^{-1}	T, K	$AlCl_3$, mol %	100κ, S cm^{-1}	T, K
2.5	1.07	453	15.0	6.41	510
5.0	2.13	465	20.0	8.19	529
10.0	4.34	488	25.0	11.4	543

The next to last column in Table I expresses the greatest residual (difference between an observed and a computed value of ln κ) as a percentage of the observed value. The standard deviation is, of course, a significantly smaller number. For all data sets the residuals are virtually random.

In a formal sense eq 1 is the Arrhenius equation with a "correction term", $A_3T^{1/10}$. However, the three parameters are strongly correlated and the $A_3T^{1/10}$ term is by no means small so that one should be very cautious about attributing physical significance to the numerical values of parameters taken individually.[15] From our point of view

(14) See, for example, C. A. Angell and R. D. Bressel, *J. Phys. Chem.*, 76, 3244 (1972).

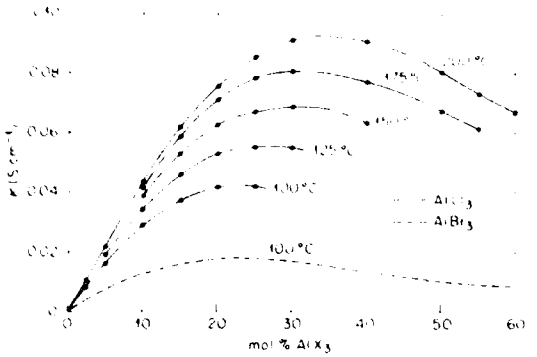

Figure 4. Conductivity isotherms for $SbCl_3$-$AlCl_3$ melts at five temperatures and for $SbBr_3$-$AlBr_3$ melts at 100 °C. Points calculated from the parameters in Table I are displayed. Data for the bromide system are from ref 16.

eq 1 is nothing more than a compact means of representing and interpolating our data.

Equation 1 passes through a maximum whose coordinates T_m and κ_m are given by eq 2 and 3, where $b = 10^{1.11}$

$$T_m = (10A_2/A_3)^{10.11} \quad (2)$$

$$\ln \kappa_m = A_1 - bA_2^{1.11}A_3^{10.11} \quad (3)$$

$+ 10^{10.11} = 1.35613$. Computed values of the maxima for melts containing 2.5–25.0 mol % $AlCl_3$ are listed in Table II. These agree with the observed values for the three cases in which maxima were measured, 2.5, 5.0, and 10.0 mol % $AlCl_3$. Because the maxima are broad, the uncertainty in both the experimental and computed values is several degrees.

The composition dependence of κ at several temperatures is shown in Figure 4 together with an isotherm for the $SbBr_3$-$AlBr_3$ system[16] that will be discussed later. These isotherms rise rapidly from zero as the $AlCl_3$ content increases and pass through a maximum that progressively shifts toward higher $AlCl_3$ content as the temperature increases. The observed shift is from ca. 25 mol % $AlCl_3$ at 100 °C to ca. 35 mol % $AlCl_3$ at 200 °C.

Conductivity measurements were made on three $SbCl_3$-rich melts in the $SbCl_3$-$AlCl_3$-NaCl system. Although NaCl is only sparingly soluble in $SbCl_3$, we found that it will dissolve in $SbCl_3$-$AlCl_3$ mixtures so long as the number of moles of NaCl does not exceed the number of moles of $AlCl_3$. When the NaCl content exceeds that of $AlCl_3$, the liquidus surface rises rather abruptly, just as it does in the $AlCl_3$-NaCl system[17] where the reaction to form $NaAlCl_4$ goes nearly to completion.

Results of these conductivity measurements are shown as solid lines in Figure 5. For comparison, the curves for two compositions in the $SbCl_3$-$AlCl_3$ system are displayed as dashed lines. Note that the 90.0-5.0-5.0 melt can be made by adding NaCl to a 94.7-5.3-0 melt, quite close in composition to the 95.0–5.0–0 melt shown, while the 85.0–10.0–5.0 and 80.0–10.0–10.0 melts can be made by adding NaCl to 89.5–10.5–0 and 88.9–11.1–0 melts, respectively. The latter two compositions have κ values a little greater than those of the 90.0–10.0–0 melts. Thus, we find that the addition of NaCl to a $SbCl_3$-$AlCl_3$ mixture

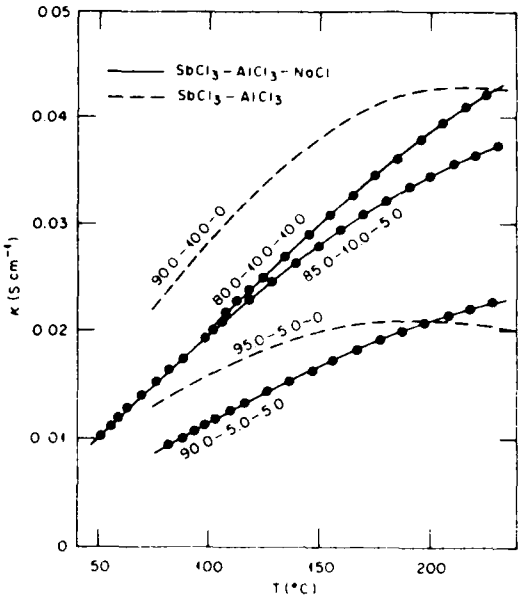

Figure 5. Temperature dependence of the conductivity for $SbCl_3$-$AlCl_3$-NaCl melts. Two curves for melts without NaCl are shown for comparison. Labels on the curves are in the format mol % $SbCl_3$–mol % $AlCl_3$–mol % NaCl.

(containing up to at least 10 mol % $AlCl_3$) substantially *decreases* the specific conductivity at low temperatures, while at higher temperatures this effect is observed to reverse for melts containing equal amounts of $AlCl_3$ and NaCl.

These data were fitted to eq 1 and the resulting parameters are listed in Table I. The fit is not as good as it was for $SbCl_3$-$AlCl_3$ melts inasmuch as the residuals show systematic trends. However, for the two melts with equimolar $AlCl_3$ and NaCl most of the residuals lie within experimental uncertainty and we regard eq 1 as a satisfactory representation of the data.

Discussion

The conductivity maxima for $SbCl_3$-$AlCl_3$ mixtures shown in Figure 4 reach values of 0.04–0.09 S cm^{-1} at 100–200 °C. These are quite substantial ionic conductivities. By comparison, highly ionized NaCl-$AlCl_3$ mixtures containing the mobile Na^+ ion have κ values on the order of 0.2–0.6 S cm^{-1} at similar temperatures,[18] while equimolar alkylpyridinum chloride-$AlCl_3$ melts have conductivities on the order of 0.04–0.08 S cm^{-1}.[19] Pure, molten SCl_3AlCl_4, in which the SCl_3^+ cation is comparable in size to $SbCl_2^+$, has a conductivity of 0.04 S cm^{-1} at 150 °C.[20]

Jander and Swart[3] reported the conductivity of $SbCl_3$-$AlCl_3$ mixtures containing from about 1 to 10 mol % $AlCl_3$ at 100 °C with values that are in fairly good agreement with ours. They proposed that the charge carriers were produced by the following reaction:

$$AlCl_3 + SbCl_3 \rightleftharpoons SbCl_2(AlCl_4) \rightleftharpoons SbCl_2^+ + AlCl_4 \quad (4)$$

Considerable work has been done on the conductivity of $SbBr_3$-$AlBr_3$ mixtures and it is interesting to note some of the qualitative similarities between the chloride and

(15) The potential for error in attributing physical significance to numerical values of individual parameters that belong to sets of coupled parameters is discussed and illustrated in M. H. Lietzke and R. W. Stoughton, *J. Tenn. Acad. Sci.*, **49**, 130 (1974).

(16) V. A. Izbekov and V. A. Plotnikov, *Z. Anorg. Chem.*, **71**, 328 (1911).

(17) W. Fischer and A.-L. Simon, *Z. Anorg. Allg. Chem.*, **306**, 1 (1960).

(18) R. C. Howie and D. W. MacMillan, *J. Inorg. Nucl. Chem.*, **33**, 3681 (1971).

(19) R. A. Carpio, L. A. King, R. E. Lindstrom, J. C. Nardi, and C. L. Hussey, *J. Electrochem. Soc.*, **126**, 1644 (1979).

(20) C. Petrovic and G. Mamantov, unpublished results.

bromide systems. Izbekov and Plotnik[16] measured the conductivity of $SbBr_3$–$AlBr_3$ mixtures over the entire compositional range at 100 °C and their results for 0–60 mol % $AlBr_3$ are shown in Figure 4. The general shape of the curve is much like that which we found for the chloride melts. On the $AlBr_3$-rich side the conductivity curve shows a slight hump and then approaches zero in a way that is almost asymptotic to the composition axis. These authors also reported the temperature dependence of Λ at two compositions, 42.80 and 88.26 mol % $AlBr_3$. On an Arrhenius plot the 42.80 mol % line shows a small departure from linearity in the same direction and of similar magnitude to that reported here for 40 mol % $AlCl_3$ in $SbCl_3$. At 88.26 mol % $AlBr_3$ the conductivity passes through a well-defined maximum like that which we report at the $SbCl_3$-rich end of the $SbCl_3$–$AlCl_3$ system.

Gorenbein[21] reported five conductivity isotherms over the full compositional range of the $SbBr_3$–$AlBr_3$ system. Unfortunately, his paper displays only a few points on the $SbBr_3$-rich side of the conductivity maximum so that no clear conclusions about the temperature dependence of Λ in this region can be drawn. However, his isotherms have the same shape as that in the earlier investigation, and their maxima shift with increasing temperature in the direction of increasing aluminum bromide content, just as in the chloride system. He assumed that the bromide analogue of reaction 4 is the source of the charge carriers. From viscosity measurements he concluded that the ionic mobilities are strongly influenced by melt composition in such a way as to cause the maxima of conductivity isotherms to occur well to the $SbBr_3$-rich side of the equimolar mixture. Jander and Weis[22] reported conductivity and cryoscopic i-factor values for dilute solutions of $AlBr_3$ in $SbBr_3$ at 100 °C. They concluded that the compound $SbBr_2AlBr_4$ is not completely dissociated.

There are also interesting qualitative similarities between conductance in $SbCl_3$–$AlCl_3$ melts and other types of liquid systems. The extreme deviations from Arrhenius behavior with a conductivity maximum at T_m that we observed in the compositional range 2.5–10 mol % $AlCl_3$ are similar to those of various pure molten metal halides and of some concentrated aqueous solutions of strong electrolytes.[23] This behavior has been attributed to a competition between increasing ion mobility with increasing temperature and increasing loss of charge carriers due to interionic association to form neutral molecules or gaslike ion pairs. Furthermore, in concentrated (as distinguished from dilute) aqueous solutions, the temperature of the conductivity maximum, T_m, increases with increasing electrolyte concentration just as it does with increasing $AlCl_3$ concentration in the $SbCl_3$–$AlCl_3$ system.

Arguments similar to those above can obviously be invoked to explain the occurrence of a conductivity maximum in $SbCl_3$–$AlCl_3$ melts. Such arguments require that the ions formed in the reaction that occurs when $SbCl_3$ and $AlCl_3$ are mixed be in equilibrium with neutral molecules, such as $SbCl_2AlCl_4$ in reaction 4, and that the concentration of the latter be quite significant in the temperature range of our measurements. Therefore, we shall now turn to a consideration of the structural entities that may be present in our melts.

The compound $SbBr_2AlBr_4$ provides the model upon which reaction 4 is based. However, as noted in the Introduction, no such binary compound occurs in the chloride system. We do not regard this difference with respect to solid compound formation as a matter of fundamental importance insofar as the liquid state is concerned. We attribute this difference to differences between the properties of crystalline $AlCl_3$ and crystalline $AlBr_3$ so that in the solid-state reaction

$$SbX_2AlX_4(s) = SbX_3(s) + AlX_3(s) \qquad (5)$$

the forward reaction is favored for X = Cl but the reverse is favored for X = Br. Thus, it is possible for similar reactions to occur in both the bromide and chloride melts but, upon freezing, a solid compound is recovered in one case but not in the other.

This proposal is based on the plausible assumption that the coordination of aluminum in $SbCl_2AlCl_4$ is tetrahedral, just as it is in $SbBr_2AlBr_4$,[24] Al_2Cl_6,[25] and Al_2Br_6.[25] The solid AlX_3 compounds, however, are quite different. Solid $AlBr_3$ consists of Al_2Br_6 molecules and melts at 97.4 °C with a $\Delta H°$ of 11.3 kJ mol^{-1}.[25] In contrast solid $AlCl_3$ has a compact layer lattice with 6-fold coordination about aluminum and melts at 192.4 °C with a $\Delta H°$ of 35.3 kJ mol^{-1}.[25] Thus, for the chloride system the solid-state decomposition of $SbCl_2AlCl_4$ is favored by the relatively large lattice energy of $AlCl_3$. Even crystalline $SbBr_2AlBr_4$ is not very stable since $\Delta H°_{298}$ for reaction 5 with X = Br is only 18.0 ± 2.5 kJ mol^{-1} according to Malkova and Suvorov.[26]

The best evidence regarding the solid-state structure of $SbBr_2AlBr_4$ is provided by NQR spectra reported by Okuda et al.[24] They concluded that the structural entities are a V-shaped $SbBr_2^+$ ion and a distorted tetrahedral $AlBr_4^-$ ion with weak bridge bonds between Sb atoms and the Br atoms in $AlBr_4^-$ ions.

The evidence presented thus far lends some support to the assertion that reaction 4 and its bromide analogue are reasonable guesses as to the ionizing processes in antimony trihalide-rich melts.

In keeping with the supposition that $SbCl_2AlCl_4$ molecules are favored at high temperatures, Raman spectra[27] of $SbCl_3$–$AlCl_3$ melts at 210–220 °C do not show the bands of either $AlCl_4^-$ or $Al_2Cl_7^-$. Moderately small concentrations of $AlCl_4^-$ or $Al_2Cl_7^-$ probably would not be detected in these spectra because of interferences from the relatively intense bands due to Sb–Cl variations but, nevertheless, the large concentrations required by a high degree of ionization are clearly not present.

The above considerations lead to the conclusion that at 210–220 °C the concentration of charge carriers is not large even for those melt compositions whose specific conductivity is quite large. This implies that at least one of the ionic species has an exceptionally high ionic mobility. We shall return to this point later.

It is interesting to see what can be inferred about the weak bonds reported to occur between $SbBr_2^+$ and $AlBr_4^-$ ions in crystalline $SbBr_2AlBr_4$. Although the X-ray crystal structure of this compound has not been determined, structures are known for related compounds such as $TeCl_3AlCl_4$, $SbCl_2GaCl_4$, and many anionic bromo and chloro complexes of antimony(III). In $TeCl_3AlCl_4$,[28] Te

(21) E. Va. Gorenbein, *J. Gen. Chem. USSR (Engl. Transl.)*, **15**, 729 (1945).
(22) G. Jander and J. Weis, *Z. Elektrochem.*, **61**, 1275 (1957).
(23) S. J. Smedley, "The Interpretation of Ionic Conductivity in Liquids", Plenum Press, New York, 1980, Chapters 4 and 5.
(24) T. Okuda, K. Yamada, H. Ishihara, and H. Negita, *Bull. Chem. Soc. Jpn.*, **50**, 3136 (1977).
(25) C. R. Boston, "Advances in Molten Salt Chemistry", Vol. 1, J. Braunstein, G. Mamantov, and G. P. Smith, Eds., Plenum Press, New York, 1971, Chapter 3.
(26) A. S. Malkova and A. V. Suvorov, *Russ. J. Inorg. Chem. (Engl. Transl.)*, **14**, 1049 (1969).
(27) R. Huglen, G. Mamantov, G. M. Begun and G. P. Smith, *J. Raman Spectrosc.*, **9**, 188 (1980).
(28) B. Krebs, B. Buss, and D. Altena, *Z. Anorg. Allg. Chem.*, **386**, 257 (1971).

is surrounded by a distorted octahedron of six Cl atoms, three of which have short bond distances of about 227 ppm and three of which have long bond distances of 301–313 pm. Each short-bonded Cl atom is trans related to a long-bonded Cl atom and each long-bonded Cl atom belongs to a different $AlCl_4^-$ moiety. If one ignores the long Te···Cl bonds, the crystal might be described as consisting of $TeCl_3^+$ and $AlCl_4^-$ ions. However, this description would not be entirely accurate because the long Te···Cl bonds are substantially shorter than the sum of the van der Waals radii, 400 pm.[29] When the long bonds are included in the description, one finds that the $TeCl_3^+$ and $AlCl_4^-$ moities are joined to form a crystallographically infinite network rather than small, discrete molecular ions.

The crystal structure[30] of the 1:1 adduct $SbCl_3$-$GaCl_3$ shows that each Sb atom has two short bonds (~230 pm) to two Cl atoms with a Cl-Sb-Cl angle of 97.4° and two medium-length bonds (~271 and ~277 pm) to two other Cl atoms. (Sb-Cl bond lengths are discussed in some detail below.) Each of the latter Cl atoms is bonded to a different Ga atom, while each Ga atom is coordinated to four Cl atoms with a distorted tetrahedral geometry. The overall conformation is an endless chain of alternating $SbCl_2^+$ and $GaCl_4^-$ units that are strongly linked by Ga-Cl···Sb bridges.

The anionic chloro and bromo complexes of antimony(III)[31] have structural features similar to those of $TeCl_3$-$AlCl_4$ and $SbCl_2GaCl_4$ except that halogen bridge bonds join pairs of Sb atoms rather than Te and Al atoms or Sb and Ga atoms. We will confine our discussion to the chloro complexes, which differ only in detail from their bromo analogues. In nearly all cases Sb atoms are surrounded by a distorted octahedron of chlorine atoms. Trans-related chlorines may be paired with short and long bonds, respectively, or with more nearly equal bonds of intermediate length. The only case of a chlorine atom without a trans-related partner is the discrete $SbCl_5^{2-}$ ion in which one of the octahedral positions is unoccupied.[32,36] When this occurs, the halide atom trans to the empty position has an especially short bond length.

Generally, antimony achieves 6-fold coordination by chlorine bridge bonds to one or more other Sb atoms. The only cases in which bridge bonds are absent are the discrete $SbCl_5^{2-}$ and $SbCl_6^{3-}$ ions.[33] Chlorines in bridging positions are often short bonded to one Sb atom and long bonded to another. However, there are examples of chlorine atoms that have only long bonds to Sb.[38] In verbal descriptions of such structures the longer bonds are sometimes ignored. For example, on this basis the α and β forms of $Cs_3Sb_2Cl_9$ were described as consisting of $SbCl_3$ molecules together with Cl⁻ and Cs^+ ions.[34] In these crystals, the distances between the supposed Cl⁻ ions and nearest Sb atoms were 282–289 pm compared with Sb–Cl distances of 242–245 pm in the supposed $SbCl_3$ molecules and a sum of van der Waals radii of 360 pm (according to Hulme and Szymański[43]) or 400 pm (according to Pauling[29]). Crystal structures of chloro complexes of antimony(III) display Sb–Cl distances ranging from 236 to 342 pm without a significant gap. At the extremes of this range the bonds might be described as being largely covalent and largely ionic, respectively, but in between these extremes there would appear to be a continuous transition from one type to the other.

There is evidence that chlorine bridge bonding plays a structural role of some importance in molten $SbCl_3$. X-ray and neutron diffraction measurements on molten $SbCl_3$ at 80 °C indicate the presence of pyramidal molecules (like those in the gas) attached to one another by chlorine bridges to form short chains in which the dipole axes of the molecules are strongly correlated over several molecular diameters.[44] Thus, a given $SbCl_3$ molecule in the melt shares its chlorine atoms via long bonds to the antimony atom of a neighboring molecule. Raman spectra of liquid $SbCl_3$ in the 2–100-cm^{-1} range are due to intermolecular motions between molecules attracted by middle-range forces.[45] These spectra are due to the collective motions of a linear chain structure. They also provide evidence that the chain rupture energy is about 10 kJ mol^{-1} and that chain making is a thermally activated process with a barrier of about 3 kJ mol^{-1}.

The above structural considerations suggest that $SbCl_2^+$ may to a significant extent be bridge bonded to $SbCl_3$ molecules when the latter are present. This can be schematically represented by reaction 6. Such an equilibrium

$$SbCl_2^+ + nSbCl_3 \cdots SbCl_2^+ \cdot nSbCl_3 \qquad (6)$$

implies that the ionization of $SbCl_2AlCl_4$ molecules proceeds not only via reaction 4 but also via an equilibrium that involves $SbCl_3$ molecules, such as reaction 7, with the partitioning between these processes determined by reaction 6.

$$SbCl_2AlCl_4 + nSbCl_3 \cdots SbCl_2^+ \cdot nSbCl + AlCl_4^- \qquad (7)$$

If $SbCl_3$ molecules assist the ionization of $SbCl_2AlCl_4$ (as in reaction 7), then one expects the maximum concentration of ions to occur in the $SbCl_3$-rich composition region. Thus, the conductivity maximum would also be expected to occur in the $SbCl_3$-rich composition region, although not at the composition of the maximum in ionic concentration. This is due to the difference in the mobility of the $SbCl_2^+$ and $SbCl_2^+ \cdot nSbCl_3$ ions as a consequence of their sizes. The shift in the conductivity maximum in the direction of 50 mol % $AlCl_3$ as the temperature increases can be rationalized in terms of a thermal dissociation of $SbCl_2^+ \cdot nSbCl_3$ (reaction 6).

Up to this point we have discussed our results in terms of a conventional Stokesian mechanism, that is, one in which ions migrate by a normal diffusional process. However, there are several types of molten halides and halide solutions in which the conductivity is reported to be anomalously large, so that a non-Stokesian process appears to be aiding ionic transport. Although we have

(29) L. Pauling, "The Nature of the Chemical Bond", 3rd ed., Cornell University Press, Ithaca, NY, 1960, p 260.
(30) C. Peylhard, P. Teulon, and A. Potier, *Z. Anorg. Allg. Chem.*, **483**, 236 (1981).
(31) Examples of anionic chloro complexes are given in ref 32–39. Examples of anionic bromo complexes are given in ref 40–42.
(32) M. Edstrand, M. Inge, and N. Ingri, *Acta Chem. Scand.*, **9**, 122 (1955); M. Webster and S. Keats, *J. Chem. Soc. A*, 298 (1971).
(33) S. K. Porter and R. A. Jacobson, *J. Chem. Soc. A*, 1356 (1970).
(34) K. Kihara and T. Sudo, *Z. Kristallogr.*, **134**, 142 (1971); *Acta Crystallogr., Sect. B*, **30**, 1088 (1974).
(35) D. R. Schroeder and R. A. Jacobson, *Inorg. Chem.*, **12**, 210 (1973).
(36) R. K. Wismer and R. A. Jacobson, *Inorg. Chem.*, **13**, 1678 (1974).
(37) A. Lipka and D. Mootz, *Z. Anorg. Allg. Chem.*, **440**, 231 (1978).
(38) F. J. Kruger, F. Zettler, and A. Schmidt, *Z. Anorg. Allg. Chem.*, **449**, 135 (1979).
(39) A. Lipka, *Z. Anorg. Allg. Chem.*, **469**, 218, 229 (1980).
(40) S. L. Lawton and R. A. Jacobson, *Inorg. Chem.*, **5**, 743 (1966).
(41) S. K. Porter and R. A. Jacobson, *J. Chem. Soc. A*, 1359 (1970).
(42) P. W. DeHaven and R. A. Jacobson, *Cryst. Struct. Commun.*, **5**, 31 (1976).
(43) R. Hulme and J. T. Szymański, *Acta Crystallogr., Sect. B*, **25**, 753 (1969).
(44) E. Johnson, A. H. Narten, W. E. Thiessen, and R. Triolo, *Faraday Discuss. Chem. Soc.*, **66**, 287 (1978).
(45) F. Aliotta, G. Maisano, N. Micali, P. Migliardo, C. Vasi, F. Wanderlingh, R. Triolo, and G. P. Smith, *J. Chem. Phys.*, **76**, 3987 (1982).

no direct evidence for such a process in $SbCl_3$–$AlCl_3$, it is structurally plausible, and the assumption that it plays a role leads to a rather simple accounting of the observed behavior.

It is well established that the chloride ion has an abnormally high mobility in molten $SbCl_3$, as does the bromide ion in $SbBr_3$ as discussed by Porter and Baughan.[46] They attributed this high mobility to a Grotthus-type mechanism based on the chloride-transfer process $SbCl_4^- + SbCl_3 \rightleftharpoons SbCl_3 + SbCl_4^-$. A similar anomalous conductivity has been noted in liquid $AsCl_3$.[47] Recently Poulsen and Bjerrum[48] reported evidence for anomalous ionic conductivity in molten $BiCl_3$–$AlCl_3$, $TeCl_4$–$AlCl_3$, and KCl–$TeCl_4$ mixtures. They attributed this behavior to a Grotthus-like chloride-transfer mechanism between labile donor and acceptor units simultaneously present in the melt. For solutions of aluminum halides and alkali-metal halides in toluene, Gilandi and co-workers[49] recently observed a 10^4-fold increase in the equivalent conductivity over a 10-fold increase in solute concentration. They interpreted the abnormally high conductivity in terms of a non-Stokesian, relay-type process involving the addition of an ion to one end of a large neutral aggregate of ions while another ion of the same type leaves the aggregate at the opposite end. This virtual movement of an ion through an aggregate results in an enhanced apparent ionic mobility.

Given the above precedents, it is plausible to suppose that a non-Stokesian mechanism may contribute to conductivity in $SbCl_3$–$AlCl_3$ melts through a chloride-transfer process between $SbCl_2^+$ and a suitably oriented $SbCl_3$ molecule, thus

$$Cl_2Sb^+ + ClSbCl_2 \rightleftharpoons Cl_2Sb^+\cdots Cl\cdots SbCl_2^+ \rightleftharpoons Cl_2SbCl + SbCl_2^+ \quad (8)$$

The occurrence of *trans-related short* and long Sb–Cl bonds, as discussed above, shows that transition states of the sort called for in eq 8 are within the known capability of chloro (and bromo) antimony(III) complexes. Chains (oriented pairs, trios, etc.) of the sort that occur in liquid $SbCl_3$ would greatly augment the chloride-transfer process. As soon as the positive charge was transferred from $SbCl_2^+$ to a $SbCl_3$ molecule at the end of a chain, the next $SbCl_3$ molecule would be correctly oriented to receive the charge. After the charge had thus moved through a chain, the $SbCl_3$ molecules would have to reorient before transferring another charge. The possibilities are like those envisaged for H^+ or OH^- transfer through H_2O with the long Sb–Cl bonds playing the structural role of hydrogen bonds in an aqueous system.[50] The structural similarities between chloro and bromo complexes of antimony(III) suggest that non-Stokesian conduction is also plausible in $SbBr_3$–$AlBr_3$ melts.

The occurrence of a conductivity maximum upon heating can be rationalized by a loss of $SbCl_2^+$ upon formation of $SbCl_2AlCl_4$, just as in the Stokesian model, but this effect is also augmented by the thermal degradation of $SbCl_3$ chains. The fact that the isothermal conductivity maximum occurs far on the $SbCl_3$-rich side of the equimolar composition is readily rationalized by the fact that $SbCl_3$ molecules must be present in addition to $SbCl_2^+$ ions for the chloride-transfer process to occur. This maximum is a consequence of a balance between the increase in $SbCl_2^+$ and the decrease in $SbCl_3$ as more and more $AlCl_3$ is added. The presence of $SbCl_2^+$-$n$$SbCl_3$ cations augments this effect. The shift of this maximum toward the equimolar composition with increasing temperature is due to an increasing importance of Stokesian conduction at high temperatures.

Sodium chloride is a much stronger Lewis base than any plausible entities in $SbCl_3$–$AlCl_3$ mixtures. Therefore, when this substance is added to $SbCl_3$-rich melts, the Cl^- ion will titrate the $SbCl_2^+$ or $SbCl_2^+$-$n$$SbCl_3$ cations to form neutral $SbCl_3$ molecules and will break up the $SbCl_2AlCl_4^-$ complex entities, thus

$$NaCl + SbCl_2^+ \rightarrow Na^+ + SbCl_3 \quad (9)$$

$$NaCl + SbCl_2AlCl_4^- \rightarrow Na^+ + AlCl_4^- + SbCl_3 \quad (10)$$

In reaction 9, $SbCl_2^+$ ions are replaced by Na^+ ions with no net change in the total number of ions, while, in reaction 10, neutral $SbCl_2AlCl_4$ complexes are replaced by Na^+ and $AlCl_4^-$ ions. Since Na^+ ions are much smaller than any ions in SbCl–$AlCl_3$ melts, the above reactions should substantially increase the specific conductivity if the conduction mechanism was Stokesian and if the Na^+ ions were not immobilized by pairing. However, experiment shows that at low temperatures quite the opposite happens, as will be seen from Figure 5. Thus, a purely Stokesian transport mechanism requires ion pairing as shown in reaction 11,

$$NaAlCl_4 \rightleftharpoons Na^+ + AlCl_4^- \quad (11)$$

where $NaAlCl_4$ is a gaslike ion pair. This equilibrium can by no means be shifted far to the left because the conductivity of melts containing equimolar NaCl and $AlCl_3$ have a substantial specific conductivity. Furthermore, reaction 11 must have a $\Delta H°$ of much smaller magnitude than that for reaction 4 in melts with similar, large concentrations of $SbCl_3$ molecules. This follows from the temperature dependences of the 80–10–10 and 90–5–5 mol % melts as compared with those for the 90–10–0 and 95–5–0 mol % melts (without NaCl). The conductance curves for the latter pass through maxima within the temperature interval shown in Figure 5 (as a consequence of a substantial shift in reaction 4 toward neutral molecules), whereas the conductance curves for melts containing equimolar NaCl and $AlCl_3$ have only a small curvature indicative of a much smaller influence of temperature on equilibrium 4.

A simpler, more straightforward explanation of the consequences of adding NaCl is provided if the non-Stokesian chloride-transfer mechanism augments Stokesian diffusional transport. The addition of NaCl removes $SbCl_2^+$ (or $SbCl_2^+$-$n$$SbCl_3$), which is one of the two species required by the chloride-exchange magnesium (reaction 8). At low temperatures the high ionic mobility of Na^+ together with the increased number of ions (eq 10) is insufficient to compensate for the elimination of non-Stokesian transport so that the specific conductivity decreases. With increasing temperature the importance of non-Stokesian transport becomes diminished as $SbCl_2^+$ is removed by $SbCl_2AlCl_4$ formation, while Stokesian transport is enhanced by an increase in ionic mobility so that at high temperatures the addition of Na^+ ions more than compensates for the loss of $SbCl_2^+$ ions.

Acknowledgment. This research was sponsored by Aero Propulsion Laboratory, Air Force Wright Aeronautical Laboratories, Wright-Patterson Air Force Base, Ohio,

(46) G. B. Porter and E. C. Baughan, *J. Chem. Soc.*, 744 (1958).
(47) V. Gutmann, *Sven. Kem. Tidskr.*, **68**, 1 (1956), known through ref 48.
(48) F. W. Poulsen and N. J. Bjerrum, *J. Phys. Chem.*, **79**, 1610 (1975).
(49) A. Reger, E. Peled, and E. Gileadi, *J. Phys. Chem.*, **83**, 873 (1979); E. Peled, M. Brand, and E. Gileadi, *J. Electrochem. Soc.*, **128**, 1697 (1981).
(50) See, For example, D. A. Lown and H. R. Thirsk, *Trans. Faraday Soc.*, **67**, 132 (1971), and references therein.

under contract No. F33615-78-C-2075, and by the Division of Chemical Sciences, Office of Basic Energy Sciences, U.S. Department of Energy, under contract W-7405-eng-26 with the Union Carbide Corp. M.S. is grateful for financial assistance from Norges Teknisk-Naturvitenskapelige Forskningsråd. We note with thanks the technical assistance of J. Cobb and D. Goff, and helpful advice from J. Brynestad and C. A. Angell.

* U.S. GOVERNMENT PRINTING OFFICE 1983-659-062/1022

END

DATE
FILMED

9 — 83

DTIC